Fisheries and Oceans Canada | Pêches et Océans Canada
Ecosystems and Oceans Science | Sciences des écosystèmes et des océans

Canadian Science Advisory Secretariat (CSAS)

Research Document 2020/030

Quebec Region

Physical Oceanographic Conditions in the Gulf of St. Lawrence during 2019

P.S. Galbraith[1], J. Chassé[2], J.-L. Shaw[1], J. Dumas[1], C. Caverhill[3], D. Lefaivre[1], C. Lafleur[1]

(1) Fisheries and Oceans Canada, Québec Region,
Maurice Lamontagne Institute,
P.O. Box 1000, Mont-Joli, Québec, G5H 3Z4

(2) Fisheries and Oceans Canada, Gulf Region,
Gulf Fisheries Centre,
P.O. Box 5030, Moncton, New Brunswick, E1C 9B6

(3) Fisheries and Oceans Canada, Maritimes Region,
Bedford Institute of Oceanography,
P.O. Box 1006, Dartmouth, Nova Scotia, B2Y 4A2

August 2020

Canada

Foreword

This series documents the scientific basis for the evaluation of aquatic resources and ecosystems in Canada. As such, it addresses the issues of the day in the time frames required and the documents it contains are not intended as definitive statements on the subjects addressed but rather as progress reports on ongoing investigations.

Published by:

Fisheries and Oceans Canada
Canadian Science Advisory Secretariat
200 Kent Street
Ottawa ON K1A 0E6

http://www.dfo-mpo.gc.ca/csas-sccs/
csas-sccs@dfo-mpo.gc.ca

ISSN 1919-5044

Correct citation for this publication:

Galbraith, P.S., Chassé, J., Shaw, J.-L., Dumas, J., Caverhill, C., Lefaivre, D. and Lafleur, C. 2020. Physical Oceanographic Conditions in the Gulf of St. Lawrence during 2019. DFO Can. Sci. Advis. Sec. Res. Doc. 2020/030. iv + 84 p.

Aussi disponible en français :

Galbraith, P.S., Chassé, J., Shaw, J.-L., Dumas, J., Caverhill, C., Lefaivre, D. et Lafleur, C. 2020. Conditions océanographiques physiques dans le golfe du Saint-Laurent en 2019. Secr. can. de consult. sci. du MPO, Doc. de rech. 2020/030. iv + 88 p.

TABLE OF CONTENTS

ABSTRACT

An overview of physical oceanographic conditions in the Gulf of St. Lawrence (GSL) in 2019 is presented as part of the Atlantic Zone Monitoring Program (AZMP). AZMP data as well as data from regional monitoring programs are analysed and presented in relation to long-term means. The annual average freshwater runoffs of the St. Lawrence River measured at Québec City and its combination with rivers flowing into the Estuary (RIVSUM II) were at their highest level since 1976. Sea-ice maximum volume was near normal, but the winter mixed layer volume was at a record high aided by the second largest inflow since 1997 of Labrador Shelf Water. The August cold intermediate layer (CIL) and the seasonally averaged minimum temperature index were near normal. Surface water temperatures were at a record low in September, but this was caused by strong vertical mixing from tropical storm Dorian rather than from heat loss to the atmosphere. The May to November average was below normal, but the warmest month of the year, August, was above normal. Deep water temperatures have been increasing overall in the Gulf since 2009, with inward advection from Cabot Strait. Gulf-wide average temperatures at 150 and 200 m are lower than the 2015 record highs but remain above normal at 3.3°C (+0.8°C, +1.6 SD) and 5.5°C (+1.0°C, +2.4 SD). New series record highs (since 1915) were set at 250 and 300 m, at 6.3°C (+1.0°C, +3.8 SD) and 6.5°C (+1.0°C, +6.6 SD) respectively. Bottom area covered by waters warmer than 6°C remained high in Anticosti Channel and Esquiman Channel and were at record highs in the northwest Gulf and Central Gulf.

INTRODUCTION

This document examines the physical oceanographic conditions and related atmospheric forcing in the Gulf of St. Lawrence in 2019 (Fig. 1). It complements similar reviews of the environmental conditions on the Newfoundland and Labrador Shelf and the Scotian Shelf and Gulf of Maine as part of the Department of Fisheries and Oceans' (DFO) Atlantic Zone Monitoring Program (AZMP; see Therriault et al. 1998 for background information on the program, as well as Cyr et al. 2020 and Hebert et al. 2018 for examples of past reviews in other AZMP regions) in support of zonal state of the ocean report provided as a Scientific Advisory Report (DFO 2020). The last detailed report of physical oceanographic conditions in the Gulf of St. Lawrence was produced for the year 2018 (Galbraith et al. 2019).

Some of the variables presented are spatially averaged over distinct regions of the Gulf (Fig. 2) into what will be termed "regional averages". The report uses data obtained from the AZMP, other DFO surveys, and other sources. Environmental variables are usually expressed as anomalies, i.e., deviations from their long-term mean. The long-term mean or normal conditions are calculated for the standard 1981–2010 reference period when possible. Furthermore, because these series have different units (°C, m^3, m^2, etc.), each anomaly time series is normalized by dividing by its standard deviation (SD), also calculated for the standard reference period when possible. This allows a more direct comparison of the various series. Missing data are represented by grey cells in the tables, values within ±0.5 SD of the average as white cells, and conditions corresponding to warmer than normal (higher temperatures, reduced ice volumes, reduced cold-water volumes or areas) by more than 0.5 SD as red cells, with more intense reds corresponding to increasingly warmer conditions. Similarly, blue represents colder than normal conditions. Higher than normal freshwater inflow is shown as red, but does not necessarily correspond to warmer-than-normal conditions.

The summertime water column in the Gulf of St. Lawrence consists of three distinct layers: the surface layer, the cold intermediate layer (CIL), and the deeper water layer (Fig. 3). Surface temperatures typically reach maximum values in early to mid-August (Galbraith et al. 2012). Gradual cooling occurs thereafter, and wind forced mixing during the fall leads to a progressively deeper and cooler mixed layer, eventually encompassing the CIL. During winter, the surface layer thickens partly because of buoyancy losses (cooling and reduced runoff) and brine rejection associated with sea-ice formation, but mostly from wind-driven mixing prior to ice formation (Galbraith 2006). The surface winter layer extends to an average depth of 75 m, but may reach >150 m in places such as the Mécatina Trough where near freezing waters (-1.8 to 0ºC) from the Labrador shelf entering through the Strait of Belle Isle may extend from the surface to the bottom in depths >200 m (Galbraith 2006). During spring, surface warming, sea-ice melt waters, and continental runoff produce a lower-salinity and higher-temperature surface layer. Underneath this surface layer, cold waters from the previous winter are partly isolated from the atmosphere and form the summer CIL. This layer will persist until the next winter, gradually warming up and deepening during summer (Gilbert and Pettigrew 1997; Cyr et al. 2011) and more rapidly during the fall as vertical mixing intensifies.

This report considers air temperature and freshwater runoff, both significant drivers of the surface layer which is discussed next. Winter sea ice conditions and the winter mixed layer are then presented. The latter is the precursor to the summer CIL, which affects bottom temperatures on the Magdalen Shallows. The deeper waters, mostly isolated from exchanges with the surface, are presented last along with a summary of major oceanographic surveys, some modelling results on currents and transports, and details of observations at high frequency sampling stations.

AIR TEMPERATURE

The air temperature data are the second generation of homogenized surface air temperature data, part of the Adjusted and Homogenized Canadian Climate Data (AHCCD), which accounts for shifts due to the relocation of stations, changes in observing practices and automation (Vincent et al. 2012). The monthly air temperature anomalies for several stations around the Gulf are shown in Fig. 4 for 2018 and 2019, as well as the average of all station anomalies.

Fig. 5 shows the annual, winter (December-March), and April-November mean air temperature anomalies averaged over all available stations shown in Fig. 4 since 1873. Record-high annual and winter temperatures occurred in 2010 and record-high April-November temperatures in 2012. Galbraith et al. (2012) found the average April-November air temperature over the Gulf from Environment Canada's National Climate Data and Information Archive (NCDIA) to be a good proxy for May-November sea-surface temperature over the Gulf (but excluding the estuary) and found within the former a warming trend of 0.9°C per century between 1873 and 2011; the same trend is found here over the selected ACCHD stations between 1873 and 2019 (Fig. 5). The NCDIA December-March air temperatures in the western Gulf were found to be highly correlated (R^2=0.67) with sea-ice properties, as well as with winter mixed layer volumes (Galbraith et al. 2010). Galbraith et al. (2013) found slightly higher correlations (R^2=0.72) with sea-ice using December-February ACCHD averages, possibly because March temperatures are of less importance during low sea-ice cover since much of the sea-ice cover decrease has occurred much earlier in February.

There were no monthly records set at any station around the Gulf in 2019. Averaged over all stations, air temperatures were mostly near normal in winter, below normal in spring, mixed in summer and near normal in fall. However November 2018 was the coldest since 1992 and this has likely led to early onset of sea-ice. Temperatures peaked at higher than normal in August (+1.2°C, +1.5 SD), but weren't as warm as a year earlier. Averaged over all stations, the December-March air temperature average (-0.5°C, -0.3 SD), the annual average (-0.3°C, -0.3 SD), and the April-November average (-0.4°C, -0.5 SD) were all near normal.

PRECIPITATION AND FRESHWATER RUNOFF

A freshwater runoff hindcast for the St. Lawrence River is updated using the model and methods described in Lefaivre et al. (2016). Observations of water levels at the Saint-Joseph-de-la-Rive station were used at the downstream boundary of the model. The runoff at the upstream boundary of the model was calculated using the stage-discharge relationships at the outlets of lake Deux-Montagnes and lake Saint-Louis. In addition, a correction was made so that the model minimizes the difference in water level observation at the Varennes station; this station is directly influenced by the exit from both lakes and allows the validation of the upstream flow of the St. Lawrence River. The runoff at Quebec City is extracted from the model at 3 minute intervals, filtered to remove the tidal signal and sub-sampled at noon local time (EST) every day (Fig. 6). To combine it with runoffs downstream to recreate the runoff that feeds the Estuary, the time series is then lagged by 21 days to approximate the time taken to reach the Estuary at the height of the Saguenay mouth, and new monthly means are computed (Fig. 7, lower curve).

A hydrological watershed model was used to estimate the monthly runoff since 1948 for all other major rivers flowing into the Gulf of St. Lawrence, with discharge locations as shown in Fig. 8. The precipitation data (NCEP reanalysis, six hourly intervals) used as input in the model were obtained from the NOAA-CIRES Climate Diagnostics Center (Boulder, Colorado, USA; Kalnay et al. 1996). The data were interpolated to a ¼° resolution grid and the water routed to river mouths using a simple algorithm described here. When air temperatures were below freezing,

the water was accumulated as snow in the watershed and later melted as a function of warming temperatures. Water regulation is modelled for three rivers that flow into the estuary (Saguenay, Manicouagan, Outardes) for which the annual runoff is redistributed following the climatology of the true regulated runoffs for 12 months thereafter. Runoffs were summed for each region shown and the climatology established for the 1981–2010 period. The waters that flow into the Estuary (region 1, Fig 7.) were added to the lagged St. Lawrence River runoff (above) to produce the RIVSUM II index (Fig. 7, upper curve). In 2019, the RIVSUM II spring freshet extended in time into June. The average runoff for May-June tied for first place of the time series with 1974 at 30,900 $m^3 s^{-1}$ (+3.1 SD).

Monthly anomalies of the summed runoffs for 2018 and 2019 are shown in Fig. 9. Rivers other than the St. Lawrence contribute about 5,000 $m^3 s^{-1}$ runoff to the Estuary, the equivalent of 40% of the St. Lawrence River, while the other tributaries distributed along the border of the GSL provide an additional 3,900 $m^3 s^{-1}$ in freshwater runoff to the system. River regulation has a strong impact on the relative contributions of sources. For example, in May 2015 the higher-than-average river runoff into the Estuary (an effect of the heavy precipitation in 2014 and river regulation) was almost as important as the below normal St. Lawrence run-off (Galbraith et al. 2017). The long-term time series are shown, summed by large basins, in Fig. 10. The methodology used in this year's report is different than in prior years and the details of the modeled time series have changed. Broad long-term patterns of runoff over the large basins were similar to that of the St. Lawrence River but interannual variability is low in the Northeast basin and Magdalen Shallows basin. The annual average runoff of the St. Lawrence River at Québec City and RIVSUM II both show a general downward trend from the mid-1970s until 2001, an upwards trend between 2001 and 2009 followed by another since 2012 (Fig. 10). In 2019, the annual runoff was above normal at 15,100 $m^3 s^{-1}$ (+2.3 SD) for the St. Lawrence River and 20,200 $m^3 s^{-1}$ (+2.0 SD) for the RIVSUM II index, at their highest level since 1976.

SURFACE LAYER

The surface layer conditions of the Gulf are monitored by various complementary methods. The first is the shipboard thermosalinograph network (Galbraith et al. 2002), which consists of temperature-salinity sensors (SBE-21; Sea-Bird Electronics Inc., Bellevue, WA) that have been installed on various ships starting with the commercial ship Cicero of Oceanex Inc. in 1999 (retired in 2006) and on the Cabot from 2006 to fall 2013. The Oceanex Connaigra, was outfitted with a thermosalinograph in early 2015.

The second data source is the Maurice Lamontagne Institute thermograph network (Pettigrew et al. 2016), which consists of a number of stations with moored instruments recording water temperature every 5 to 30 minutes (Fig. 11). Most instruments are installed on Coast Guard buoys that are deployed in the ice-free season, but a few stations are monitored year-round. The data are typically only available after the instruments are recovered except for oceanographic buoys that transmit data in real-time.

The third data source are a blend of daily composites of Advanced Very High Resolution Radiometer (AVHRR) satellite images from three products. The first is Pathfinder version 5.3 (Casey et al. 2010), a 4-km resolution product available for August 1981 to present, although only data up to 2014 were available when this blend was constructed. The two others were generated using data from the National Oceanic and Atmospheric Administration (NOAA) and European Organisation for the Exploitation of Meteorological Satellites (EUMETSAT). One is an archived 1.1-km resolution product available from the Maurice Lamontagne Institute (MLI) for the period of 1985-2013 (details in Galbraith and Larouche 2011, and Galbraith et al. 2012). The other product has 1.5-km resolution and is provided by the Bedford Institute of Oceanography

(BIO) Operational Remote Sensing group and spans 1997 to present. Since the SST product has changed since prior annual reports, the details of the time series presented here have also changed slightly.

The BIO and MLI products were inter-calibrated by comparing monthly climatological values for the period of 1998–2012 common to both products at all pixels in NAFO Divisions 3L to 4X-SS to avoid coastal errors and sea-ice masking issues. The BIO product was adjusted to the MLI product as $SST_{MLI} = 0.9730 \cdot SST_{BIO} - 0.097$ (-0.1°C adjustment at 0°C; -0.64°C at 20°C). This is in part explained by the fact that the MLI product used all available SST images while the BIO product uses only daytime passes, introducing a slight diurnal bias.

The climatological reference was chosen to be the MLI product spanning 1985–2010; it has the highest spatial resolution of the three products and spans a period close to the 1981–2010 climatological standard. Climatologies were then constructed for each day of the year. Daily anomalies were computed based on these for each MLI daily composite and for each BIO adjusted daily composite, while Pathfinder anomalies were calculated based on its own daily 1985–2010 climatologies. Weekly and Monthly mean anomaly composites were then computed as the average of all pixel-level anomalies in each period, and then weekly and monthly composites were created by adding these mean anomalies to the climatogical fields for the same week or month of the year.

SEA SURFACE TEMPERATURE

The May to November cycle of weekly averaged surface temperature over the Gulf of St. Lawrence is illustrated in Fig. 12. Galbraith et al. (2012) have shown that Gulf-averaged monthly air temperature and SST climatologies match up quite well with SST lagging air temperature by half a month. Maximum sea-surface temperatures are reached on average during the second week of August but that can vary by a few weeks from year to year. The maximum surface temperature averages to 15.6ºC over the Gulf during the second week of August (1985–2010), but there are spatial differences: temperatures on the Magdalen Shallows are the warmest in the Gulf, averaging 18.1ºC over that area, and the coolest are at the head of the St. Lawrence Estuary (7.0°C) and in upwelling areas along the lower north shore.

Fig. 13 shows a mean annual cycle of water temperature at a depth of 8 m along the Montréal to St. John's shipping route based on thermosalinograph data collected from 2000 to 2019. The data were averaged for each day of the year at intervals of 0.1 degree of longitude to create a climatological composite along the ship track. The most striking climatological feature is the area at the head of the Laurentian Trough (69.5°W), where strong vertical mixing leads to cold summer water temperatures (around 5°C to 6°C and sometimes lower) and winter temperatures that are always above freezing (see also Fig. 12). The climatological cycle shows the progression to winter conditions, first reaching near-freezing temperatures in the Estuary and then progressing eastward with time, usually reaching Cabot Strait by the end of the winter (but no further).

Thermosalinograph data show that near-freezing surface layer conditions first appeared earlier than normal, in early December 2018, and lasted longer than normal into April 2019 (Fig. 13). The exception was the Estuary where waters were warmer than normal starting in early March. Temperatures throughout the year were mostly below normal to normal in the estuary and Gulf, except some above normal anomalies from late June to August, and from mid-October to mid-November. Anomalies in the Gulf changed from above normal when it went offline on August 19th to as much as 7°C below normal when the system came back online and crossed the Gulf immediately after the passage of tropical storm Dorian.

Monthly mean sea-surface temperatures from AVHRR imagery are presented as maps (Fig. 14), temperature anomaly maps (Fig. 15), spatial averages expressed as anomalies (Fig. 16) or as mean temperatures (Fig. 17). Since the products are new for this year, we also include the time series since 1982 (Fig. 18 and Fig. 19). In the Estuary, the seasonal maximum was reached 5 weeks early in late June when the weekly average temperature reached 12.1°C, an anomaly of +2.8°C for that week and still warmer than the climatological high expected in late July of 11.4°C.

There were series record lows (since 1981) in September in 5 regions (anomaly records ranging from -1.6°C to -3.4°C) as well as averaged over the Gulf (-2.1°C, -2.7 SD), caused by the passage of tropical storm Dorian over the Gulf on September 7-8. The Viking buoy AZMP-ESG (East Southern Gulf) recorded a 60 mBar drop of atmospheric pressure to 960 mBar, 13 m waves, winds of 120 km/h and a remarkable drop in surface water temperature of 8°C. However, the ocean didn't lose any heat; temperature-salinity profiles from the Viking buoy done before the storm on August 23 and after the storm on September 10 show evidence of mixing down to a depth of 45 m and nearly identical 0-45 m depth-averaged temperature. The heat was mixed down, creating cold anomalies at the surface compensated by warm anomalies at depth. Surface temperatures then remained nearly constant for some time, warming even in some areas, until fall cooling of air temperature caught up and cooling of the mixed layer continued. Averaged over the gulf, the May to November 2019 average was just below normal (-0.3°C, -0.5 SD) but the warmest month of the year, August, was above normal (+0.9°C, +1.1 SD).

Sea-surface temperature monthly climatologies and time series were also extracted for more specific regions of the Gulf. The Magdalen Shallows, excluding Northumberland Strait, is divided into western and eastern areas as shown in Fig. 20. The monthly average SST for the Magdalen Shallows as a whole (region 8) is repeated in Fig. 21 along with averages for the western and eastern areas. Climatologies differ by roughly 0.5°C to 1°C between the western and eastern regions. Temperatures were at a series record low in September on both the Eastern Shelf and the Western Shelf because of mixing caused by the tropical storm.

Seasonal trends in relation to air temperature are examined by first displaying weekly averaged AVHRR SST in the GSL for all years between 1982 and 2019 (Fig. 22) with years on the x-axis and weeks of the year on the y-axis (See Galbraith and Larouche 2013 for a full description). Isotherms show the first and last occurrences of temperature averages of 12°C over the years, chosen to be representative of spring (and fall) transitions to (and from) typical summer temperatures. Although the selected temperature is arbitrary, the results that follow are not particularly sensitive to the exact temperature chosen because the surface mixed layer tends to warm and cool linearly in spring and fall (e.g. Fig. 12). A 10°C threshold is also used to demonstrate this. The Gulf had experienced earlier summer onset between 1985 and 2017 of -0.5 weeks per decade, but later-than-normal warming in 2018 by 1 week had rendered this trend no longer statistically significant, and this remains the case with the addition of later-still warming of 2019 (+1.5 SD, +1.3 weeks) in spite of the addition of the cool 1982-1984 period to the analysis with this new SST dataset. The progressively later fall cooling trend that was still reported last year has also disappeared with the addition of the second-earliest fall cooling of the time series for 2019 (-2.0 SD, +2.0 weeks), caused by tropical storm Dorian. In spite of the disappeared trends, the interannual variability in the time of year when the 12°C threshold is crossed remains correlated with June-July average air temperature for the summer onset (0.9 week sooner per 1°C increase; R^2=0.61) and with September average air temperature for the fall (0.7 week later per 1°C increase; R^2=0.52). These air temperature averages, shown in Fig. 22, can be used as proxies prior to 1982 and for climate change predictions. The implication is that the duration of the Gulf of Lawrence warm season has increased and will increase by about

2 weeks for each 1°C of seasonal warming (e.g. associated with anthropogenic climate change).

Thermograph network observations are compared to daily average temperatures (or salinities) calculated using all available years of data for each day of the year at each station and depth (Fig. 23 to Fig. 26). The seasonal cycle of near-surface temperature is measured by shallow instruments, while Cold Intermediate Layer warming from spring to fall is captured by instruments moored between 30 and 120 m depth. Monthly averages are also shown, with the magnitude of their anomaly colour-coded. Monthly shallow-water anomalies were fairly consistent across all stations of each of the regions. As with AVHRR data sources and in spite of different climatological periods, summer months shows mostly below normal to normal shallow temperatures except for above normal temperatures in August in the Gulf. Stations in the estuary also showed temperatures peaking to seasonal maximal values early. Many stations recorded a sudden drop in near-surface temperature associated with the tropical storm Dorian (Mont-Louis, Sept-Îles, Port Menier, Rivière-au-Tonnerre, Natasquan, La Romaine, Shediac Valley, East Southern Gulf, Île Shag, Old Harry).

The new station Saguenay Sill 1 is located just inside of the first sill connecting the Saguenay Fjord to the St. Lawrence Estuary. Fig. 23 and Fig. 26 show temperature and salinity data collected there since 2015. The salinity of the water (hence its density) determines the type of circulation that renews basin waters. These time series extend those first presented in Belzile et al. (2016) and Galbraith et al. (2018).

The Île Shag (10 m) station shows bottom temperatures close to Îles-de-la-Madeleine that are important to the lobster fishery. April and May temperatures were near normal and below normal, respectively, at this station (Fig. 25). The Île Shag panel shows with a red line spanning historical dates when spring temperature last increased over 1.5°C, a temperature associated with increased lobster mobility, as well as the mean date (April 27th) plus and minus 0.5 SD (4 days). In 2019, this crossing occurred on May 6th, the same day that the lobster fishery began. It must therefore have been in cold waters (<1.5°C) since it can take up to two weeks for waters to warm at 30 m starting from the time recorded at 10 m.

SEA ICE

Ice cover area, duration and volume are estimated from ice cover products obtained from the Canadian Ice Service (CIS), further processed into regular grid that are used in analyses. These are weekly Geographic Information System (GIS) charts covering the period 1969-2019 and daily charts covering the period 2009-2019. All charts were gridded on a 0.01° latitude by 0.015° longitude grid (approximately 1 km resolution). Thickness (and therefore volume) are estimated from stages of ice growth from new ice (5 cm), nilas (5 cm), grey ice (12.5 cm), grey-white ice (22.5 cm), thin first year ice (50 cm), medium first year ice (95 cm) and thick first year ice (160 cm). Prior to 1983, the CIS reported ice categories into fewer classifications using a single category of first year ice (≥ 30 cm) with a suggested average thickness of 65 cm. While we used this thickness in prior annual reports, we have now found this value to lead to underestimates of the seasonal maximum thickness and volume based on high inter-annual correlations obtained between the estimated volume and area of the weekly seasonal maximums. The comparison pre- and post-1983 provided an estimate of 85 cm in the Gulf of St. Lawrence and of 95 cm on the Newfoundland and Labrador Shelf. To avoid a spatial discontinuity and preferring slightly underestimating ice volume in the northeast Gulf rather than over-estimating it everywhere else, we choose to set it at 85 cm.

Several products were computed to describe the sea-ice cover interannual variability: day of first and last occurrence and duration maps (Fig. 27) and their regional averages (Fig. 28);

distribution of ice thickness during the week of maximum volume (Fig. 29, upper panels) and maximum thickness reached at any week during the season (Fig. 29, lower panels); daily evolution of the estimated sea-ice volume in relation to the climatology and historical extremes (Fig. 30); estimated seasonal maximum ice volumes within the Gulf as well as on the Scotian Shelf (Fig. 31); time series of seasonal maximum ice volume, area (excluding thin new ice) and ice season duration in relation with December-to-March air temperature anomaly (Fig. 32).

There has been a declining trend in ice cover severity since 1990 with rebounds in 2003 and 2014 (Fig. 32). The correlation between annual maximum ice volume (including the cover present on the Scotian Shelf) and the December-February air temperature averaged over five Western Gulf stations (Sept-Îles, Mont-Joli, Gaspé, Charlottetown and Îles-de-la-Madeleine) accounted for 72% of the variance using the 1969–2012 time series (Galbraith et al. 2013). Fig. 32 shows a similar comparison using ice volume and the ACCHD December-to-March air temperature anomaly from Fig. 5 also yielding $R^2 = 0.72$. The correlations between air temperature and the ice parameters season duration and area are also very high ($R^2 = 0.78$-0.80). Correlation coefficients are slightly higher when using January to February air temperatures, perhaps because March air temperatures have no effect on ice cover that has almost disappeared by then during very mild winters. Sensitivity of the ice cover to air temperature increase (e.g. through climate change) can be estimated using 1969-2019 co-variations between winter air temperature and sea-ice parameters, which indicate losses of 18 km^3, 31,000 km^2 and 13 days of sea-ice season for each 1°C increase in winter air temperature.

Ice typically forms first in December in the St. Lawrence estuary and in shallow waters along New Brunswick, Prince Edward Island and the lower north shore and melts last in the northeast Gulf where the ice season duration tends to be longest apart from shallow bays elsewhere (Fig. 27). Offshore sea ice is typically produced in the northern parts of the Gulf and drifts towards Îles-de-la-Madeleine and Cabot Strait during the ice season.

In 2019, the sea-ice cover formed much earlier than normal in the Estuary, the Western portion of the Gulf and along the coast of the lower north shore, but later than normal in offshore regions of the Gulf (Fig. 27, Fig. 28). It was the earliest first occurrence of ice on record in the Upper Estuary; the first time it occurred in November. Ice volume progressed normally until early-January, then progressed about 1 SD below normal until mid-February when progression quickened until the maximum was reached at a normal period in mid-March (Fig. 30). The near normal seasonal maximum ice volume of 77 km^3 (+0.3 SD) occurred the week of March 11th (Fig. 29). The duration of 54 days (calculated differently this year using an area-weighted method) was overall near normal (-0.3 SD), and the area was above normal (+0.7 SD) (Fig. 32). These sea-ice conditions were consistent with the coldest November air temperatures since 1992, followed by near normal winter air temperatures (-0.5°C, -0.3 SD). In the 10 year span since 2010, 7 of the 10 lowest maximum ice volumes of the time series have occurred (Fig. 32), although this does not include 2019. A near normal volume of ice was exported from the Gulf of St. Lawrence onto the Scotian Shelf in 2019 (Fig. 29, Fig. 31), the largest volume since 2015.

WINTER WATER MASSES

A wintertime survey of the Gulf of St. Lawrence waters (typically 0–200 m) has been undertaken in early March since 1996, typically using a Canadian Coast Guard helicopter but from Canadian Coast Guard ships in 2016 and 2017. The survey, sampling methods, and results of the cold-water volume analysis in the Gulf and the estimate of the water volume advected into the Gulf via the Strait of Belle Isle over the winter are described in Galbraith (2006) and in Galbraith et al. (2006). Fig. 33 and Fig. 34 show gridded interpolations of near-surface temperature, temperature difference above freezing, salinity, cold layer thickness and bottom

contacts, and thickness of the Labrador Shelf water intrusion for 2019 as well as climatological means.

The March surface mixed layer is usually very close (within 0.1°C) to the freezing point in most regions of the Gulf but thickness of the surface layer varies, leaving variability in the cold-water volume between mild and severe winters rather than in temperature. One exception was 2010 when, for the first time since the inception of the winter survey, the mixed layer was on average 1°C above freezing. During typical winters, surface waters in the temperature range of ~ 0°C to -1°C are only found from the northeast side of Cabot Strait spreading into the Gulf. Some of these warm waters presumably enter the Gulf during winter and flow northward along the west coast of Newfoundland, however it is also possible that local waters could have simply not cooled close to freezing. Conditions in March 2019 were near-freezing throughout the Gulf (Fig. 33), consistent with the sea-ice cover present across all of Cabot Strait and spilling out onto the Scotian Shelf (Fig. 29).

Near-freezing waters with salinities of around 32 are responsible for the (local) formation of the CIL since that is roughly the salinity at the temperature minimum during summer. These are coded in green-blue in the salinity panel of Fig. 33 and are typically found to the north and east of Anticosti Island. Surface salinities were higher than the climatology in this part of the Gulf during the winter of 2019.

Near-freezing waters with salinity >32.35 (colour-coded in violet) are considered to be too saline to have been formed from waters originating within the Gulf (Galbraith 2006) and are presumed to have been advected from the Labrador Shelf through the Strait of Belle Isle. These waters were present throughout the surface of Mécatina Trough in March 2019 (Fig. 33). A T-S water mass criterion from Galbraith (2006) was used to identify intruding Labrador Shelf waters that have exhibited no evidence of mixing with warm and saline deep Gulf water. These waters occupied all the water column in Mécatina Trough in March 2019 (top-right panel of Fig. 34). The recent history of Labrador Shelf water intrusions is shown in Fig. 35, where its volume is shown as well as the fraction it represents of all the cold-water volume in the Gulf. This volume was second highest of the 1997-2019 time series in March 2019 at 3700 km³ (+2.1 SD), and represented 24% (+1.2 SD) of the cold water (T< -1°C) in the Gulf. It extended further into the Gulf, reaching Anticosti Channel.

The cold mixed layer depth typically reaches about 75 m in the Gulf and is usually delimited by the -1°C isotherm because the mixed layer is typically near-freezing and deeper waters are much warmer (Galbraith 2006). In March 2010 and 2011 much of the mixed layer was warmer than -1°C such that the criterion of T<0°C was also introduced (see middle panels of Fig. 34). The cold surface layer is the product of local formation as well as cold waters advected from the Labrador Shelf, and can consist either of a single water mass or of layers of increasing salinity with depth. This layer reaches the bottom in many regions of the Gulf, with interannual variability in whether the deepest parts of the Magdalen Shallows or of Mécatina Trough are reached (see bottom panels of Fig. 34). The thickness of the winter layer is usually greatest north and northeast of Anticosti Island, and the doming of the Anticosti Gyre isopycnals appears in the climatology as a thinner center part. In 2019, the typical thickness gradient towards the northeast was present, but the T< -1°C layer was also thicker than the climatology in central Gulf and Cabot Strait.

Integrating the cold layer depth over the area of the Gulf (excluding the Estuary and the Strait of Belle Isle) yields a cold-water (< -1°C) volume of 15,200 km³ in 2019, the highest of the time series and +1.2 SD above the 1996–2019 average. This record was aided by the large inflow of Labrador Shelf water into the Gulf; subtracting out the above-normal volume of Labrador Shelf water from the total volume would bring it down to near-normal (+0.3 SD) but of course the

inflow through the Strait of Belle Isle has also forced some presumably cold water onto the Scotian Shelf that otherwise would have remained in the Gulf.

The interannual variability of winter volumes of water colder than 0 and 1°C are shown in Fig. 36. The mixed layer volume only increases to 16,000 km³ when water temperatures <0°C are considered which is also 1.2 SD above the 1996–2019 average. This last volume of cold water corresponds to 48% of the total water volume of the Gulf (33,500 km³, excluding the Estuary).

COLD INTERMEDIATE LAYER

FORECAST FROM THE MARCH 2018 SURVEY

The summer CIL minimum temperature index (Gilbert and Pettigrew 1997) has been found to be highly correlated with the Gulf (excluding the estuary) volume of cold water (<-1°C) measured the previous March when much of the mixed layer is near-freezing (Galbraith 2006; updated relation in right panel of Fig. 32). This is expected because the CIL is the remnant of the winter cold surface layer. A measurement of the volume of cold water present in March is therefore a valuable tool for forecasting the coming summer CIL conditions. The winter mixed layer in 2019 was near-freezing throughout most the Gulf. The volume of the layer with T < -1°C was highest of the time series at +1.2 SD. The Cold Intermediate Layer for summer 2019 was therefore forecasted to be colder than in 2018, with a Gilbert and Pettigrew (1997) index of around -0.64°C compared to -0.05°C in 2018 (Galbraith et al. 2019).

AUGUST–SEPTEMBER CIL

The CIL minimum temperature, thickness and volume for T<0°C and <1°C were estimated using temperature profiles from all sources for August and September. Most data are from the multi-species surveys in September for the Magdalen Shallows and August for the rest of the Gulf. Using all available temperature profiles, spatial temperature interpolations of the Gulf were done for each 1-m depth increment, with the interpolated field bound between the minimum and maximum values observed within each of the different regions of the Gulf (Fig. 2) to avoid spurious extrapolations. The CIL thickness at each grid point is simply the sum of depth bins below the threshold temperature, and the CIL minimum temperature is only defined at grid points where temperature rises by at least 0.5°C at depths greater than that of the minimum, or if the grid point minimum temperature is below the CIL spatial average of the Gulf.

Fig. 37 shows the gridded interpolation of the CIL thickness <1°C and <0°C and the CIL minimum temperature for August–September 2019 as well their 1981–2010 climatology (1994–2010 for Mécatina Trough). Similar maps were produced for all years back to 1971 (although some years have no data in some regions), allowing the calculation of volumes for each region for each year as well as the climatologies shown on the left side of Fig. 37. The climatological period used here begins in 1985 instead of 1981 because there are too few data prior to 1985, when oceanographic data began to be sampled during multi-species surveys. The CIL thickness for T<0°C and T<1°C increased compared to 2018, with Gulf volumes reaching near normal values. The 2019 CIL temperature minimum distribution was on average similar to the climatology, but was colder in the northeast Gulf, perhaps an after effect of the larger-than-normal winter intrusion of Labrador Shelf Water.

The time series of the regional August–September CIL volumes are shown in Fig. 38 (for <0°C and <1°C). Esquiman Channel and central Gulf showed strong increases in CIL volumes in 2019 compared to 2018, while the Estuary volumes decreased. Fig. 39 shows the Gulf total volume of CIL water (<0°C and <1°C) and the average CIL minimum core temperature from the August–September interpolated grids (e.g., Fig. 37). The CIL areal minimum temperature

average and volume shown in Fig. 39 exclude data from Mécatina Trough which has very different water masses from the rest of the Gulf; it is influenced by inflow through the Strait of Belle Isle and is therefore not indicative of the climate in the rest of the Gulf. The CIL volumes as defined by T<0°C and <1°C increased significantly (to -0.1 and -0.2 SD) compared to 2018 conditions (-1.6 and -1.7 SD).

The time series of the CIL regional average minimum core temperatures are shown in Fig. 40. All regions except for the Estuary and northwest Gulf showed a strong decrease in minimum core temperature compared to 2018, reaching below normal in Esquiman Channel. The 2019 average temperature minimum (excluding Mecatina Trough, the Strait of Belle Isle and the Magdalen Shallows) was normal at -0.2°C, a decrease of 0.5°C from 2018, and is shown in Fig. 39 (bottom panel, green line). The average difference between this CIL index and the Gilbert and Pettigrew (1997) index (described below) is 0.27°C because of the warming between mid-June and the August survey. This index corresponds to a Gilbert and Pettigrew (1997) index of -0.5°C after rounding to the nearest decimal.

NOVEMBER CIL CONDITIONS IN THE ST. LAWRENCE ESTUARY

Since 2006, the AZMP November survey usually provides a good number of conductivity-temperature-depth (CTD) casts in the St. Lawrence, allowing a good estimation of CIL properties in the Estuary. The data show the temporal warming (Fig. 40) and thinning (Fig. 38) of the CIL since the August survey. Fig. 40 shows that the fairly rapid increase of the CIL minimum temperature occurring between August and November is fairly constant inter-annually in spite of the differences in August temperature. Results indicate a thinner CIL in the fall of 2019 than a year earlier, but with similar minimum core temperatures.

SEASONAL MEAN CIL INDEX

The Gilbert and Pettigrew (1997) CIL index is defined as the mean of the CIL core temperatures observed between 1 May and 30 September of each year, adjusted to 15 July with a region-dependant warming rate. It was updated using all available temperature profiles measured within the Gulf between May and September inclusively since 1947 (black line of the bottom panel of Fig. 39). As expected, the CIL minimum core temperature interpolated to 15 July is almost always colder than the estimate based on August and September data for which no temporal corrections were made. This is because the CIL is eroded over the summer and therefore its minimum core warms over time.

This CIL index for summer 2019 was -0.45°C, near normal at -0.1 SD. The 0.4°C decrease from the summer 2018 CIL index is consistent with the increase in CIL volume between August 2018 and 2019 discussed above and the decrease of 0.5°C in the areal average of the minimum temperature in August. The warm winter conditions from 2010 to 2012 led to CIL indices that were still far below the record highs observed in the 1960s and 1980s. The earlier CIL temperature minimums will need to be re-examined to confirm that they were calculated using data with sufficient vertical resolution to correctly resolve the core minimum temperature.

SUMMARY OF CIL CONDITIONS

As a summary, Fig. 41 shows selected time series of winter and summertime CIL conditions (June and September bottom temperatures also related to the CIL are outlined below) and highlights the strong correlations between these various time series. Conditions related to the CIL were typically near normal in 2019 except for warmer than normal bottom temperatures on the Magdalen Shallows (leading to below normal areas in Fig. 41), somewhat surprisingly following the record high winter cold layer volume.

MAGDALEN SHALLOWS JUNE SURVEY

A long-standing assessment survey covering the Magdalen Shallows has taken place in June for mackerel assessments and was since merged with the June AZMP survey. This survey provides good coverage of the temperature conditions that are greatly influenced by the cold intermediate layer that reaches the bottom at roughly half of the surface area at this time of the year.

Near-surface waters warm quickly in June, mid-way between the winter minimum and the annual maximum in early August. This can introduce a bias if the survey dates are not the same each year. To account for this, the seasonal warming observed at the Shediac Valley AZMP monitoring station was evaluated. A linear regression was performed of temperature versus time for each meter of the water column for each year with monitoring data at Shediac Valley between May and July. Visual inspection showed that the depth-dependent warming rate was fairly constant for all years and an average was computed for every depth. Warming is maximal at the surface at 18°C per 100 days and, in spite of some uncertainties between 30 and 55 m, decreases almost proportionally with depth to reach 2°C per 100 days at 40 m, followed by a further linear decrease to reach 1°C per 100 days at 82 m (Galbraith and Grégoire 2015).

All available temperature profiles taken in June from a given year are binned at 1 m depth intervals (or interpolated if the resolution is too coarse) and then adjusted according to the sampling date to offset them to June 15th according to the depth-dependent warming rate extracted from Shediac Valley monitoring data. An interpolation scheme is used to estimate temperature at each 1 m depth layer on a 2 km resolution grid. Fig. 42 shows temperatures and anomalies at depths of 20, 30, 40 and 50 m. Fig. 43 shows averages over the grids at 10, 20, 30, 50 and 75 m for all years when interpolation was possible, as well as SST June averages since 1982, for both western and eastern regions of the Magdalen Shallows (Fig. 20). Temperatures were on average below normal to normal, except at 40 m and deeper on the Western Shelf where they were above normal (Fig. 42 and Fig. 43).

BOTTOM WATER TEMPERATURES ON THE MAGDALEN SHALLOWS

Bottom temperature is also estimated at each point of the grids constructed from the June survey by looking up the interpolated temperature at the depth level corresponding to a bathymetry grid provided by the Canadian Hydrographic Service with some corrections applied (Dutil et al. 2012). The method is fully described in Tamdrari et al. (2012). A climatology was constructed by averaging all available temperature grids between 1981 and 2010, and anomaly grids were then computed for each year based on that climatology. The June bottom temperature climatology as well as the 2019 reconstructed temperature and anomaly fields are shown in Fig. 44. The same method was applied using the available CTD data from August and September, mostly from the multispecies surveys for the northern Gulf in August and for the Magdalen Shallows in September. These results are also shown in Fig. 44. While much of the deeper bottom water temperatures are climatologically still below 0°C in June, a remnant from the winter near-freezing mixed layer that reached the bottom, most of the area usually warms to below 1°C by August-September. Temperature anomalies in coastal shallow waters range from <-2.5°C to >+2.5°C, but anomalies tend to be of smaller magnitude in deeper waters.

Time series of the bottom area covered by water in various temperature intervals were estimated from the gridded data for the June surveys as well as for the September multispecies survey on the Magdalen Shallows (Fig. 45). The time series of areas of the Magdalen Shallows covered by water colder than 0, 1, 2, and 3°C in June and September are also shown in Fig. 41 as part of the CIL summary. In June 2019, none of the bottom of the Magdalen Shallows was covered by water with temperatures <-1°C, in contrast to somewhat colder conditions in June

2017, two years prior. By September, none of the bottom was covered by water with temperatures <0°C. These are warmer than normal conditions (Fig. 38) that are nevertheless colder than during the recent 2010-2012 period. The area covered by water temperatures <0°C in June and <1°C in September had then reached a low (warm conditions) not seen since the early 1980s, but rebounded to near normal in 2014 and 2015, and again in 2017. The areas were overall smaller than normal (warmer waters) in June 2019 (-0.9 SD) and in September (-1.2 SD). At higher threshold temperatures, areas with T< 2°C and < 3°C were below normal (warmer) in both June and September 2019.

DEEP WATERS (>150 M)

The deeper water layer (>150 m) below the CIL originates at the entrance of the Laurentian Channel at the continental shelf break and circulates towards the heads of Laurentian, Anticosti, and Esquiman channels without much exchange with the upper layers. The layer from 150 to 540 m is characterized by temperatures between 1 and >7°C and salinities between 32.5 and 35 (except for Mécatina Trough where near-freezing waters may fill the basin to 235 m in winter and usually persist throughout the summer). Decadal changes in temperature, salinity, and dissolved oxygen of the deep waters entering the Gulf at the continental shelf are related to the varying proportion of the source cold–fresh and oxygen-rich Labrador Current water and warm–salty and oxygen-poor slope water (McLellan 1957, Lauzier and Trites 1958, Gilbert et al. 2005). The deeper waters travel from the mouth of the Laurentian Channel to the Estuary in roughly three to four years (Gilbert 2004), decreasing in dissolved oxygen from in situ respiration and oxidation of organic material as they progress to the channel heads. The lowest levels of dissolved oxygen (below 20 percent saturation in recent years) are therefore found in the deep waters at the head of the Laurentian Channel in the Estuary.

BOTTOM WATER TEMPERATURES IN AUGUST AND SEPTEMBER

The same method used to calculate bottom water temperature on the Magdalen Shallows was applied to the entire Gulf by combining all available CTD data from August and September, mostly from the multispecies surveys for the northern Gulf in August and for the Magdalen Shallows in September, into a single map (Fig. 46). All of the Gulf deep bottom water temperatures were above normal, with large areas of Central Gulf, Anticosti and Esquiman Channels, and northwest Gulf above 6°C, with this isotherm appearing in the Estuary in 2019.

As done for the Magdalen Shallows (Fig. 45), time series of the bottom area covered by water in various temperature intervals were also estimated for the other regions of the Gulf based on August-September temperature profile data (Fig. 47 and Fig. 48). The figures show compression of the bottom habitat area in the temperature range of 5–6°C in 1992, offset by the larger colder 4–5°C habitat. In 2012, a return of >6°C temperatures to the sea floor began. By 2015, it had caused a large decrease of the 5–6°C habitat in Anticosti and Esquiman Channels, this time replaced by a warmer 6–7°C habitat. The 6–7°C area then increased sharply in Central and northwest Gulf in 2017, and increased sharply again in northwest Gulf in 2018 and again in 2019. The 6–7°C habitat was in 2019 at a record high in the northwest Gulf, Anticosti Channel, Esquiman Channel and Central Gulf. Anticosti Channel and Esquiman Channel also saw a strong return of bottom waters colder than 0°C in August 2019 associated with the Cold Intermediate Layer.

DEEP TEMPERATURE MAXIMUM

The warm waters found at the bottom of the Laurentian Channel and elsewhere are associated with the deep temperature maximum evident in the temperature profiles in these areas (e.g. Fig.

3). The recent inter-annual progression to current conditions of the deep temperature maximum is shown on Fig. 49. Temperatures above 7°C have been recorded since 2012 in the Gulf near Cabot Strait. The Gulf-wide average and regional areal averages of the deep temperature maximum are shown in Fig. 50. The Gulf-wide average was at a series record high in 2019, at 6.60°C.

TEMPERATURE AND SALINITY ANNUAL MEANS

Monthly temperature and salinity averages were constructed for various depths using a method used by Petrie et al. (1996) but for the geographical regions shown in Fig. 2. In this method, all available data obtained during the same month within a region and close to each depth bin are first averaged together for each year. Monthly averages from all available years from 1981 to 2010 and their standard deviations are then computed for climatologies. This two-fold averaging process reduces the bias that occurs when the numbers of profiles in any given year are different. These monthly averages were further averaged into regional yearly time series that are presented in Fig. 50 (temperature) and Fig. 51 (salinity) for 200 and 300 m. The 300 m observations suggest that temperature anomalies are advected up-channel from Cabot Strait to the northwestern Gulf in two to three years, consistent with the findings of Gilbert (2004), while variability at 200 m often appears or disappears everywhere at the same time, suggesting vertical changes. The regional averages are weighted into a Gulf-wide average in accordance to the surface area of each region at the specified depth. These Gulf-wide averages are shown for 150, 200 and 300 m in Fig. 50, Fig. 51 and Fig. 52. Linear trends in temperature and salinity at 300 m of 2.3°C and 0.3 per century, respectively are shown on Fig. 52 (See also Galbraith et al. 2013 for other long term trends), although the temperature increase has been of 1.3°C per decade since 2009 (5.6 times more rapidly).

In 2019, the gulf-wide average salinities continued to bounce back at all depths after decreases in 2017 (Fig. 51 and Fig. 52), reaching a series record at 300 m of 34.75. Gulf-wide average temperatures at 150 and 200 m are lower than the 2015 record highs but remain above normal at 3.3°C (+1.6 SD) and 5.5°C (+2.4 SD). New series record highs (since 1915) were set at 250 and 300 m, at 6.3°C (+3.8 SD) and 6.5°C (+6.6 SD) respectively. At 300 m, temperature increased to regional record highs in all deep regions of the Gulf: Estuary (5.9°C, +4.1 SD), Northwest Gulf (6.2°C, +5.6 SD), Central Gulf (6.6°C, +5.7 SD) and Cabot Strait (7.1°C, +5.8 SD).

The warm anomalies present since 2010 at Cabot Strait have been progressing up the channel towards the Estuary since then, but waters that have followed into the gulf have also remained very warm and even increased in temperature such that the average overall temperature may continue to increase (Fig. 49). The potential for still warmer waters entering the Gulf exists, as evidenced by average temperatures observed at the Laurentian Mouth in 2019 of 10.2°C at 200 m and of 8.4°C at 300 m (Fig. 50), both record highs since the series began in 1914.

SEASONAL AND REGIONAL AVERAGE TEMPERATURE STRUCTURE

In order to show the seasonal progression of the vertical temperature structure, regional averages are shown in Fig. 53 to Fig. 56 based on the profiles collected during the March helicopter survey, the June AZMP and mackerel surveys, the August multi-species survey (September survey for the Magdalen Shallows), and the October-November AZMP survey. All additional archived CTD data for those months were also used. The temperature scale was adjusted to highlight the CIL and deep-water features; the display of surface temperature variability is best suited to other tools such as remote sensing and thermographs. Average discrete depth layer conditions are summarized for the months of the 2018 and 2019 AZMP

surveys in Fig. 57 for temperature and in Fig. 58 for salinity and 0-50 m stratification. For each survey the anomalies were computed relative to monthly temperature and salinity 1981–2010 climatologies calculated for each region, shown in grey as the mean value ± 0.5 SD in Fig. 53 to Fig. 56.

Caution is needed in interpreting the March profiles. Indeed, regional averaging of winter profiles does not work very well in the northeast Gulf (regions 3 and 4) because very different water masses are present in the area such as the cold Labrador Shelf intrusion with saltier and warmer deeper waters of Anticosti Channel or Esquiman Channel. For example, the sudden temperature changes near the bottom of Mécatina Trough in 2018 resulted from the deepest cast used that contained colder deep waters. The highlights of March water temperatures shown in Fig. 53 include the previously discussed record-setting winter mixed layer depth. Waters in the deepest parts of Mécatina Trough were near-freezing, with the Labrador Shelf intrusion occupying all of the area.

Temperatures in June and August 2019 were characterized by very thick and cold CIL conditions in Anticosti Channel, Esquiman Channel and central Gulf, but this had subsided somewhat by the fall. Deep-water temperatures were above normal in all regions along the Laurentian Channel, with most regions showing increases compared with 2018 conditions at the depth of the temperature maximum (200 to >250 m), most notably in Cabot Strait.

CURRENTS AND TRANSPORTS

Currents and transports are derived from a numerical model of the Gulf of St. Lawrence, Scotian Shelf, and Gulf of Maine. The model is prognostic, i.e., it allows for evolving temperature and salinity fields. It has a spatial resolution of 1/12° with 46 depth-levels in the vertical. The atmospheric forcing is taken from the Global Environmental Multiscale (GEM) model running at the Canadian Meteorological Center (CMC). Freshwater runoff is obtained from observed data and the hydrological model, as discussed in the freshwater runoff section, but does not use the new daily calculation of runoff at Québec City. The spring freshet may therefore differ from what was described in an earlier section of this document. A simulation was run for 2006–2019 from which transports were calculated. The reader is reminded that the results outlined below are not measurements but simulations and improvements in the model may lead to changes in the transport values.

Fig. 59 to Fig. 61 show seasonal depth-averaged currents for 0–20 m, 20–100 m, and 100 m to the bottom for 2019. Currents are strongest in the surface mixed layer, generally 0–20 m, except in winter months when the 20–100 m averages are almost as high, and the 100 m to bottom averages are still much higher than during other seasons (note the different scale for this depth). Currents are also strongest along the slopes of the deep channels. The Anticosti Gyre is usually evident but strongest during winter months, when it even extends strongly into the bottom-average currents, but in 2019 the Gyre circulation didn’t close up very strongly, instead feeding transport into the Gaspé Current (Fig. 59). The Gaspé Current was shifted along the north shore of the estuary in winter but was stable along the south shore for the rest of the year, combining with the Anticosti Gyre and then along the Laurentian Channel slope except for a branch that ran across the entire Magdalen Shallows.

Monthly averaged transports across seven sections of the Gulf of St. Lawrence are shown in Fig. 62 for sections with estuarine circulation, and in Fig. 63 for sections where only net transports are relevant. In Fig. 62, the net transport integrates both up and downstream circulation and, for example, corresponds to freshwater runoff at the Pointe-des-Monts section. The outflow transport integrates all currents heading toward the ocean, while the estuarine ratio corresponds to the outflow divided by the net transports. Note that the only section where

estuarine circulation is dominant is at Pointe-des-Monts. The net transport at Honguedo is on average 15 times higher, consisting mostly of circulation around Anticosti Island first observed at the Jacques-Cartier section. Similarly, the net transport at Cabot Strait is mostly balanced by inflow from Belle Isle Strait such that an estuarine ratio is perhaps a misleading description. Transports through sections under the direct estuarine influence of the St. Lawrence River (e.g., Pointe-des-Monts) have a more direct response to change in freshwater runoff while others (e.g., Cabot Strait, Bradelle Bank) have a different response, presumably due to redistribution of circulation in the GSL under varying runoff. The estuarine circulation ratio is determined by the mixing intensities within the estuary and is greatly influenced by stratification. It is on average greatest during winter months and weakest during the spring freshet. In fact, it is sufficiently reduced in spring that the climatological outward transport at Pointe-des-Monts reaches its minimum value in June even though this month corresponds to the third highest net transport of the year, i.e. the estuary becomes sufficiently stratified that fresh water runoff tends to slip on top of the denser salty waters underneath. This occurred in 2017 when the exceptionally high April freshet led to decreased modeled estuarine circulation and decreased outward transport by entrainment at the Pointe-des-Monts section. In 2019, the above average run-off in April 2019 coincided with increased outward transport and estuarine ratio, while a similarly above average run-off in May led to a decreased estuarine ratio.

HIGH FREQUENCY SAMPLING AZMP STATIONS

Sampling by the Maurice Lamontagne Institute began in 1991 at a station offshore of Rimouski (48° 40' N 68° 35' W, 320 m depth; Plourde et al. 2009), typically once a week during summer and less often during spring and fall and almost never in winter (Fig. 64). In 2013, following several analyses that identified good correlations and correspondences between the prior AZMP Anticosti Gyre and Gaspé Current stations with the Rimouski station, it was decided to drop sampling efforts at these logistically difficult stations and integrate the Rimouski station officially in the AZMP program and begin winter sampling there when opportunities arose. The AZMP station in the Shediac Valley (47° 46.8' N, 64° 01.8' W, 84 m depth) is sampled by the Bedford Institute of Oceanography, by DFO Gulf Region and by the Maurice Lamontagne Institute (Fig. 64). This station has been sampled irregularly since 1947, nearly every year since 1957, and more regularly during the summer months since 1999 when the AZMP program began. However, observations were mostly limited to temperature and salinity prior to 1999.

Oceanographic moorings have been deployed on rotation since the summer of 2015 at these two AZMP stations, providing data to fill sampling gaps in winter or during other times of the year. In 2019, Viking oceanographic buoys equipped with an automatic temperature and salinity profiler carried out 193 full-depth casts at Shediac Valley station between June 16 and November 2, and 388 casts to 320 m at Rimouski station between April 13 and November 6.

Isotherms and isohalines as well as monthly averages of layer temperature and salinity, stratification, and CIL minimum core temperature and thickness at <1°C are shown for 2017-2019 for the Rimouski station in Fig. 65 and for the Shediac Valley station in Fig. 66. The scorecard climatologies are calculated from 1991-2010 data for Rimouski station, and for 1981-2010 for Shediac Valley. Mooring data are also used to fill winter gaps in the isotherms and isohalines, and are used throughout the tables of monthly averages when available at the corresponding depths.

At the Rimouski station, the gradual shift of cold-fresh deep anomalies present in 2010 to warmer-saltier waters advected from Cabot Strait lead to a shift to warm anomalies by May 2013 and a 320-m series record in temperature (5.99°C) observed in September 2019. The CIL was warmer and thinner than normal in 2019. In June, surface salinity was below normal (23.3;

-2.2 SD) and stratification above normal, coincident with the above normal spring freshet (Fig. 7).

Conditions at Shediac Valley station (Fig. 66) were generally normal to warmer and fresher than normal, including below normal surface salinity and above normal stratification from June through August, consistent with the strong spring freshet and expected circulation time. The passage of tropical storm Dorian is apparent with the homogenization of the temperature and salinity from the surface down to a depth of approximately 30 m in early September.

Fig. 67 shows the interannual variability of some bulk layer averages from May to October for the two stations. All but one temperature metrics were above normal at both stations, including a record high near-bottom temperature (5.81°C) at Rimouski station and a record high 0-50 m average temperature at Shediac Valley.

SUMMARY

Fig. 68 summarizes SST, summertime CIL and deep-water average temperatures. While May-November SST and August SST are somewhat well correlated (R^2 = 0.41 for the 1982-2019 AVHRR record), the August SST reached in 2012 and 2014 were very high anomalies compared the May-November averages, while in 2006 the reverse was found to be the case. Similarly, the high August SST anomaly observed in 2019 contrasts with the below normal May-November anomaly. The figure shows average temperature at 300 m at a 100+ year series record high, exceeding the 1981–2010 climatology by just over 1°C, and shows the average temperature at 200 m just reach the 1981–2010 climatological value for 300 m.

Another summary of the temperature state of the Gulf of St. Lawrence over a shorter time span (since 1971) allows the inclusion of more data sets, and three sets of four time series are chosen to represent surface, intermediate and deep conditions (Fig. 69). The SST summer and fall timing are from Fig. 22 (12°C threshold) with air temperature proxies used prior to 1982. Sea-ice is grouped as an intermediate feature since all are associated with winter formation. Fig. 69 shows the sums of these three sets of anomalies representing the state of different parts of the system and is reproduced on Fig. 70 with each time series contribution shown as stacked bars (Petrie et al. 2007). These composite indices measure the overall state of the climate system with positive values representing warm conditions and negative representing cold conditions. The plot also indicates the degree of correlation between the various measures of the environment.

The index of surface anomalies is below normal (-0.9 SD) in 2019 for the first time since 1992, mostly driven by late spring timing and near-record early fall timing, the latter associated with the tropical storm Dorian. Even the May-November sea-surface temperature average for the Gulf of St. Lawrence would have been near normal had it not been for tropical storm Dorian, mixing deeper cool waters up to the surface. The index of intermediate layer anomalies is just above (warmer than) normal (+0.7 SD), driven by Magdalen Shallows conditions which had warmer CIL conditions than in the rest of the Gulf. The index of deep temperature anomalies is at a series record high (+3.9 SD).

KEY FINDINGS

- The annual average runoff from the St. Lawrence River at Québec City and RIVSUM II were above normal at 15,100 m^3s^{-1} (+2.3 SD) and 20,200 m^3s^{-1} (+2.0 SD) respectively, at their highest level since 1976. The St. Lawrence River spring freshet extended late into June, and the May-June average June tied for first place of the time series with 1974 at 30,900 $m^3 s^{-1}$ (+3.1 SD).

- Sea-ice cover formed much earlier than normal in the Estuary, the Western portion of the Gulf and along the coast of the lower north shore, but later than normal in offshore regions of the Gulf. It was the earliest first occurrence of ice on record in the Upper Estuary; the first time it occurred in November. Sea ice maximum volume was near normal at 77 km³ (+0.3 SD). In the 10 year span since 2010, 7 of the 10 lowest maximum ice volumes of the time series have occurred, although this does not include 2019.
- The winter surface mixed cold layer (<- 1°C) volume of 15,200 km³ was the highest of the time series (+1.2 SD against 1996–2018 climatology), corresponding to 48% of the total water volume of the Gulf. The Labrador Shelf water intrusion volume into Mécatina Trough of 3700 km³ tied as the second highest of the time series (1997-2019), representing 24% of the cold water (T< -1°C) in the Gulf. It likely greatly contributed to the cold layer volume record.
- The August cold intermediate layer (CIL) average minimum temperature was normal at -0.2°C, as was the Gilbert and Pettigrew minimum temperature index, which includes data over a longer season (-0.45°C, -0.1 SD).
- The timing of summer onset and post-season cooling of the surface layer were respectively later than normal (+1.5 SD, +1.3 weeks) and earlier than normal (-2.0 SD, -2.0 weeks). This second-earliest fall cooling of the time series was caused by the mixing of the water column by tropical storm Dorian resulting in redistribution of heat within the water column rather than from heat loss to the atmosphere.
- Surface water temperatures were at a record low in September (since 1981, -2.1°C, -2.7 SD), again caused by strong vertical mixing by the passage of tropical storm Dorian. The May to November 2019 average was below normal (-0.3°C, -0.5 SD), but would have been near normal without tropical storm Dorian. The warmest month of the year, August, was above normal (+0.9°C, +1.1 SD) just prior to the storm.
- Deep water temperatures have been increasing overall in the Gulf, with inward advection from Cabot Strait. Gulf-wide average temperatures at 150 and 200 m are lower than the 2015 record highs but remain above normal at 3.3°C (+1.6 SD) and 5.5°C (+2.4 SD). New series record highs (since 1915) were set at 250 and 300 m, at 6.3°C (+0.8°C, +3.8 SD) and 6.5°C (+1.0°C, +6.6 SD) respectively. At 300 m, temperature increased to regional record highs in all deep regions of the Gulf: Estuary (5.9°C, +4.1 SD), Northwest Gulf (6.2°C, +5.6 SD), Central Gulf (6.6°C, +5.7 SD) and Cabot Strait (7.1°C, +5.8 SD).
- Bottom area covered by waters warmer than 6°C remained high in Anticosti Channel and Esquiman Channel and were at record highs in the northwest Gulf and Central Gulf.

OUTLOOK FOR 2020

Air temperatures were near normal over the Gulf in December 2019, and above in January and February 2020. This was the setting for the March 2020 survey, which provides an outlook for CIL conditions expected for the remainder of 20120. Fig. 71 shows the surface mixed layer temperature, salinity, and thickness (at T<-1°C and T<0°C), as well as the thickness and extent of the cold and saline layer that has intruded into the Gulf from the Labrador shelf. Most of the winter mixed layer was cold (below -1°C) except for the southern half of coastal Newfoundland waters. The volume of the surface mixed layer colder than -1°C was near normal at 13,100 km^3, representing 39% of all waters of the Gulf. The Cold Intermediate Layer for summer 2020 is therefore forecasted to be warmer than in 2019, with a Gilbert and Pettigrew (1997) index of around -0.34°C compared to -0.45°C in 2018.

Concerning deep waters, recall that record high temperatures have been recorded in Cabot Strait since 2012, and that overall the Gulf waters at 250 and 300 m were in 2019 at a 100+ year record high. Although the March helicopter survey only rarely samples deeper than 210 m, temperatures higher than 7°C were measured at five stations in the area of Cabot Strait, reaching 7.70°C inside the Gulf. This signifies the continuation of warmer than normal conditions at depth.

ACKNOWLEDGEMENTS

We are grateful to the people responsible for CTD data acquisition during the surveys used in this report:

- Rimouski station monitoring: Roger Pigeon, Félix St-Pierre, Michel Rousseau, Rémi Desmarais, Anthony Ouellet, Nicolas Coulombe, Antoine St-Pierre.
- Shediac Valley monitoring station: Roger Pigeon, Michel Rousseau, Félix St-Pierre, Nicolas Coulombe, Anthony Ouellet, Kevin Pauley, Tom Hurlbut.
- March survey: Peter Galbraith, Michel Rousseau, Alain Roy, Claude Beaupré and the Transport Canada group in Ottawa for the design and build of the new oceanographic winch.
- June AZMP transects: Caroline Lafleur, Félix St-Pierre, Rémi Desmarais, Nicolas Coulombe, David Leblanc, Anthony Ouellet, Isabelle St-Pierre, Antoine St-Pierre, Marie-Noëlle Bourassa, Andrew Smith, Mélanie Boudreau, Johanne Guérin; the officers and crew of the CCGS Teleost.
- August Multi-species survey: David Leblanc, Nicolas Coulombe; the officers and crew of the CCGS Teleost.
- October-November AZMP survey: David Leblanc, Félix St-Pierre, Rémi Desmarais, Anthony Ouellet, Roger Pigeon, Michel Rousseau, Marie-Noëlle Bourassa, Caroline Lafleur, Hélèna Talbot, Jean-Luc Shaw; the officers and crew of the Coriolis II.
- September Multi-species survey: Nicolas Rolland (Gulf Region) for providing the CTD data.
- Northumberland Strait survey: Renée Allain, Natalie Asselin, Joël Chassé and the officers and crew of the CCGS M. Perley.
- Data management: Caroline Lafleur, Marie-Noëlle Bourassa, Isabelle St-Pierre, Brian Boivin.

CTD maintenance: Roger Pigeon, Félix St-Pierre, Michel Rousseau, Anthony Ouellet, Nicolas Coulombe.

Data from the following sources are also gratefully acknowledged:

- Air temperature: Environment Canada.
- Sea-ice: Canadian Ice Service, Environment Canada. Processing of GIS files by Jean-Luc Shaw.
- Runoff at Québec City: Denis Lefaivre et Alain D'Astous.
- Runoff from hydrological modelling: Joël Chassé and Diane Lavoie.
- Historical AVHRR SST remote sensing (IML): Pierre Larouche, Bernard Pettigrew.
- AVHRR SST remote sensing (BIO): Carla Caverhill and Cathy Porter

All figures were made using the free software Gri (Kelley and Galbraith 2000).

We are grateful to David Hebert and Frédéric Cyr for reviewing the manuscript and providing insightful comments.

REFERENCES CITED

Belzile, M., Galbraith, P.S., and Bourgault, D. 2016. Water renewals in the Saguenay Fjord. J. Geophys. Res. Oceans, 121, 638-657, doi:10.1002/ 2015JC011085.

Benoît, H.P., Savenkoff, C., Ouellet, P., Galbraith, P.S., Chassé, J. and Fréchet, A. 2012. Impacts of fishing and climate-driven changes in exploited marine populations and communities with implications for management, in State-of-the-Ocean Report for the Gulf of St. Lawrence Integrated Management (GOSLIM) Area, H. P. Benoît, J. A. Gagné, C. Savenkoff, P. Ouellet and M.-N. Bourassa, Eds. Can. Manuscr. Rep. Fish. Aquat. Sci. 2986: viii + 73 pp.

Casey, K.S., Brandon, T.B., Cornillon, P., and Evans, R. 2010. "The Past, Present and Future of the AVHRR Pathfinder SST Program", in Oceanography from Space: Revisited, eds. V. Barale, J.F.R. Gower, and L. Alberotanza, Springer.

Cyr, F., Bourgault, D. and Galbraith, P.S. 2011. Interior versus boundary mixing of a cold intermediate layer. J. Gephys. Res. (Oceans), 116, C12029, doi:10.1029/2011JC007359.

Cyr, F., Colbourne, E., Galbraith, P.S., Gibb, O., Snook, S., Bishop, C., Chen, N., Han, G., and D. Senciall. 2020. Physical Oceanographic Conditions on the Newfoundland and Labrador Shelf during 2018. DFO Can. Sci. Advis. Sec. Res. Doc. 2020/018 iv + 48 p.

DFO. 2020. Oceanographic Conditions in the Atlantic Zone in 2019. DFO Can. Sci. Advis. Sec. Sci. Advis. Rep. 2020/028.

Dutil, J.-D., Proulx, S., Galbraith, P.S., Chassé, J., Lambert, N. and Laurian, C. 2012. Coastal and epipelagic habitats of the estuary and Gulf of St. Lawrence. Can. Tech. Rep. Fish. Aquat. Sci. 3009: ix + 87 p.

Galbraith, P.S. 2006. Winter water masses in the Gulf of St. Lawrence. J. Geophys. Res., 111, C06022, doi:10.1029/2005JC003159.

Galbraith, P.S. and Grégoire, F. 2015. Habitat thermique du maquereau bleu; profondeur de l'isotherme de 8 °C dans le sud du golfe du Saint-Laurent entre 1960 et 2014. Secr. can. de consult. sci. du MPO. Doc. de rech. 2014/116. v + 13 p.

Galbraith, P.S. and Larouche, P. 2011. Sea-surface temperature in Hudson Bay and Hudson Strait in relation to air temperature and ice cover breakup, 1985-2009. J. Mar. Systems, 87, 66-78.

Galbraith, P.S. and Larouche, P. 2013. Trends and variability in eastern Canada sea-surface temperatures. Ch. 1 (p. 1-18) In: Aspects of climate change in the Northwest Atlantic off Canada [Loder, J.W., G. Han, P.S. Galbraith, J. Chassé and A. van der Baaren (Eds.)]. Can. Tech. Rep. Fish. Aquat. Sci. 3045: x + 190 p.

Galbraith, P.S., Saucier, F.J., Michaud, N., Lefaivre, D., Corriveau, R., Roy, F., Pigeon, R. and Cantin, S. 2002. Shipborne monitoring of near-surface temperature and salinity in the Estuary and Gulf of St. Lawrence. Atlantic Zone Monitoring Program Bulletin, Dept. of Fisheries and Oceans Canada. No. 2: 26–30.

Galbraith, P.S., Desmarais, R., Pigeon, R. and Cantin, S. 2006. Ten years of monitoring winter water masses in the Gulf of St . Lawrence by helicopter. Atlantic Zone Monitoring Program Bulletin, Dept. of Fisheries and Oceans Canada. No. 5: 32–35.

Galbraith, P.S., Larouche, P., Gilbert, D., Chassé, J. and Petrie, B. 2010. Trends in sea-surface and CIL temperatures in the Gulf of St. Lawrence in relation to air temperature. Atlantic Zone Monitoring Program Bulletin, 9: 20-23.

Galbraith P.S., Larouche, P., Chassé, J. and Petrie, B. 2012. Sea-surface temperature in relation to air temperature in the Gulf of St. Lawrence: interdecadal variability and long term trends. Deep Sea Res. II, V77–80, 10–20.

Galbraith. P.S., Hebert, D., Colbourne, E. and Pettipas, R. 2013. Trends and variability in eastern Canada sub-surface ocean temperatures and implications for sea ice. Ch.5 In: Aspects of climate change in the Northwest Atlantic off Canada [Loder, J.W., G. Han, P.S. Galbraith, J. Chassé and A. van der Baaren (Eds.)]. Can. Tech. Rep. Fish. Aquat. Sci. 3045: x + 192 p.

Galbraith, P.S., Chassé, J., Caverhill, C., Nicot, P., Gilbert, D., Pettigrew, B., Lefaivre, D., Brickman, D., Devine, L., and Lafleur, C. 2017. Physical Oceanographic Conditions in the Gulf of St. Lawrence in 2016. DFO Can. Sci. Advis. Sec. Res. Doc. 2017/044. v + 91 p.

Galbraith, P.S., D. Bourgault, M. Belzile. 2018. Circulation et renouvellement des masses d'eau du fjord du Saguenay. Naturaliste Canadien, 142-2:36-46. doi:10.7202/1047147ar

Galbraith, P.S., Chassé, J., Caverhill, C., Nicot, P., Gilbert, D., Lefaivre, D. and Lafleur, C. 2019. Physical Oceanographic Conditions in the Gulf of St. Lawrence during 2018. DFO Can. Sci. Advis. Sec. Res. Doc. 2019/046. iv + 79 p.

Gilbert, D. 2004. Propagation of temperature signals from the northwest Atlantic continental shelf edge into the Laurentian Channel. ICES CM, 2004/N:7, 12 pp.

Gilbert, D. and Pettigrew, B. 1997. Interannual variability (1948-1994) of the CIL core temperature in the Gulf of St. Lawrence. Can. J. Fish. Aquat. Sci., 54 (Suppl. 1): 57–67.

Gilbert, D., Sundby, B., Gobeil, C., Mucci, A. and Tremblay, G.-H. 2005. A seventy-two-year record of diminishing deep-water oxygen in the St. Lawrence estuary: The northwest Atlantic connection. Limnol. Oceanogr., 50(5): 1654–1666.

Hammill, M.O. and Galbraith, P.S. 2012. Changes in seasonal sea-ice cover and its effect on marine mammals, in State-of-the-Ocean Report for the Gulf of St. Lawrence Integrated Management (GOSLIM) Area, H. P. Benoît, J. A. Gagné, C. Savenkoff, P. Ouellet and M.-N. Bourassa, Eds. Can. Manuscr. Rep. Fish. Aquat. Sci. 2986: viii + 73 pp.

Hebert, D., Pettipas, R., Brickman, D., and Dever, M. 2018. Meteorological, Sea Ice and Physical Oceanographic Conditions on the Scotian Shelf and in the Gulf of Maine during 2016. DFO Can. Sci. Advis. Sec. Res. Doc. 2018/016. v + 53 p..

Kalnay, E., Kanamitsu, M., Kistler, R., Collins, W., Deaven, D., Gandin, L., Iredell, M., Saha, S., White, G., Woollen, J., Zhu, Y., Chelliah, M., Ebisuzaki, W., Higgins, W., Janowiak, J., Mo, K., Ropelewski, C., Wang, J., Leetmaa, A., Reynolds, R., Jenne, R. and Josephé, D. 1996. The NCEP/NCAR 40-year reanalysis project. Bull. Am. Meteorol. Soc. 77, 437–470.

Kelley, D.E. and Galbraith, P.S. 2000. Gri: A language for scientific illustration, Linux J., 75, 92 101.

Lauzier, L.M. and Trites, R.W. 1958. The deep waters of the Laurentian Channel. J. Fish. Res. Board Can. 15: 1247–1257.

Lefaivre, D., D'Astous, A., Matte, P. 2016. Hindcast of Water Level and Flow in the St. Lawrence River over the 2005–2012 period. Atmosphere-Ocean, 54 (3), 264-277.

McLellan, H.J. 1957. On the distinctness and origin of the slope water off the Scotian Shelf and its easterly flow south of the Grand Banks. J. Fish. Res. Board. Can. 14: 213–239.

Petrie, B., Drinkwater, K., Sandström, A., Pettipas, R., Gregory, D., Gilbert, D. and Sekhon, P. 1996. Temperature, salinity and sigma-t atlas for the Gulf of St. Lawrence. Can. Tech. Rep. Hydrogr. Ocean Sci., 178: v + 256 pp.

Petrie, B., Pettipas, R.G. and Petrie, W.M. 2007. An overview of meteorological, sea ice and sea surface temperature conditions off eastern Canada during 2006. DFO Can. Sci. Advis. Sec. Res. Doc. 2007/022.

Pettigrew, B., Gilbert, D. and Desmarais R. 2016. Thermograph network in the Gulf of St. Lawrence. Can. Tech. Rep. Hydrogr. Ocean Sci. 311: vi + 77 p.

Plourde, S., Joly, P., St-Amand, L. and Starr, M. 2009. La station de monitorage de Rimouski : plus de 400 visites et 18 ans de monitorage et de recherche. Atlantic Zone Monitoring Program Bulletin, Dept. of Fisheries and Oceans Canada. No. 8: 51-55.

Tamdrari, H., Castonguay, M., Brêthes, J.-C., Galbraith, P.S. and Duplisea, D.E. 2012. The dispersal pattern and behaviour of cod in the northern Gulf of St. Lawrence: results from tagging experiments. Can. J. Fish. Aquat. Sci. 69: 112-121.

Therriault, J.-C., Petrie, B., Pépin, P., Gagnon, J., Gregory, D., Helbig, J., Herman, A., Lefaivre, D., Mitchell, M., Pelchat, B., Runge, J. and Sameoto, D. 1998. Proposal for a Northwest Atlantic zonal monitoring program. Can. Tech. Rep. Hydrogr. Ocean Sci., 194: vii + 57 pp.

Vincent, L. A., Wang, X. L., Milewska, E. J., Wan, H., Yang, F. and Swail, V. 2012. A second generation of homogenized Canadian monthly surface air temperature for climate trend analysis, J. Geophys. Res., 117, D18110, doi:10.1029/2012JD017859.

FIGURES

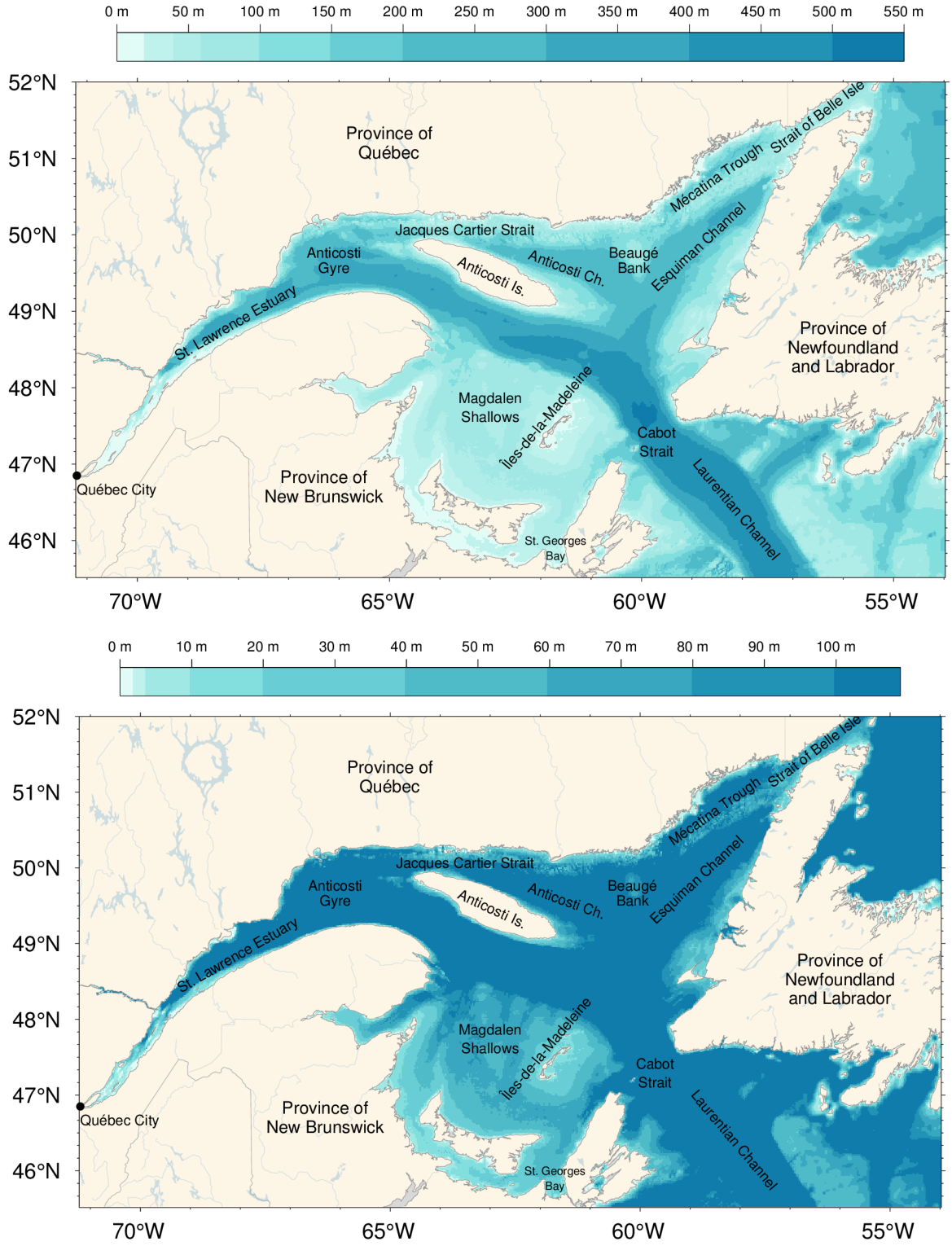

Fig. 1. The Gulf of St. Lawrence. Locations discussed in the text are indicated. Bathymetry datasets used are from the Canadian Hydrographic Service to the west of 56°47' W (with some corrections applied to the baie des Chaleurs and Magdalen Shallows) and TOPEX data to the east. Bottom panel shows detail for 0-100 m bathymetry.

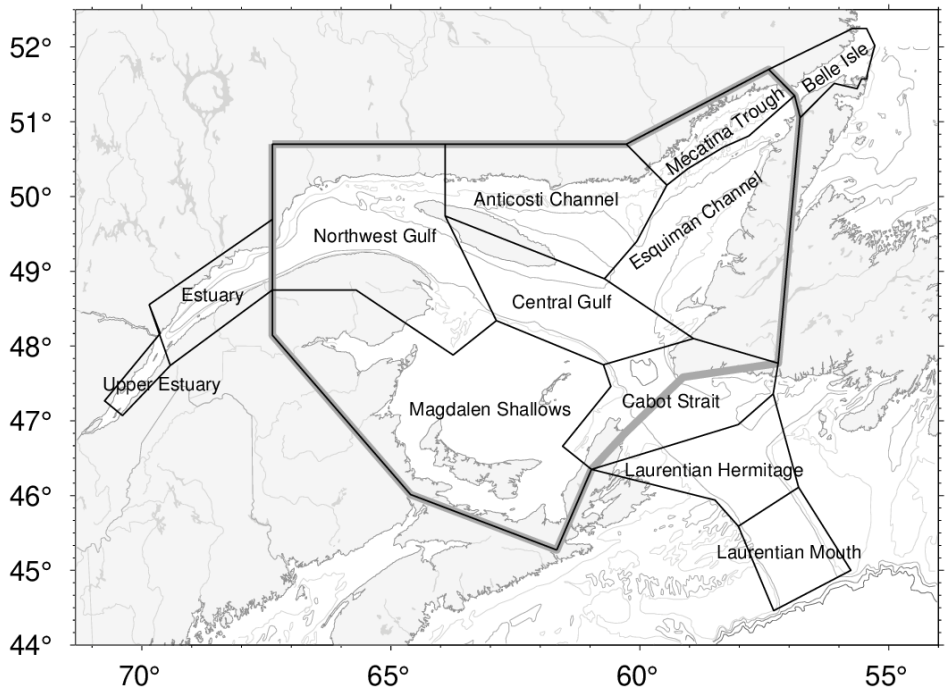

Fig. 2. Gulf of St. Lawrence divided into oceanographic regions used in spatial averaging. The thick gray outline is used for the Gulf average of sea surface temperature.

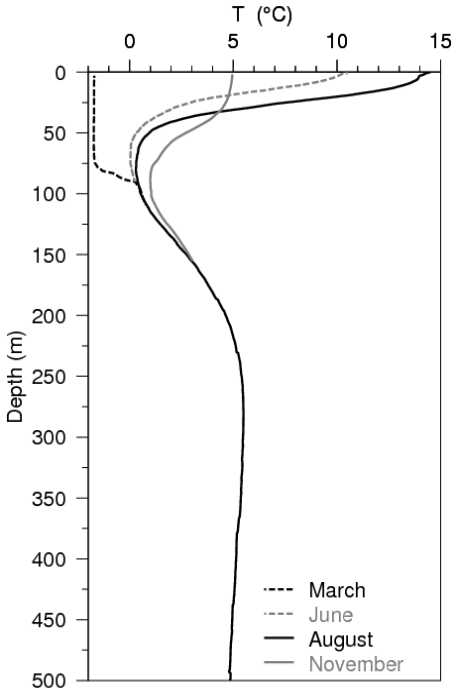

Fig. 3. Typical seasonal progression of the depth profile of temperature observed in the Gulf of St. Lawrence. Profiles are averages of observations in August, June and November 2007 in the northern Gulf. The dashed line at left shows a single winter temperature profile (March 2008), with near freezing temperatures in the top 75 m. The cold intermediate layer (CIL) is defined as the part of the water column that is colder than 1°C, although some authors use a different temperature threshold. Figure from Galbraith et al. (2012).

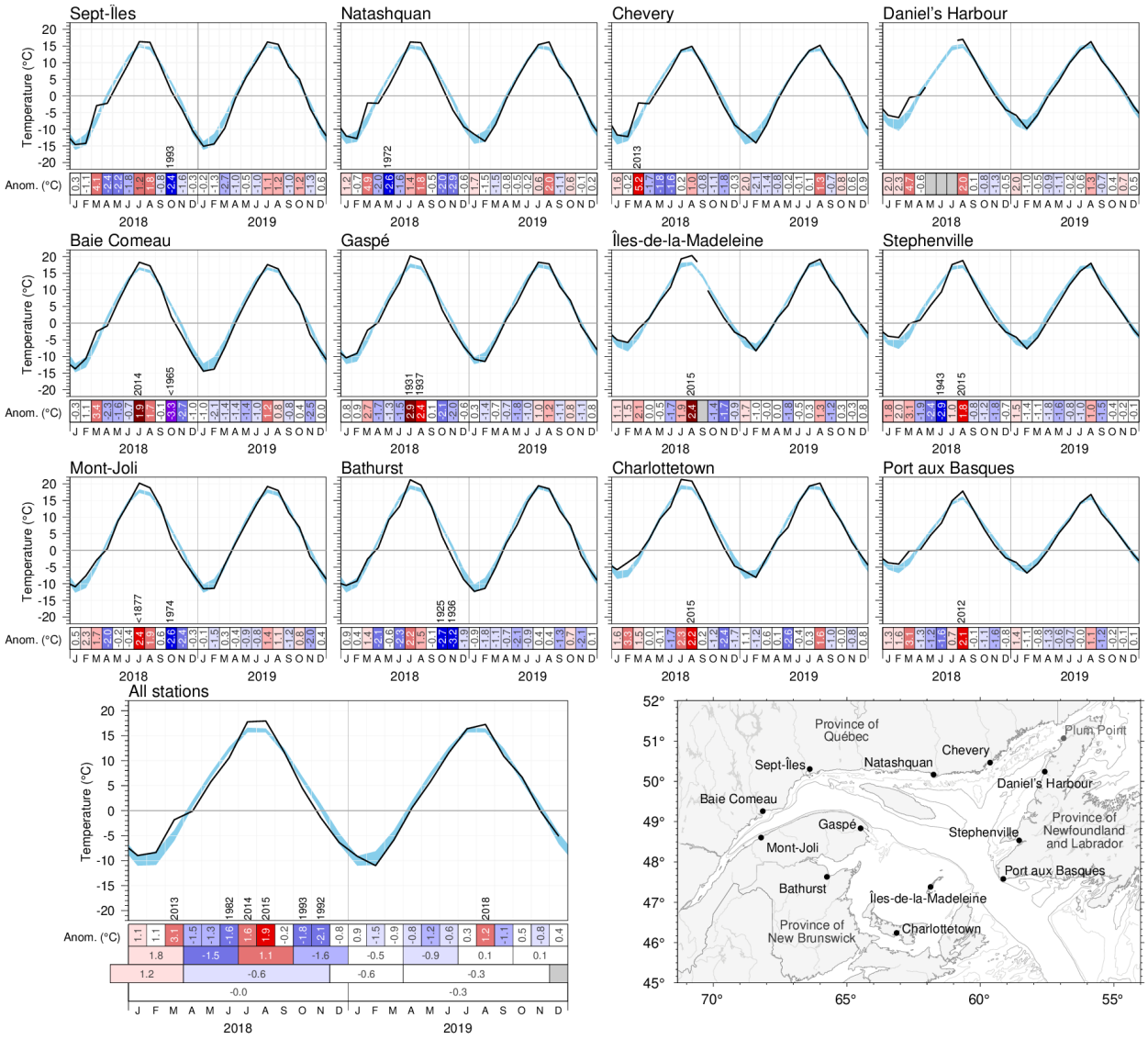

Fig. 4. Monthly air temperatures and anomalies for 2018 and 2019 at selected meteorological stations around the Gulf as well as the average for all stations. The blue area represents the 1981–2010 climatological monthly mean ± 0.5 SD. Months with 4 or more days of missing data are omitted. The bottom scorecards are colour-coded according to the monthly normalized anomalies based on the 1981–2010 climatologies for each month, but the numbers are the monthly anomalies in ºC. For anomalies greater than 2 SD from normal, the prior year with a greater anomaly is indicated. Seasonal, December-March, April-November and annual anomalies are included for the all-station average. Observations at Plum Point (not shown) had been interrupted since 2016 have reappeared since April 2019 and are included in the all-station average.

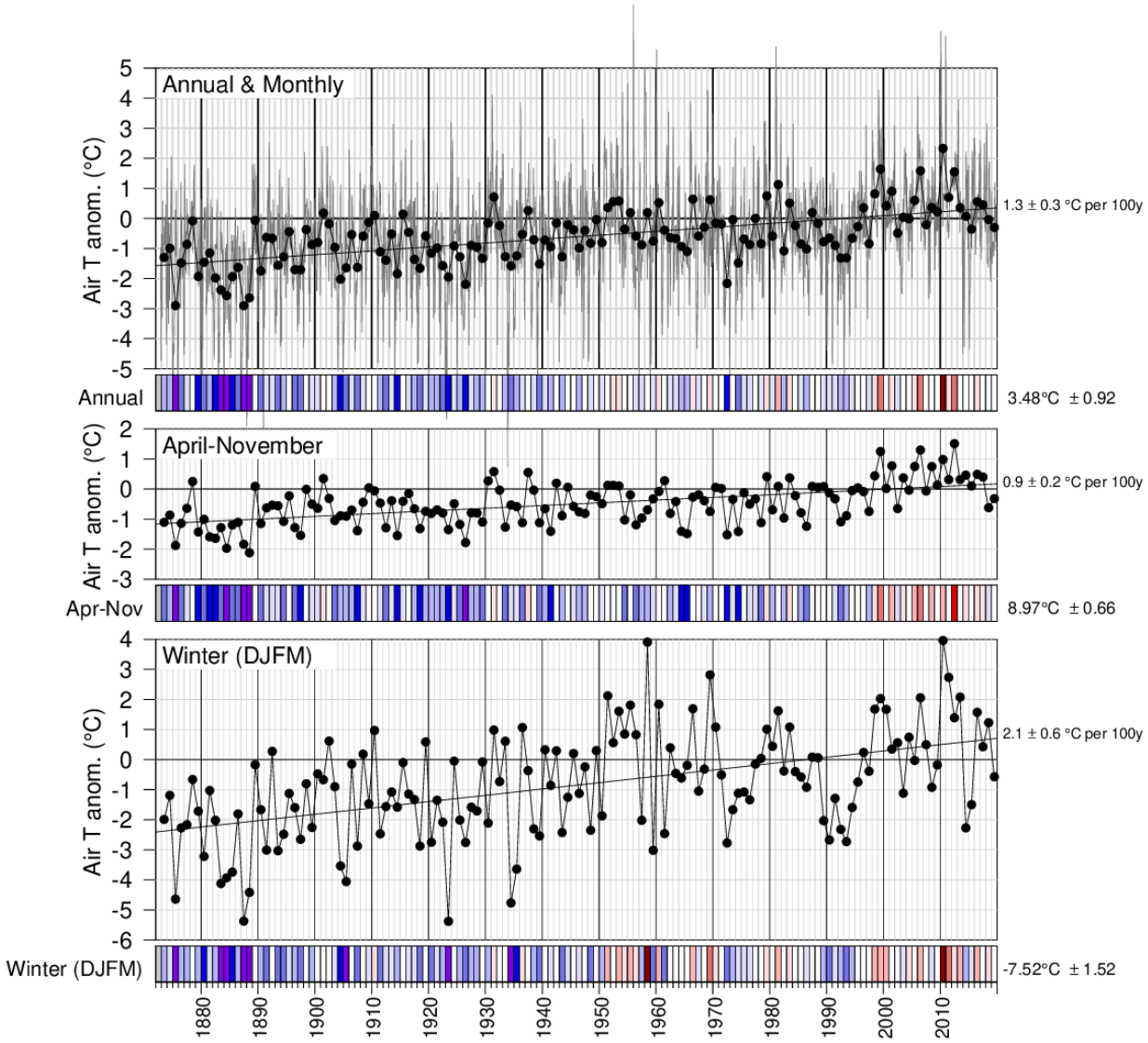

Fig. 5. Annual, April-November December-March mean air temperature anomalies averaged for the selected stations around the Gulf from Fig. 4. The bottom scorecards are colour-coded according to the normalized anomalies based on the 1981–2010 climatology. Trends plus and minus their 95% confidence intervals are shown. April-November air temperature anomalies tend to be highly-correlated with May-November sea-surface temperature anomalies (Galbraith et al. 2012; Galbraith and Larouche 2013) whereas winter air temperature anomalies correlate highly with sea-ice cover parameters and winter mixed-layer volume (Galbraith et al. 2010; Galbraith et al. 2013)

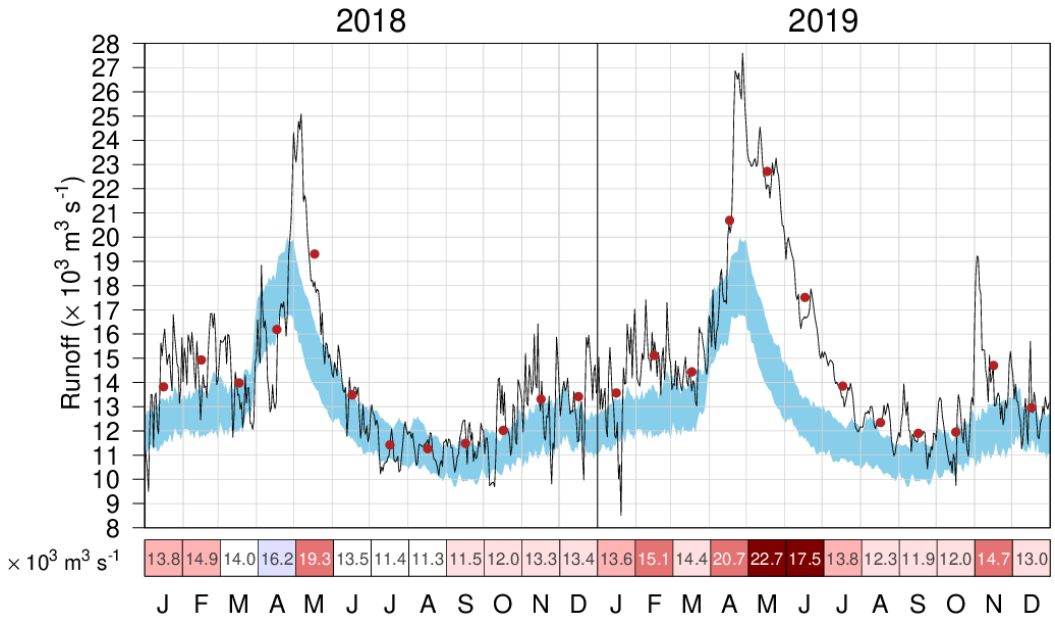

Fig. 6. Daily mean freshwater flow of the St. Lawrence River at Québec City. The 1981–2010 climatological mean (± 0.5 SD) is shown (blue shading). Monthly means are shown by red dots and displayed in the scorecard. It is colour-coded according to the monthly anomalies normalized for each month of the year, but the numbers are the actual monthly anomalies in 10^3 m^3s^{-1}.

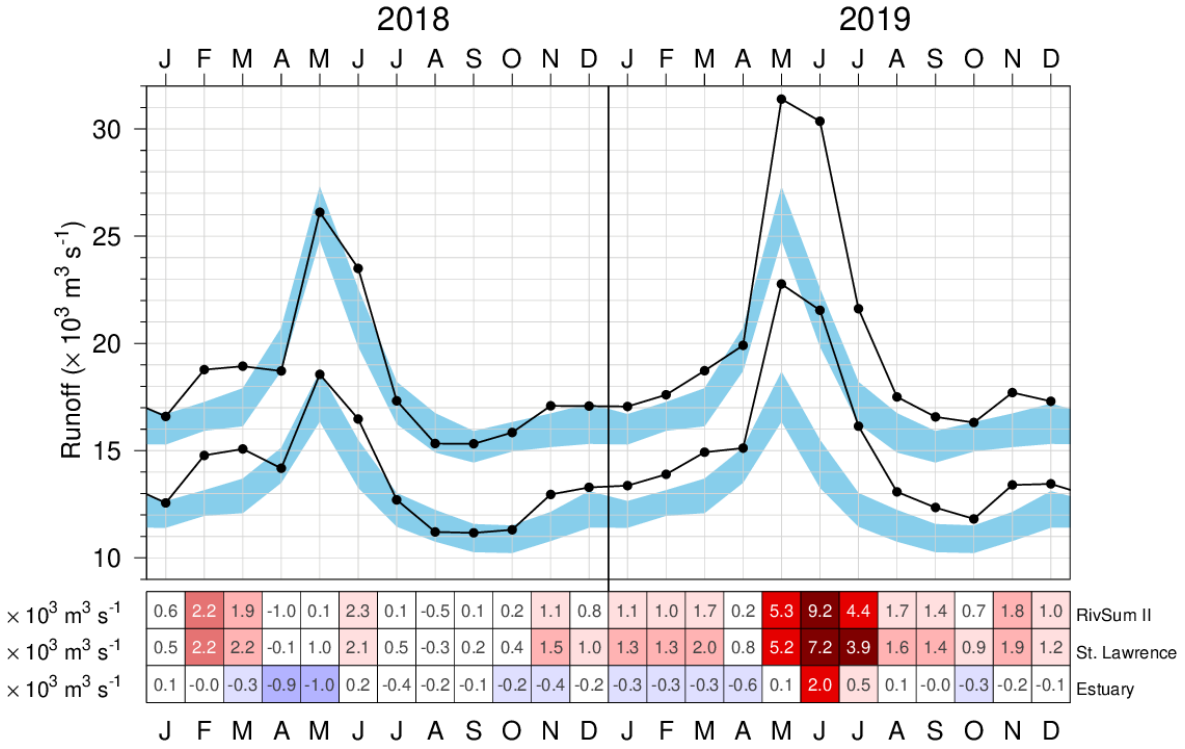

Fig. 7. Monthly mean freshwater flow of the St. Lawrence River at Québec City lagged by 21 days (lower curve) and its sum with rivers flowing into the St. Lawrence Estuary (RIVSUM II, upper curve). The 1981–2010 climatological mean (± 0.5 SD) is shown (blue shading). The scorecards are colour-coded according to the monthly anomalies normalized for each month of the year, but the numbers are the actual monthly anomalies in 10^3 m^3s^{-1}.

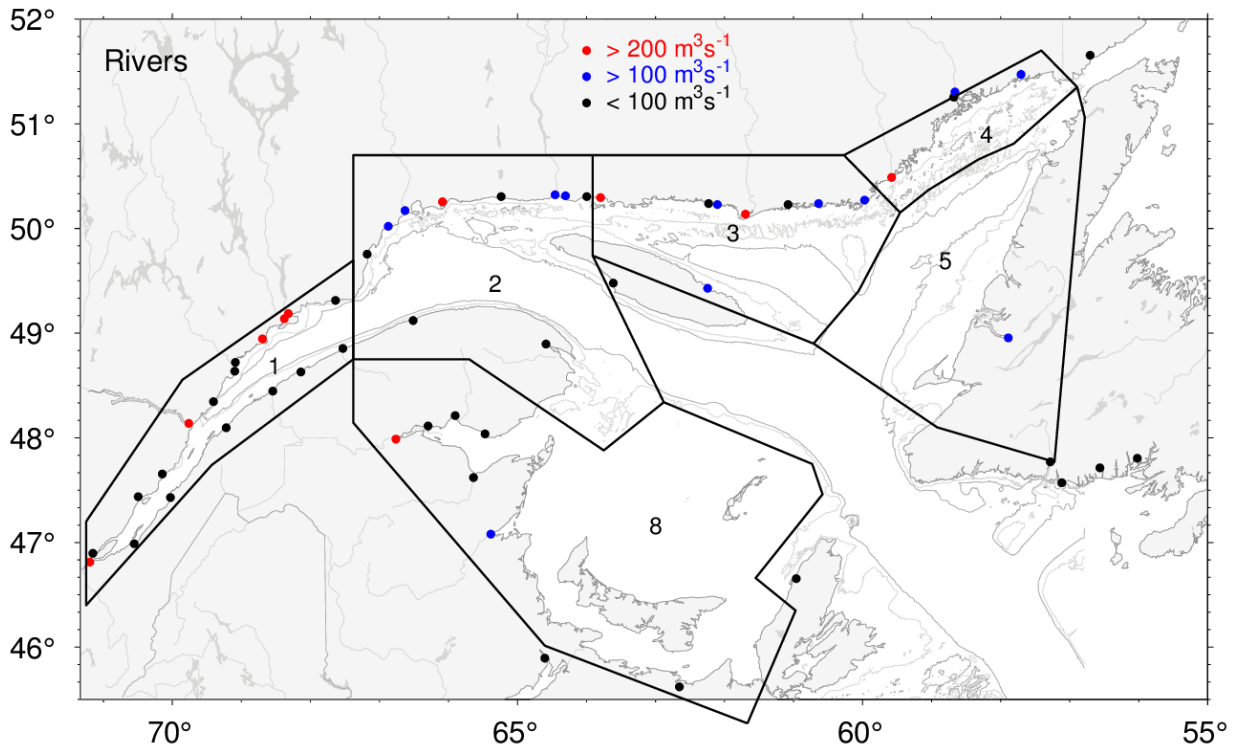

Fig. 8. River discharge locations for the regional sums of runoffs listed in Fig. 9. Red and blue dots indicate rivers that have climatological mean runoff greater than 200 m^3s^{-1} and between 100 and 200 m^3s^{-1}, respectively.

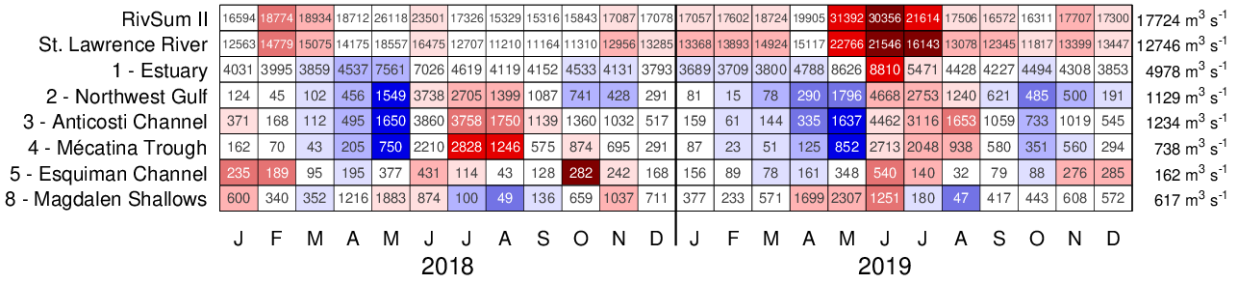

Fig. 9. Monthly anomalies of the RivSum II, the 21-day lagged St. Lawrence River runoff and sums of all other major rivers draining into separate Gulf regions for 2018 and 2019. The scorecards are colour-coded according to the monthly normalized anomalies based on the 1981–2010 climatologies for each month, but the numbers are the monthly average runoffs in $m^3\ s^{-1}$. Numbers on the right side are annual climatological means. Runoff regulation is simulated for three rivers that flow into the Estuary (Saguenay, Manicouagan, Outardes).

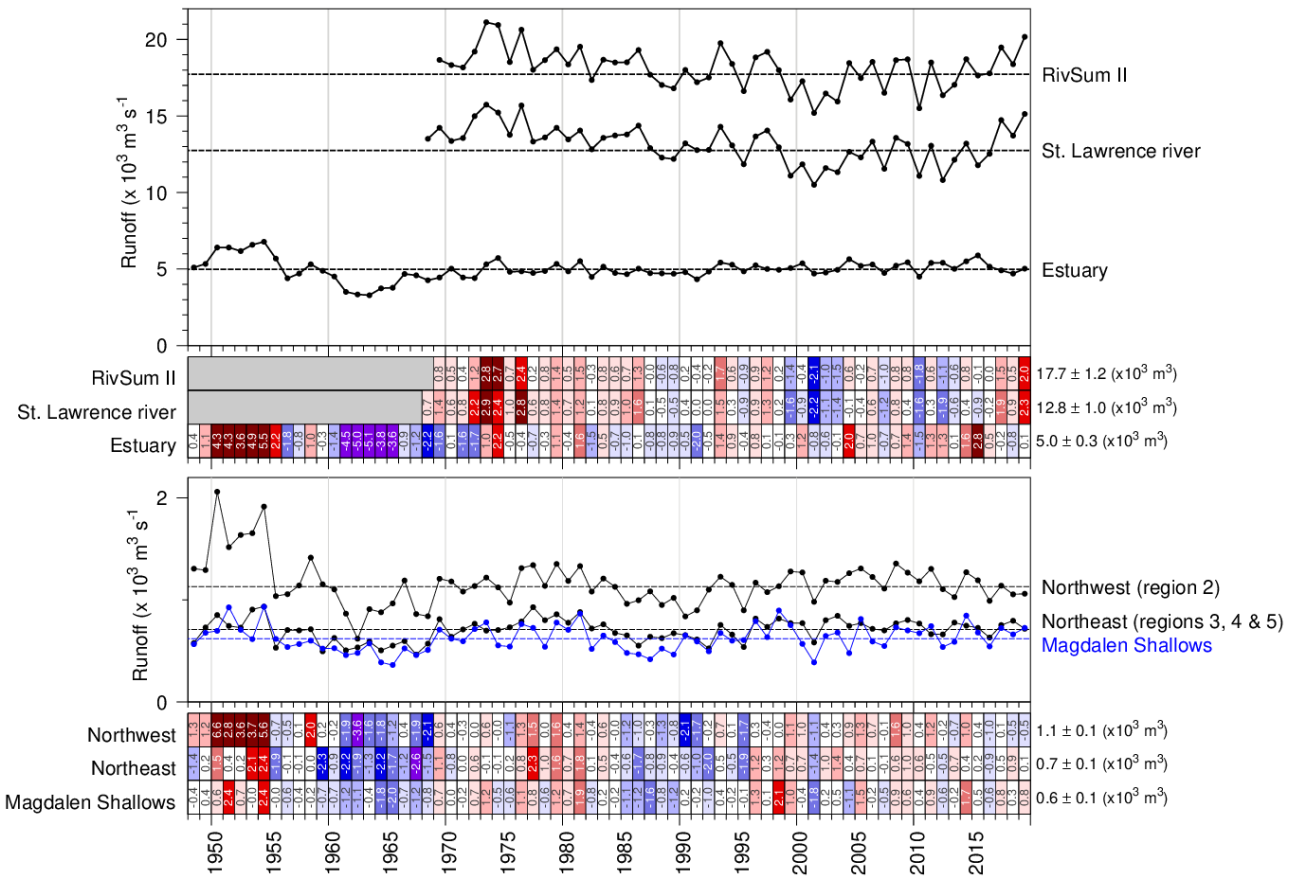

Fig. 10. Annual mean freshwater flow of the St. Lawrence River at Québec City, of the sum of all rivers flowing into regions of the Estuary, the sum of the two: the RivSum II (top panel) and into 3 other oceanographic regions of the Gulf (bottom panel). The 1981–2010 climatological mean is shown as horizontal lines and indicated on the right side of the scorecards. Numbers in scorecards are normalized anomalies.

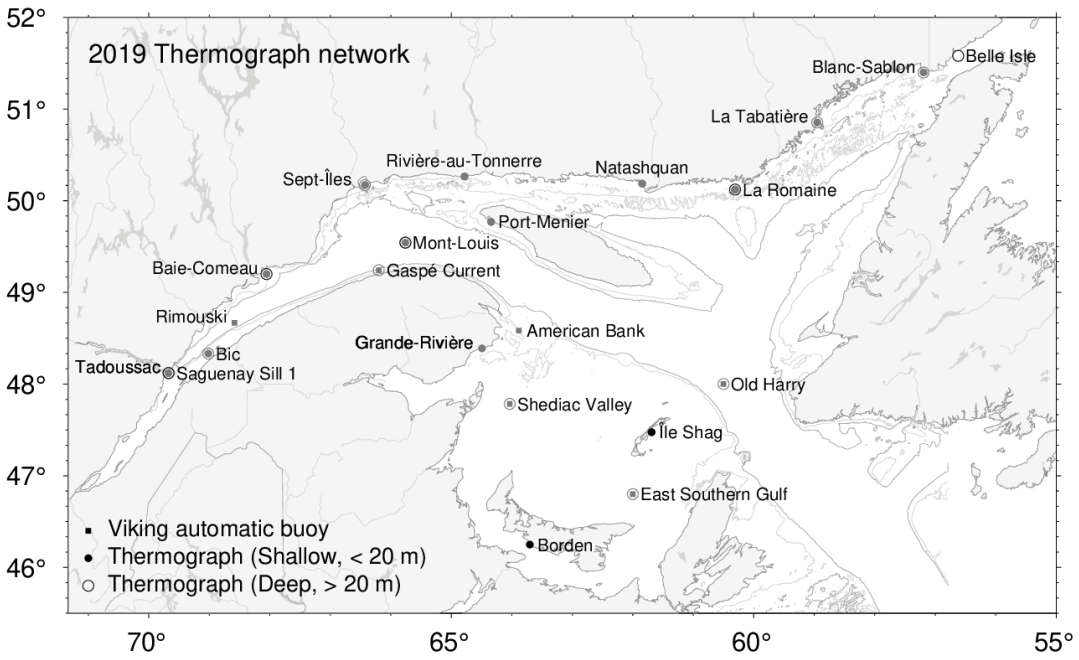

Fig. 11. Maurice Lamontagne Institute thermograph network stations in 2019, including oceanographic buoys that transmit data in real time (squares). Deep and shallow instruments are denoted by open circles and dots, while seasonal and year-round deployments are denoted by gray and black symbols.

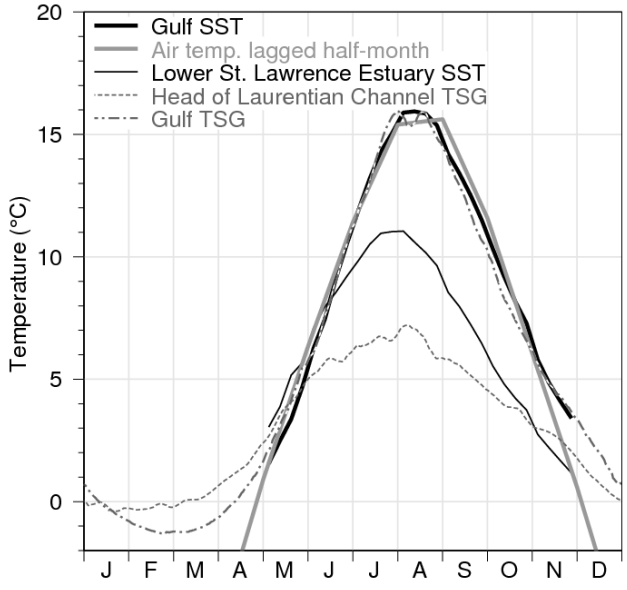

Fig. 12. Sea-surface temperature climatological seasonal cycle in the Gulf of St. Lawrence. AVHRR temperature weekly averages for 1985 to 2010 are shown from May to November (ice-free months) for the Gulf (thick black line) and the cooler Lower St. Lawrence Estuary (thin black line), defined as the area west of the Pointe-des-Monts section and east of approx 69°30'W. Thermosalinograph data averages for 2000 to 2010 are shown for the head of the Laurentian Channel (at 69°30'W, grey dashed line) and for the average over the Gulf waters along the main shipping route between the Pointe-des-Monts and Cabot Strait sections (gray dash-dotted line). Monthly air temperature averaged over eight stations in the Gulf of St. Lawrence are shown offset by 2 weeks into the future (thick grey line; winter months not shown). Figure from Galbraith et al. (2012).

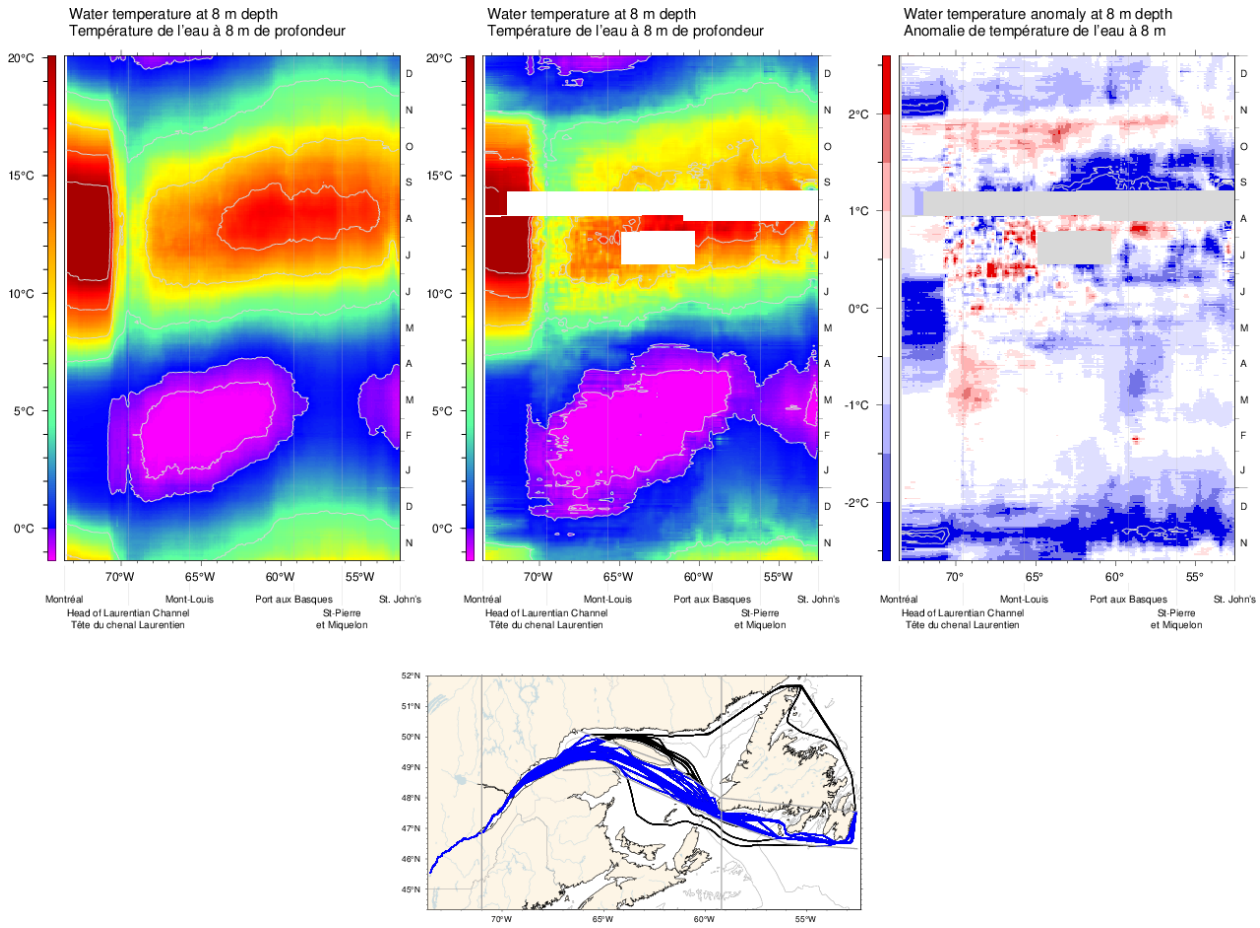

Fig. 13. Hovmöller diagram of thermosalinograph data at 8 m depth along the Montréal to St. John's shipping route: composite mean annual cycle of the water temperature for the 2000–2019 period (top left panel), composite annual cycle of the water temperature for the end of 2018 and 2019 (top middle panel), and water temperature anomaly relative to the 2000–2019 composite (top right panel). The map indicates all ship tracks in 2019, with those in blue used in the analysis.

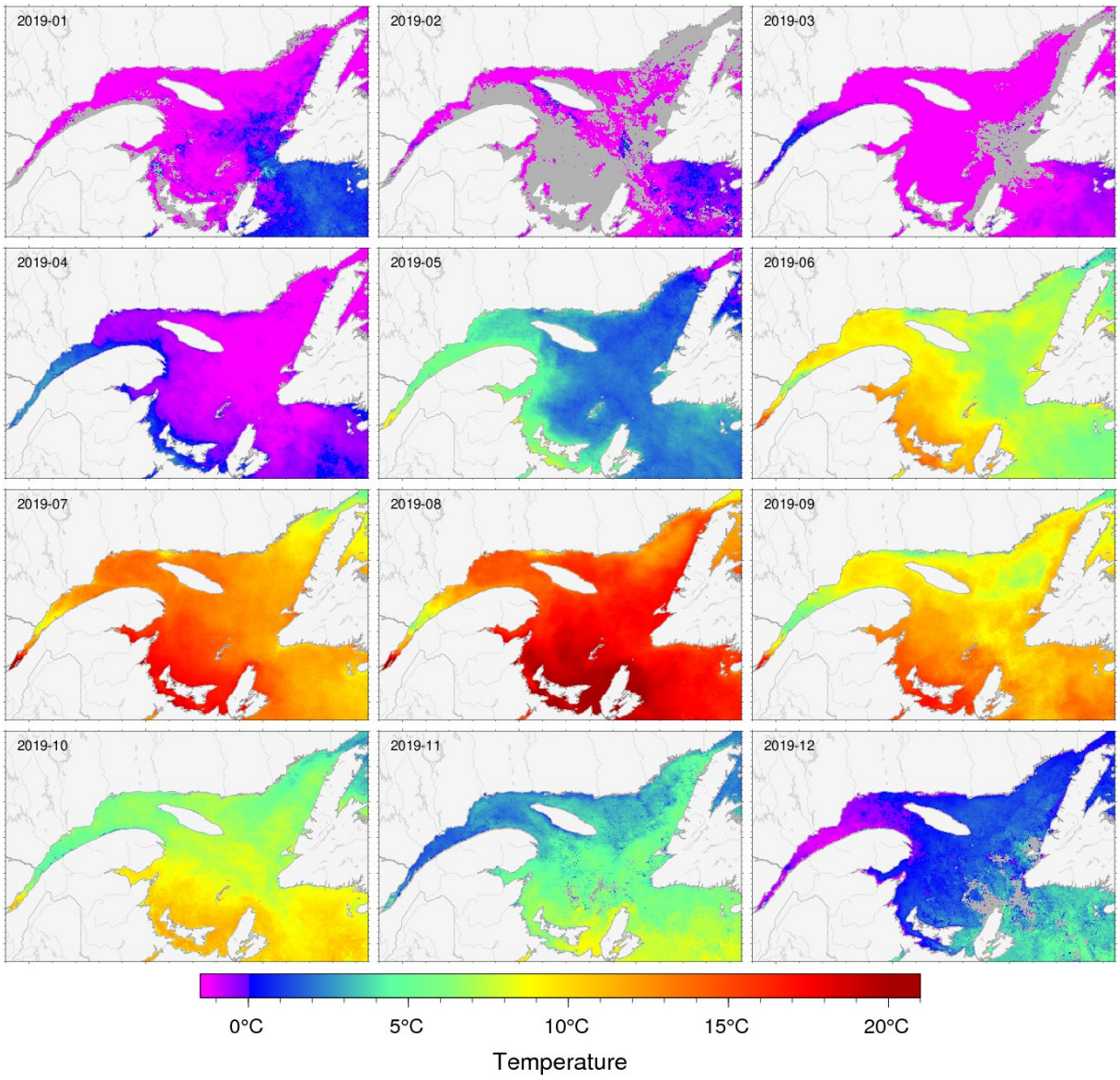

Fig. 14. Sea-surface temperature monthly averages for 2019 as observed with AVHRR remote sensing. Grey areas have no data for the period due to ice cover or clouds.

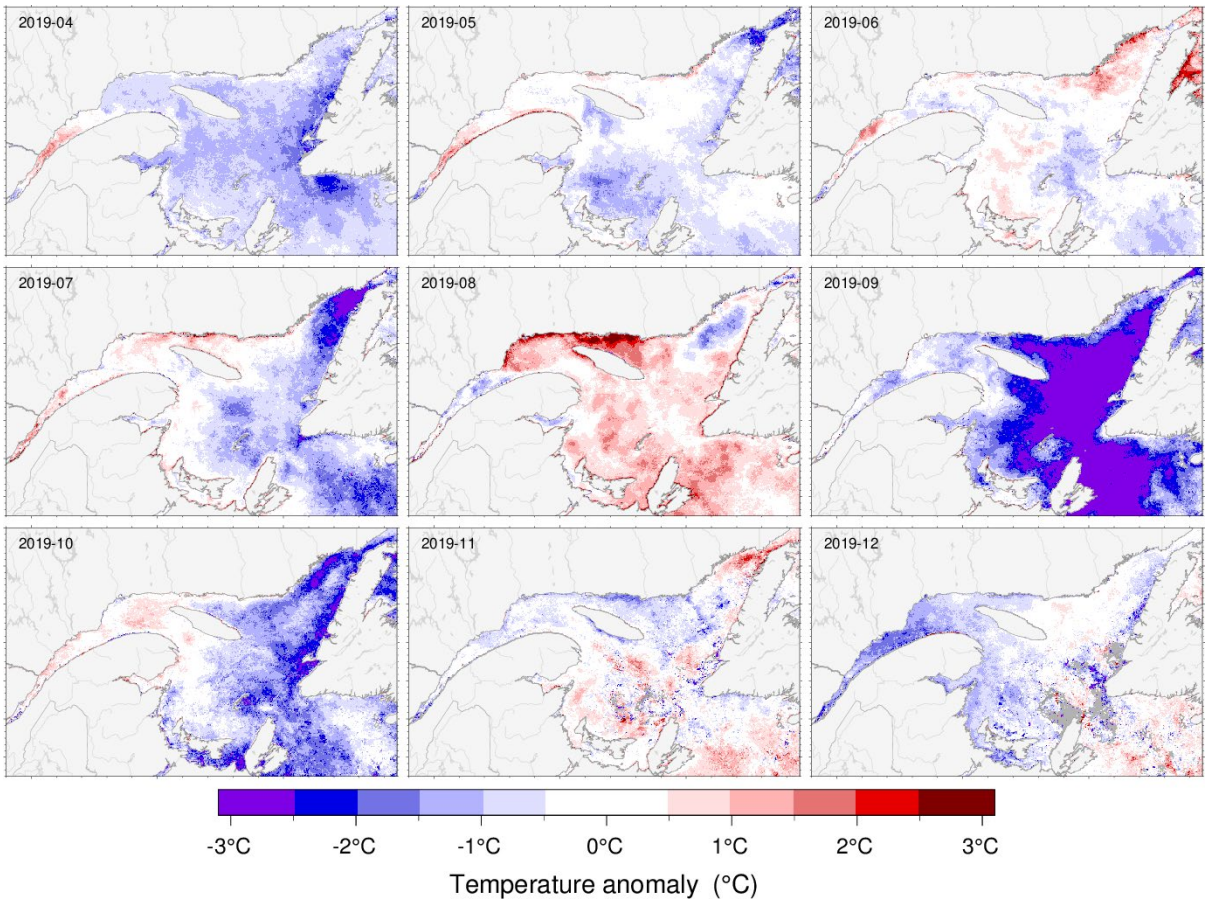

Fig. 15. Sea-surface temperature monthly anomalies for April-December 2019 based on monthly climatologies calculated for the 1981–2010 period observed with AVHRR remote sensing.

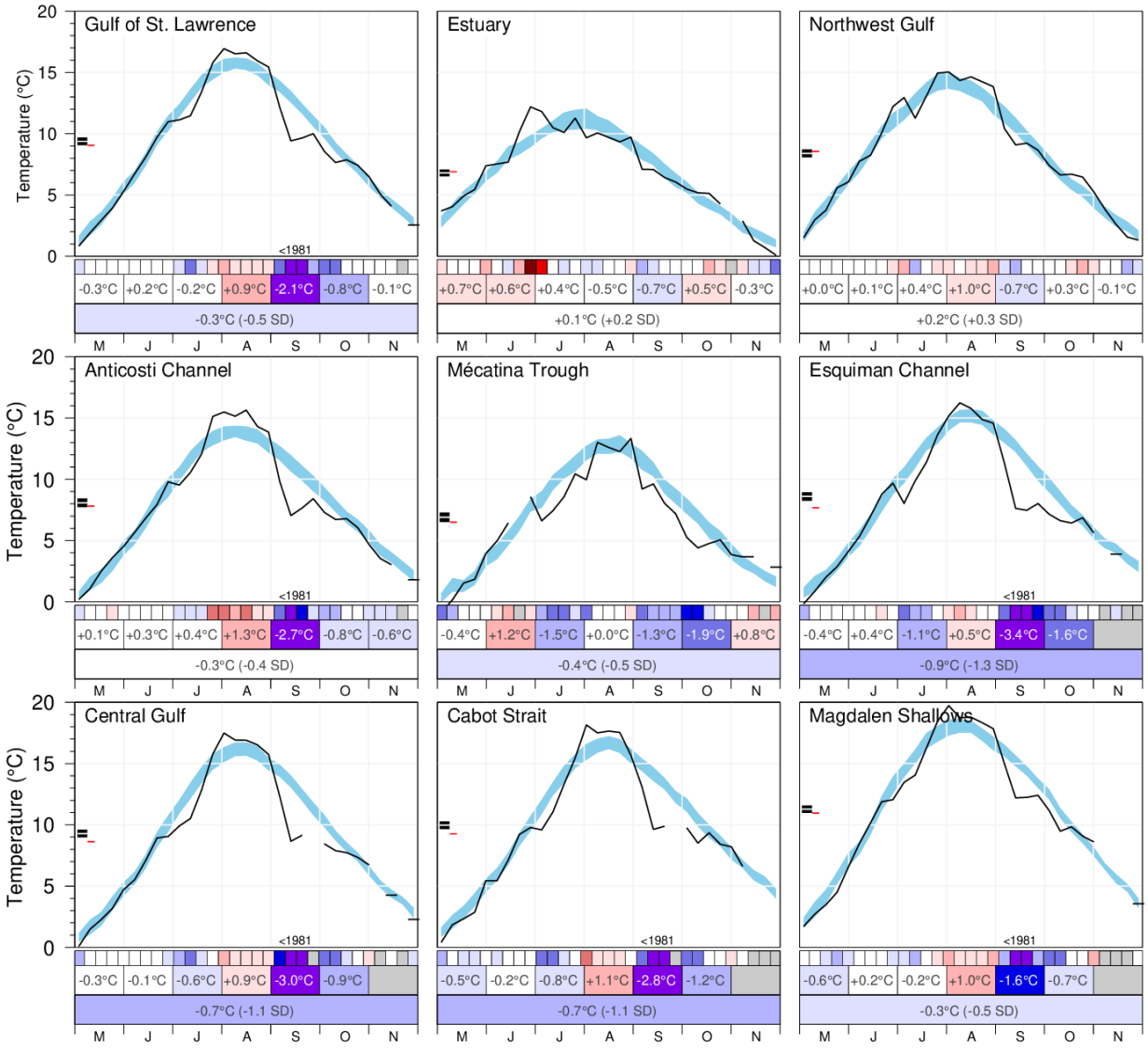

Fig. 16. AVHRR SST May to November 2019 weekly, monthly and seasonal averages over the Gulf and over eight regions of the Gulf. The blue area represents the 1981–2010 climatological weekly mean ± 0.5 SD. The climatological average plus and minus half the standard deviation of the seasonal mean temperature are indicated by the black double bars on the left side of panels, while the year's seasonal mean is indicated by the red line. The scorecards are colour-coded according to the normalized anomalies based on the 1981–2010 climatologies for each week (top row), month (middle row) or for the May-November period (bottom row), but the monthly numbers are average temperature anomalies.

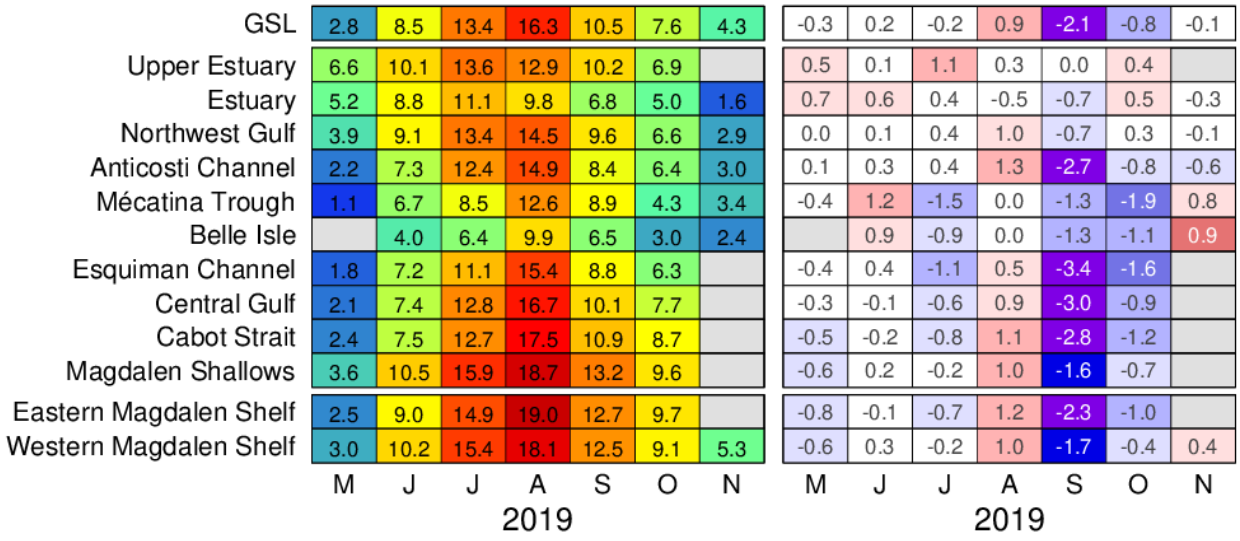

Fig. 17. AVHRR SST May to November monthly temperatures and anomalies, averaged over the Gulf and over regions of the Gulf for 2019. The numbers on the right-hand panel are area average temperatures and are colour-coded accordingly. The right-hand scorecards are colour-coded according to the monthly normalized anomalies based on the 1981–2010 climatologies for each month, but the numbers are the monthly average temperature anomalies expressed in °C.

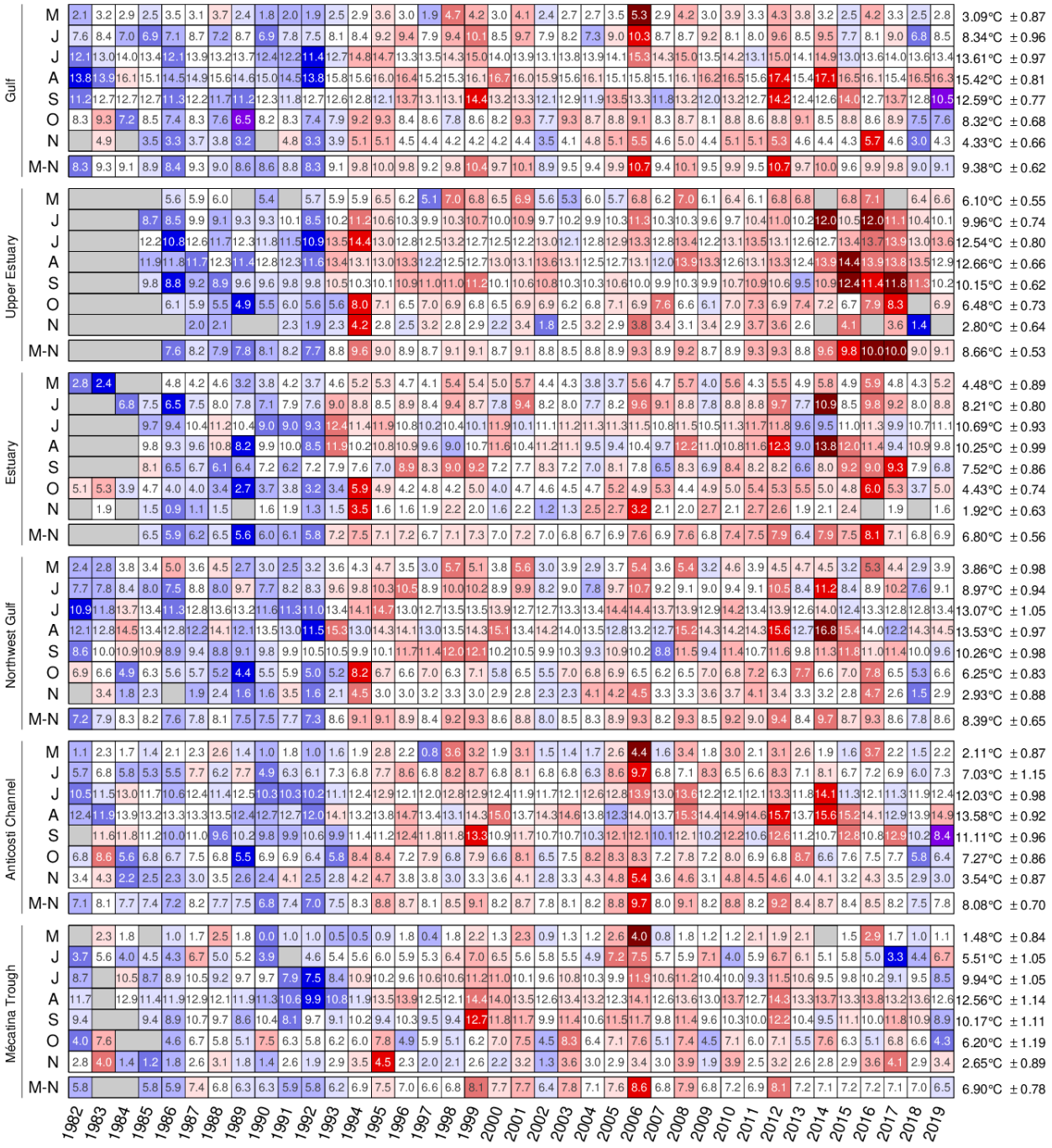

Fig. 18. AVHRR SST May to November monthly anomalies averaged over the Gulf of St. Lawrence and over the first five regions of the Gulf. The scorecards are colour-coded according to the monthly normalized anomalies based on the 1981–2010 climatologies for each month, but the numbers are the monthly average temperatures in ºC. The 1981–2010 mean and standard deviation are indicated for each month on the right side of the table. The May to November average is also included. Data for 1981 are not shown as they begin only in September.

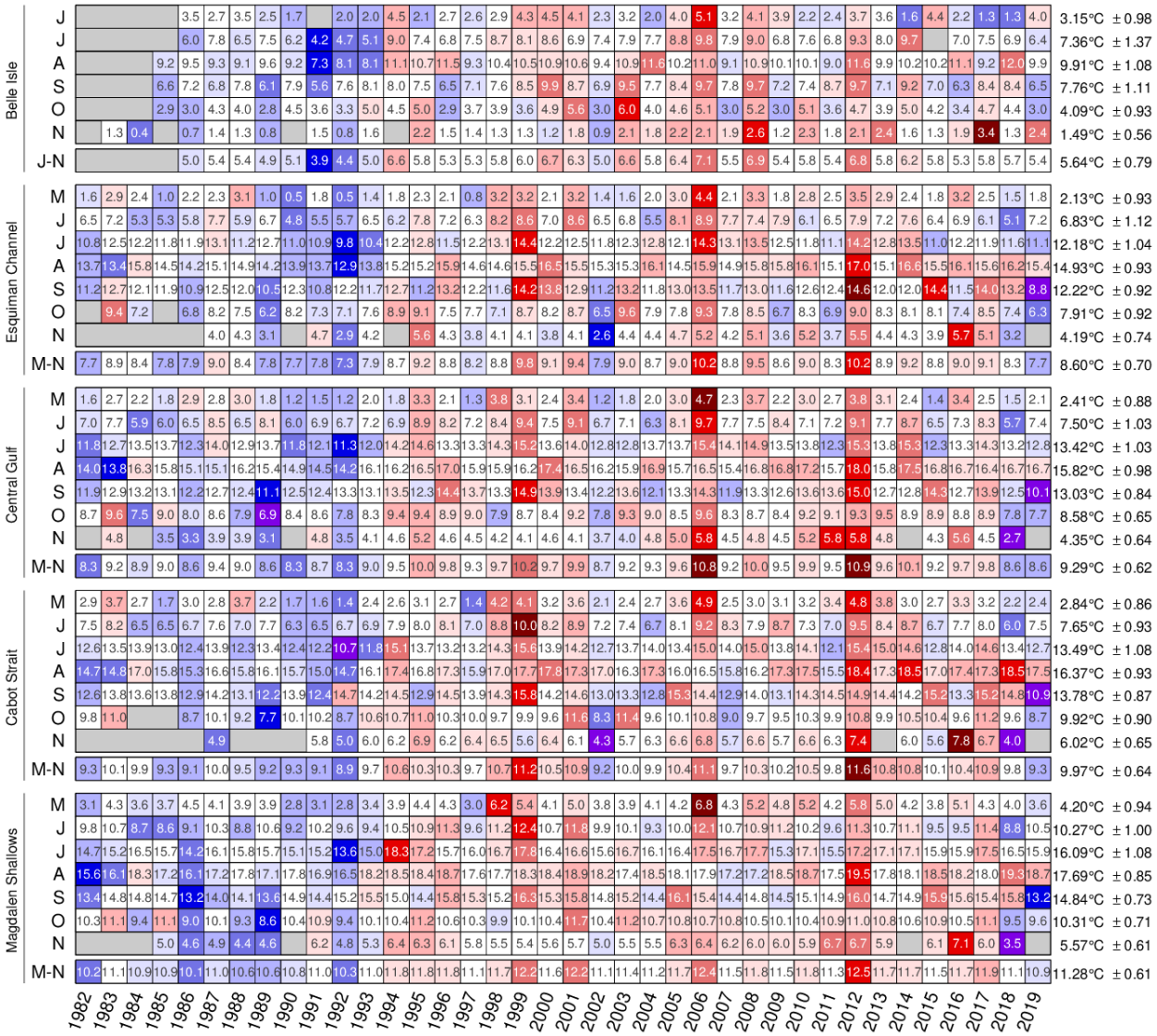

Fig. 19. AVHRR SST May to November monthly anomalies averaged over the remaining regions of the Gulf. The scorecards are colour-coded according to the monthly normalized anomalies based on the 1981–2010 climatologies for each month, but the numbers are the monthly average temperatures in ºC. The 1981–2010 mean and standard deviation are indicated for each month on the right side of the table. The May to November average is also included. Data for 1981 are not shown as they begin only in September.

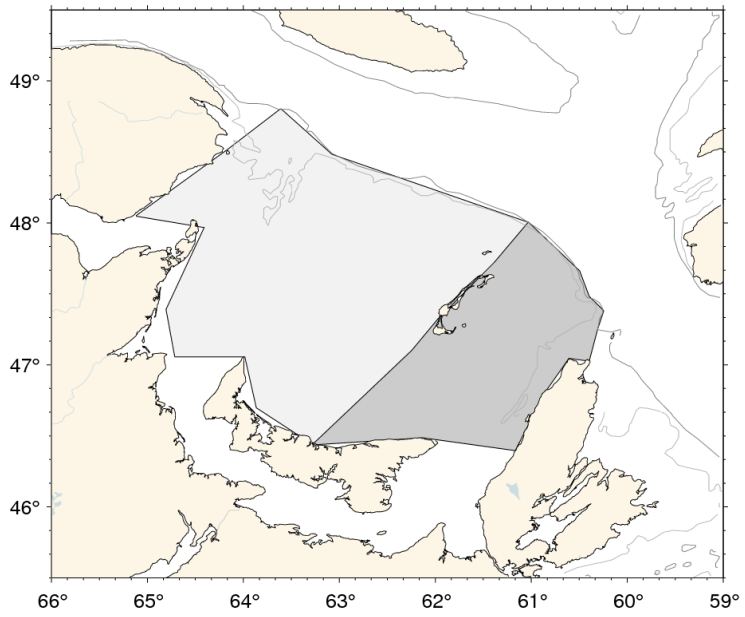

Fig. 20. Areas defined as the western and eastern Magdalen Shallows.

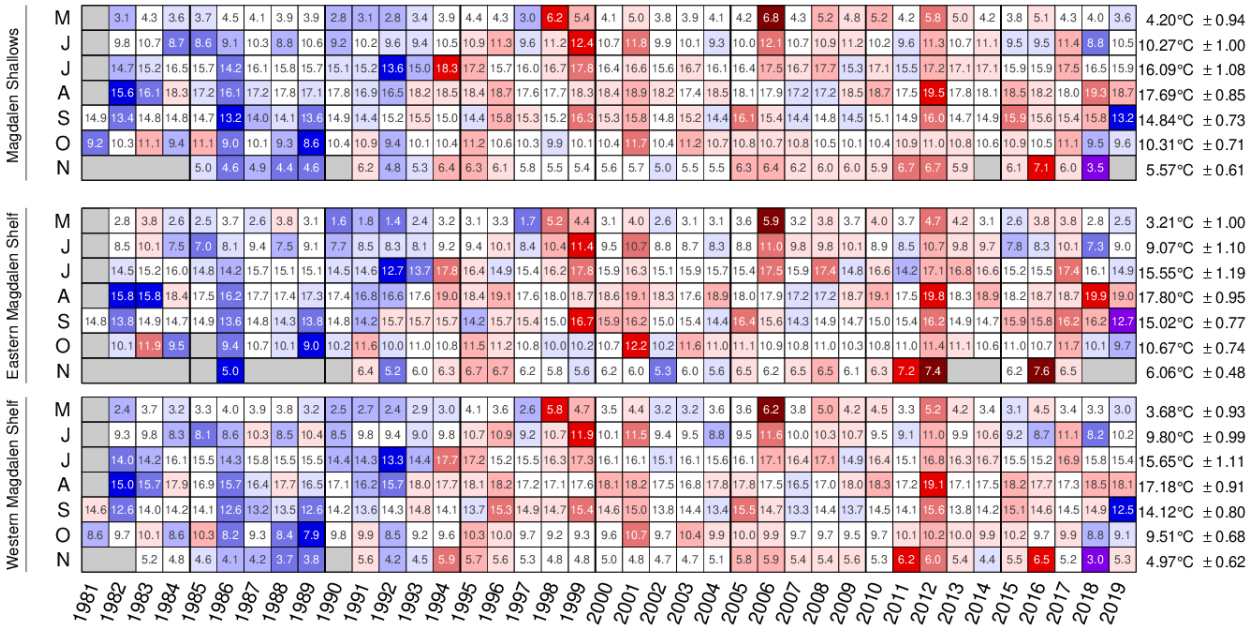

Fig. 21. AVHRR SST May to November monthly anomalies averaged over the Magdalen Shallows (region 8 of the Gulf) and the eastern and western subregions of the Magdalen Shallows (Fig. 20). The scorecards are colour-coded according to the monthly normalized anomalies based on the 1981–2010 climatologies for each month, but the numbers are the monthly average temperatures in °C. The 1981–2010 mean and standard deviation are indicated for each month on the right side of the table.

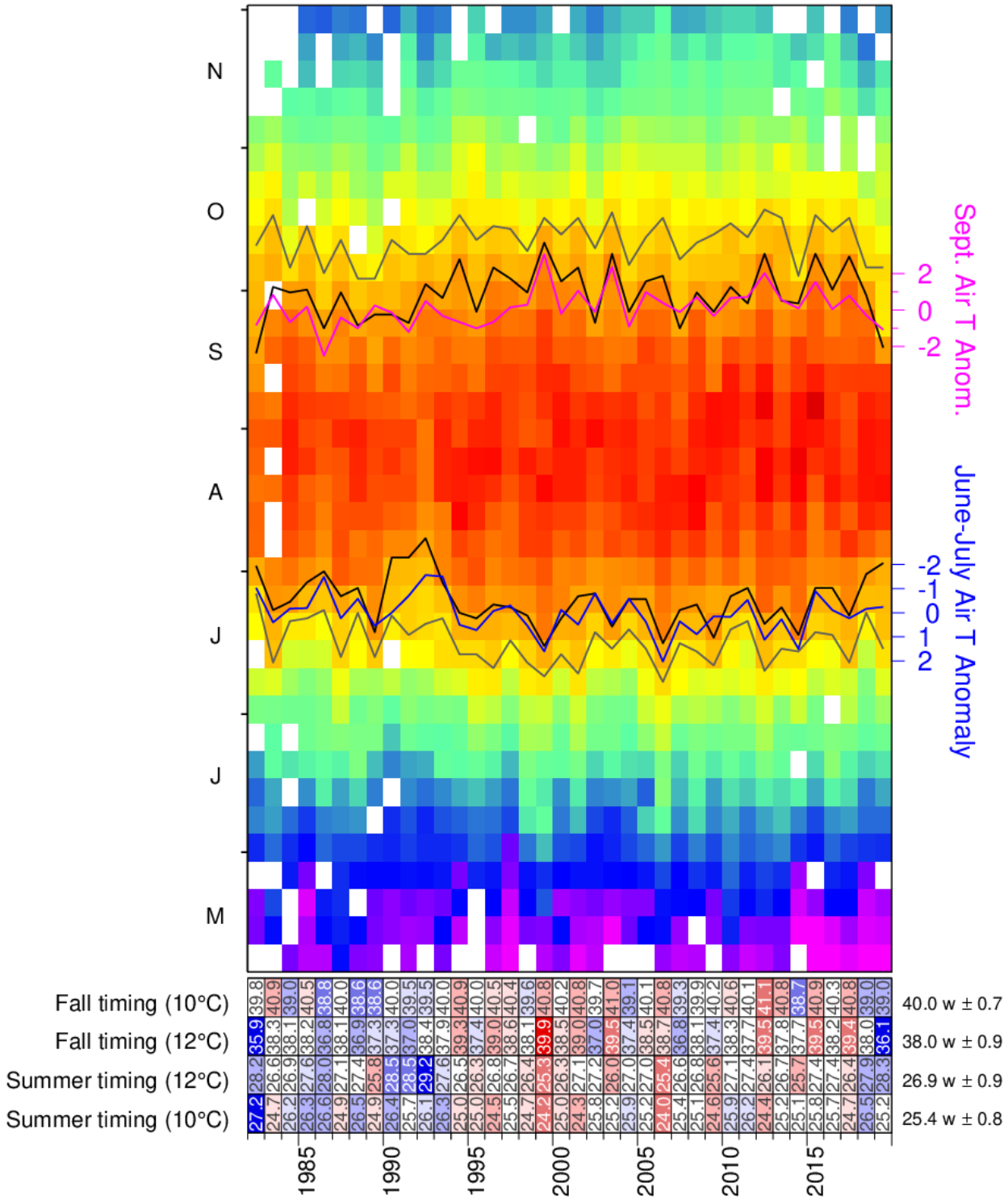

Fig. 22. Weekly average SST (1982–2019) matrix for the Gulf of St. Lawrence. Black lines show first and last occurrence of the 12°C isotherm and proxies based on June-July (blue line) and September (magenta) average air temperature are also shown (axes on right). Gray lines show first and last occurrence of the 10°C isotherm. The scorecards are colour-coded according to the normalized anomalies based on the 1982–2010 time series, but the numbers are week numbers when the threshold was crossed. Updated from Galbraith and Larouche 2013.

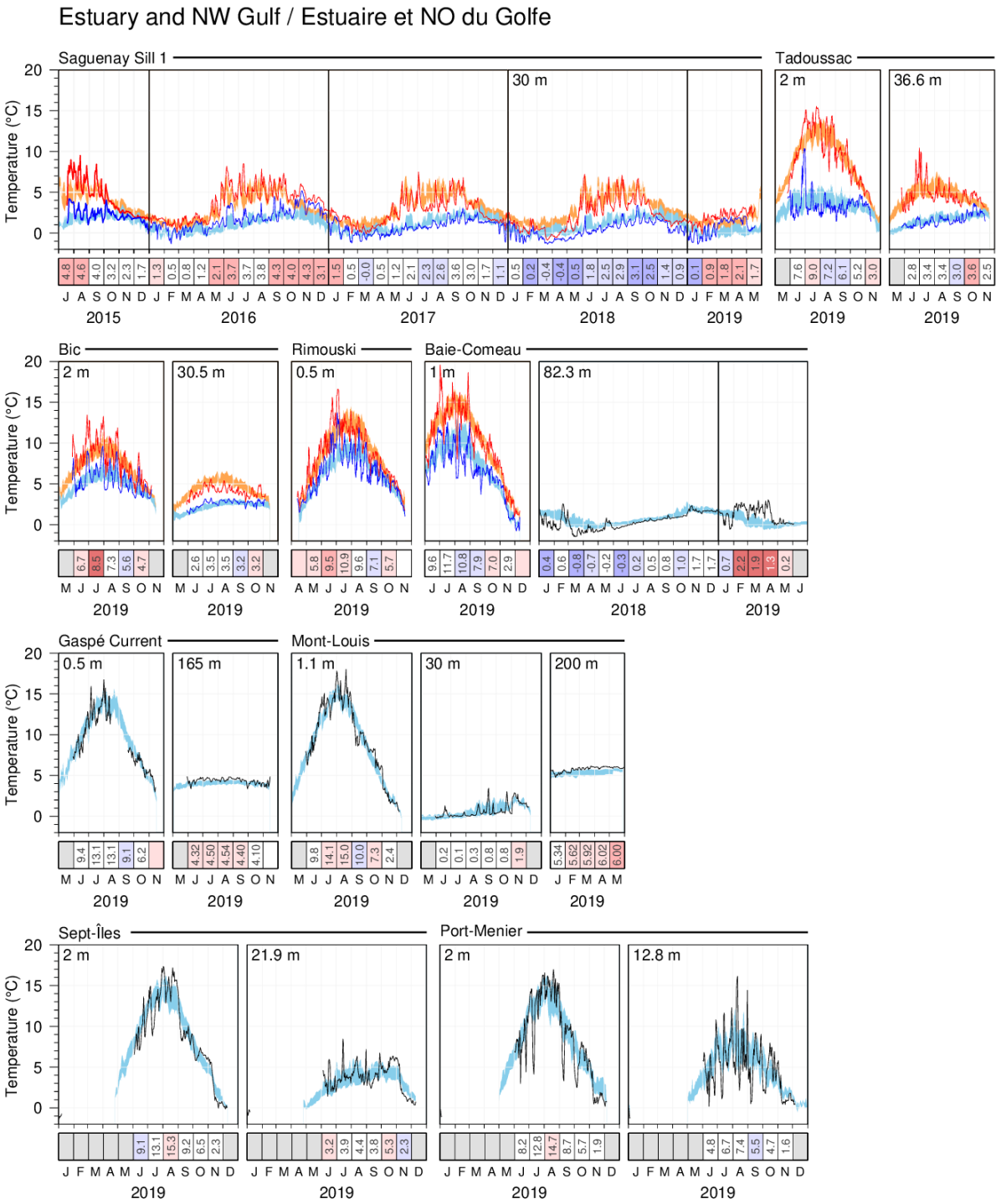

Fig. 23. Thermograph network daily mean temperatures (black line) compared with the daily climatology (blue areas are daily climatological averages ± 0.5 SD) for stations in the Estuary and northwestern Gulf. Stations that exhibit large tidal variations are displayed showing daily minimum (blue) and maximum (red) values, overlying daily climatological averages ± 0.5 SD of the minimum (blue shaded area) and maximum (orange shaded areas) values. Data from 2018 are included for stations collecting data year-round, and since 2015 for the new station Saguenay Sill 1. The scorecards show monthly average temperatures in °C colour-coded according to the monthly normalized anomalies based on the climatologies for each month.

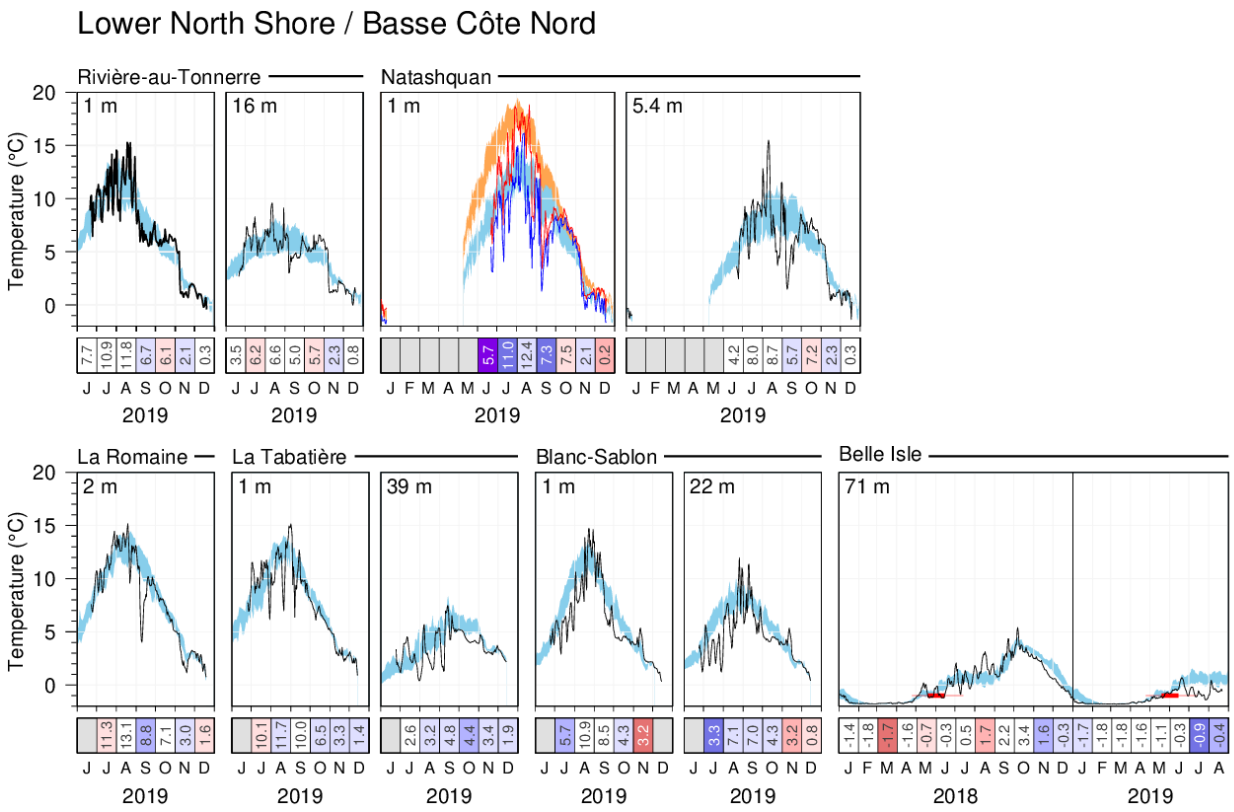

Fig. 24. Thermograph network data. Daily mean 2019 temperatures (black line) compared with the daily climatology (blue areas are daily climatological averages ± 0.5 SD) for stations of the lower north shore. Stations that exhibit large tidal variations are displayed showing daily minimum (blue) and maximum (red) values, overlying daily climatological averages ± 0.5 SD of the minimum (blue shaded area) and maximum (orange shaded areas) values. Data from 2018 are included for stations collecting data year-round. Thin red lines in the Belle Isle panel span the historical dates when spring temperature increased over -1°C, a temperature associated with inflow of winter Labrador Shelf Water into the Gulf. Thick red line indicates mean date plus and minus 0.5 SD. The scorecards show monthly average temperatures in ºC colour-coded according to the normalized anomalies based on the climatologies for each month.

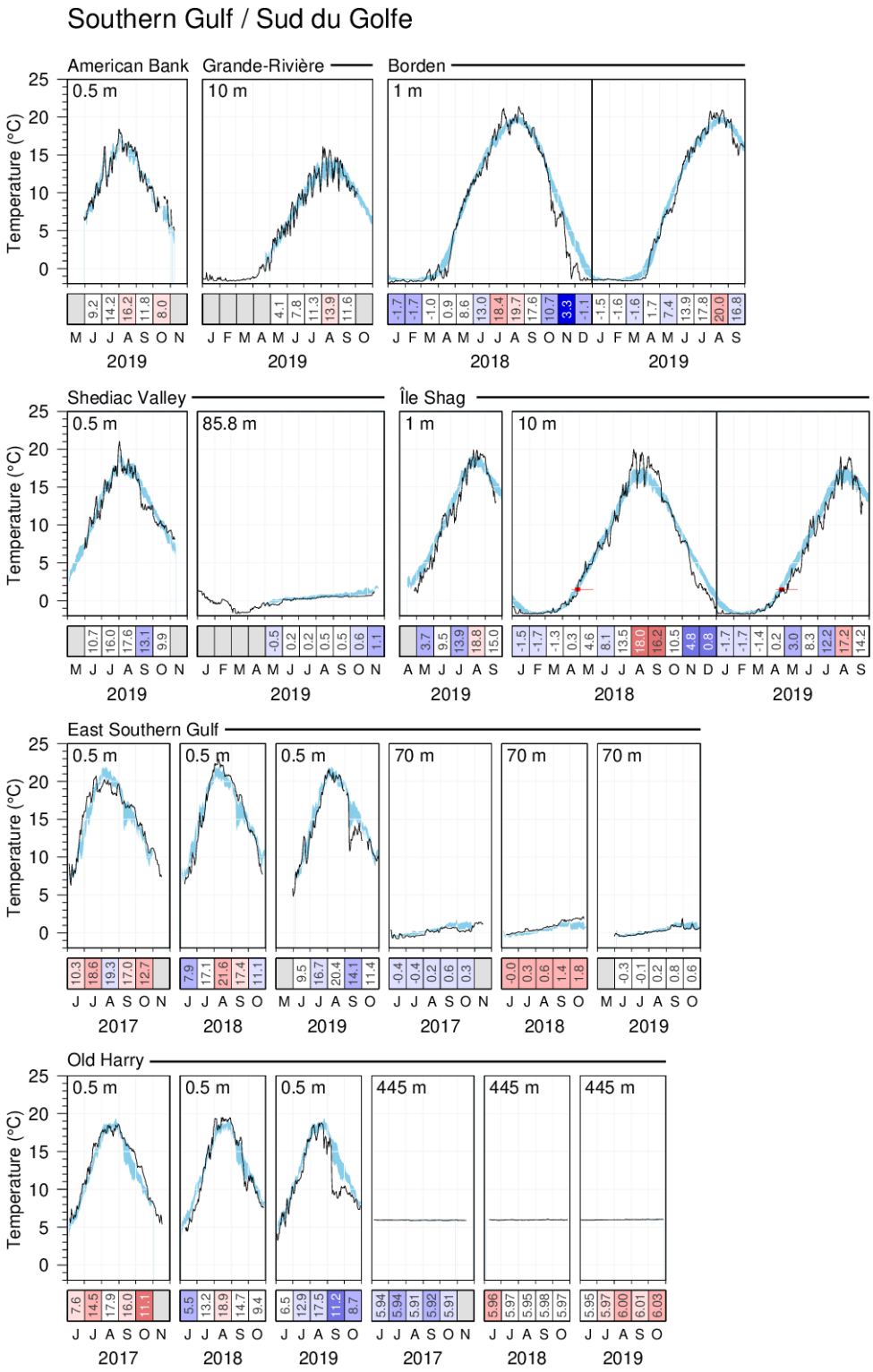

Fig. 25. Thermograph network data. Daily mean 2019 temperatures compared with the daily climatology (daily averages ± 0.5 SD; blue area) for stations of the southern Gulf. Data from 2018 are included for stations collecting data year-round, and data for the last 3 years for new stations East Southern Gulf and Old Harry. Thin red lines in the Île Shag panel span the historical dates when spring temperature increased over 1.5°C, a temperature associated with increased lobster mobility. Thick red line indicates mean date plus and minus 0.5 SD.

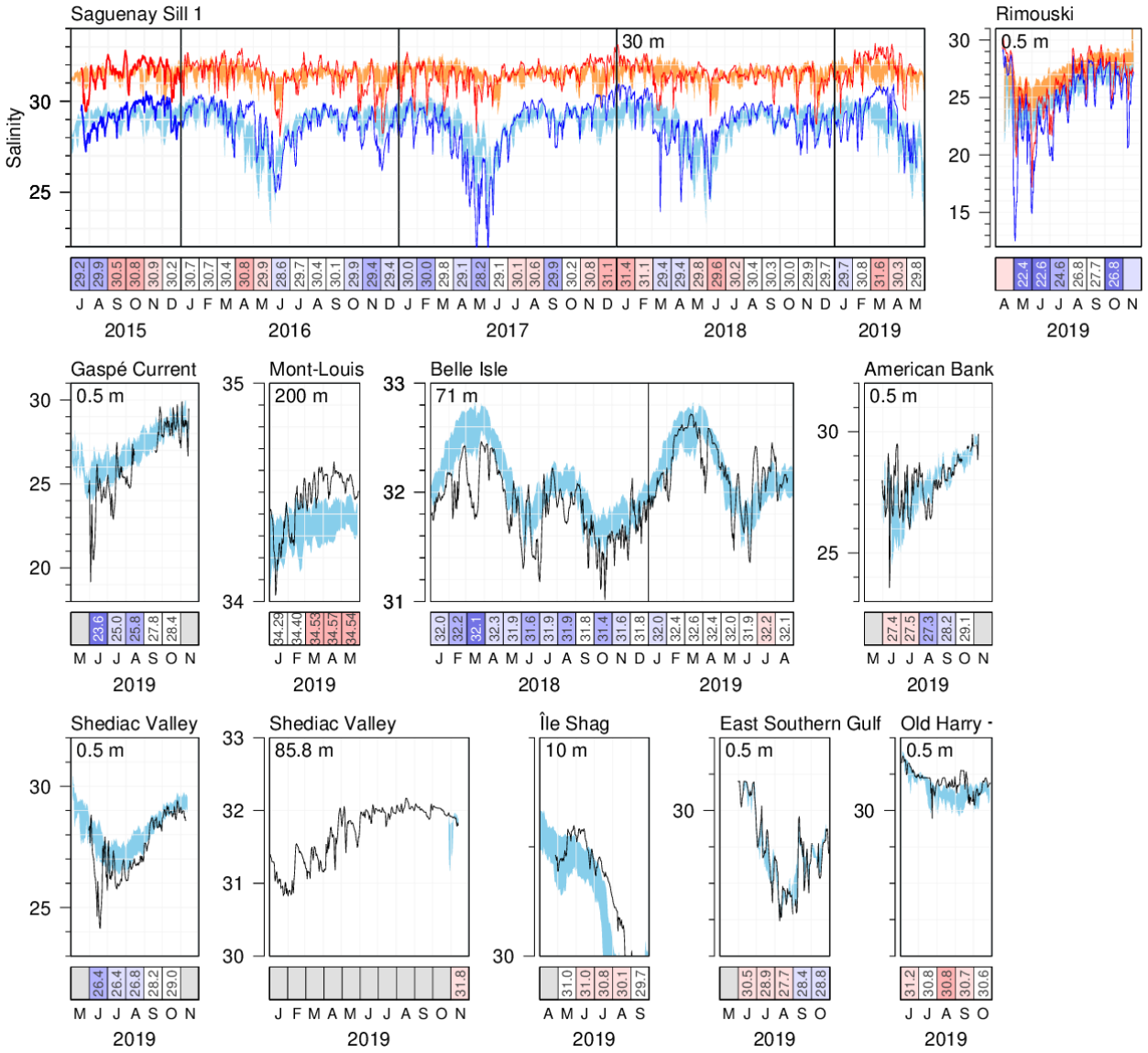

Fig. 26. Thermograph network data. Daily mean 2019 salinities (black lines) compared with the daily climatology (daily averages ± 0.5 SD; blue area) computed from all available stations. Stations that exhibit large tidal variations are displayed showing daily minimum (blue) and maximum (red) values, overlying daily climatological averages ± 0.5 SD of the minimum (blue shaded area) and maximum (orange shaded areas) values. Data from 2018 are included for stations collecting data year-round and since 2015 for the new station Saguenay Sill 1. The scorecards show monthly average salinities colour-coded according to the normalized anomalies based on the climatologies for each month.

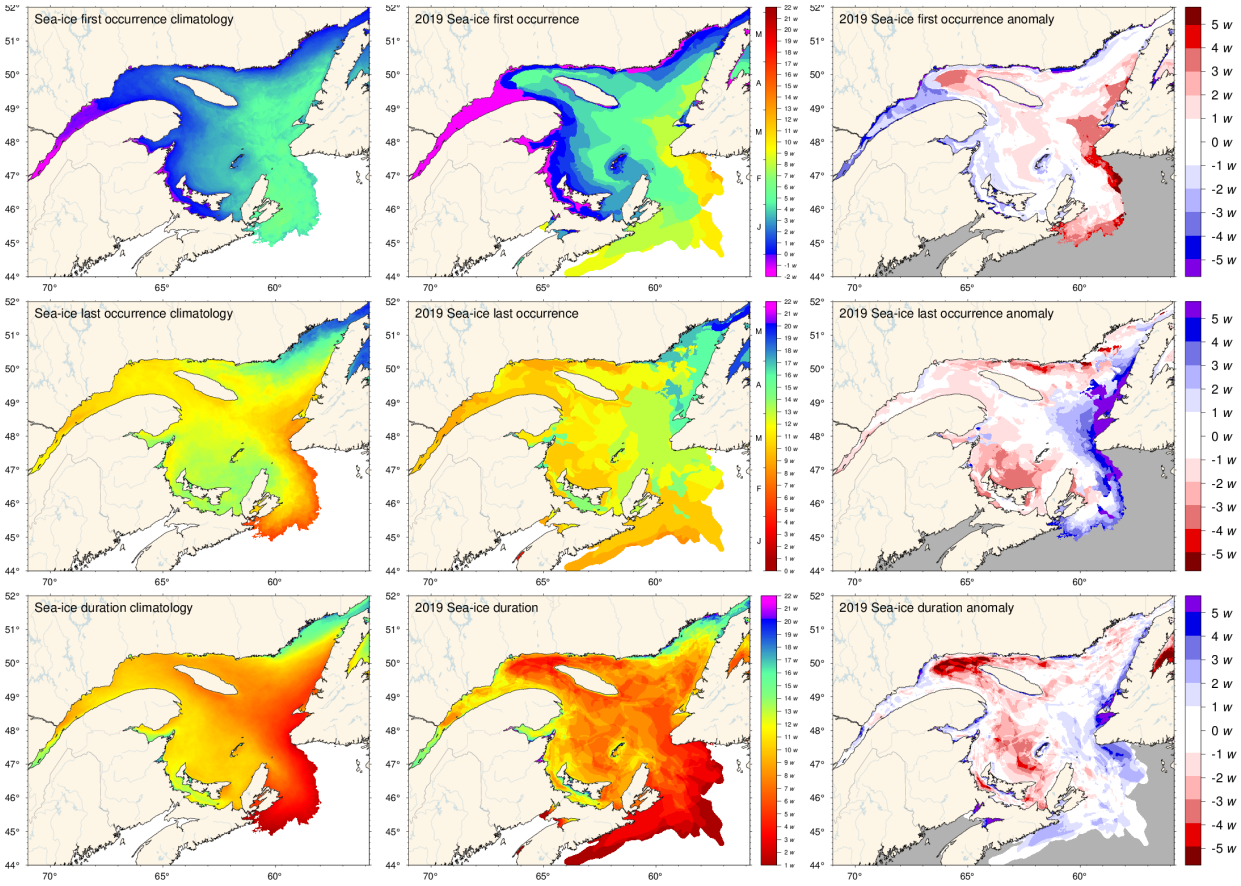

Fig. 27. First and last occurrence of ice and ice season duration based on weekly data. The 1981–2010 climatologies are shown (left) as well as the 2019 values (middle) and anomalies (right). First and last occurrence is defined here as the first and last weekly chart in which any amount of ice is recorded for each pixel and are illustrated as day-of-year. Ice duration sums the number of weeks with ice cover for each pixel. Climatologies are shown for pixels that had at least 15 years out of the 30 with occurrence of sea-ice, and therefore also show the area with 50% likelihood of having some sea-ice at any time during any given year.

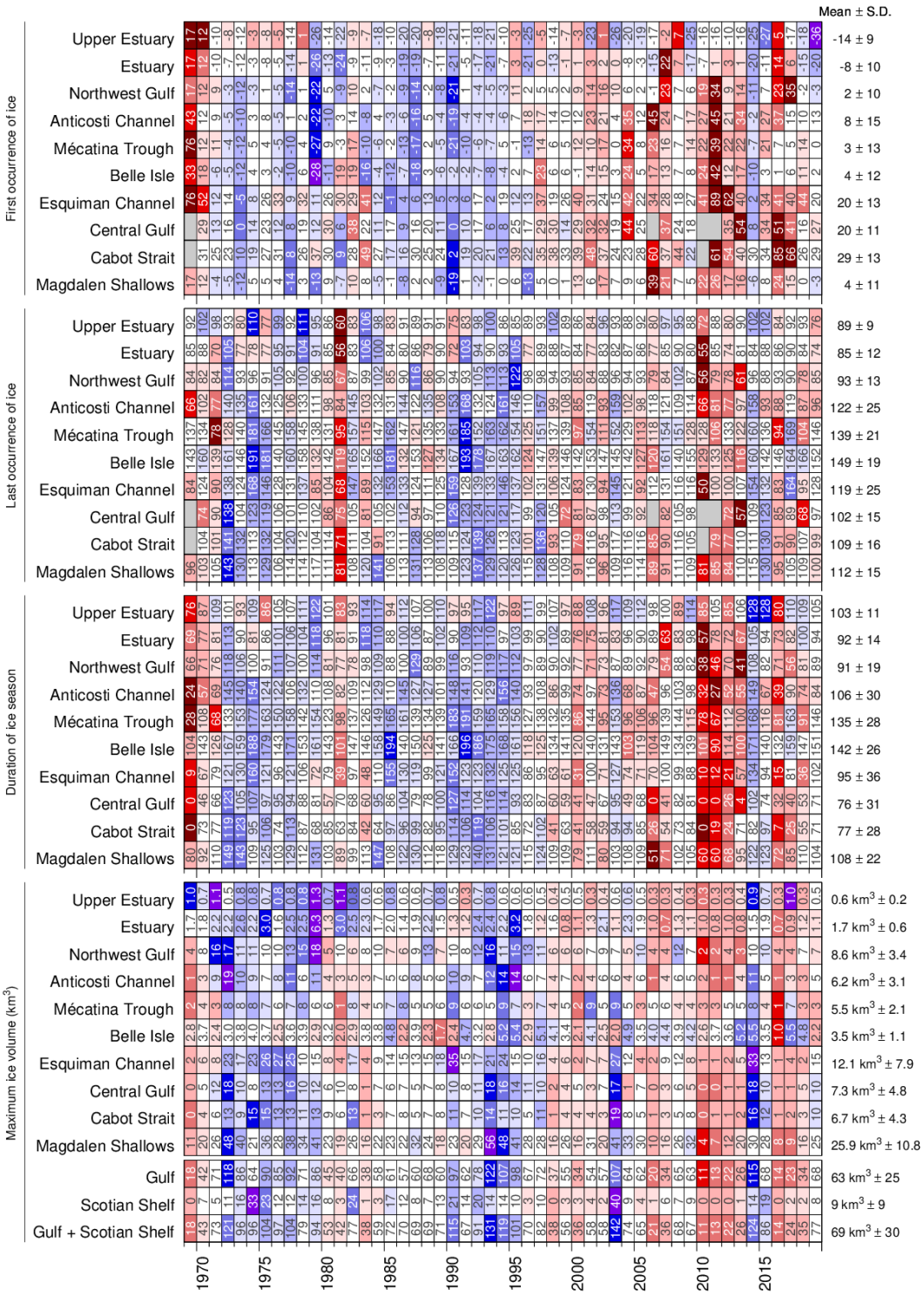

Fig. 28. First and last day of ice occurrence, ice duration and maximum seasonal ice volume by region. The time when ice was first and last seen in days from the beginning of each year is indicated for each region, and the colour code expresses the anomaly based on the 1981–2010 climatology, with blue (cold) representing earlier first occurrence and later last occurrence. The threshold is 5% of the largest ice volume ever recorded in the region. Numbers in the table are the actual day of the year or volume, but the colour coding is according to normalized anomalies based on the climatology of each region. Duration is the numbers of days that the threshold was exceeded. All results based on weekly data.

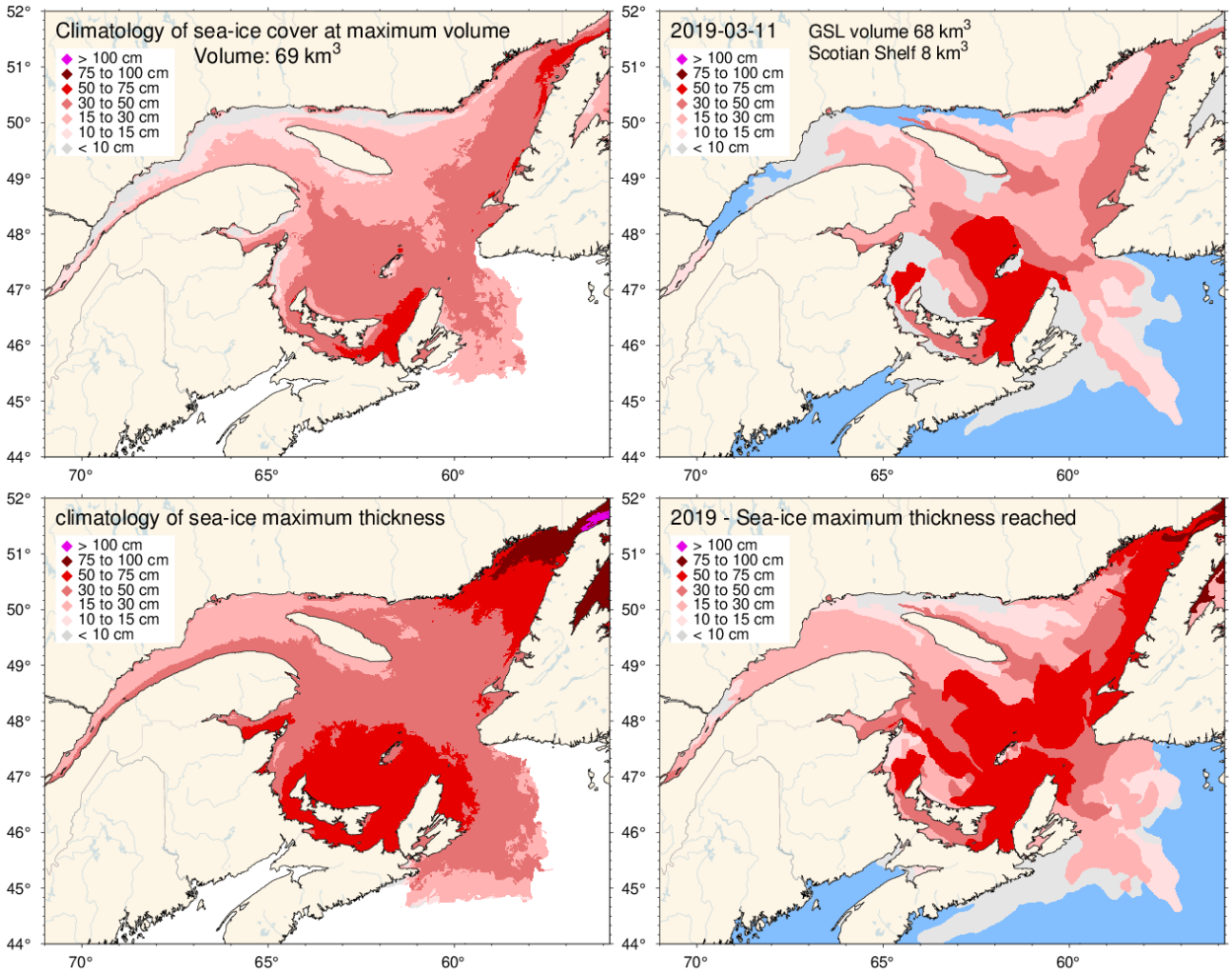

Fig. 29. Ice thickness map for 2019 for the week of the year with the maximum annual volume including the portion covering the Scotian Shelf (upper right panel) and similarly for the 1981–2010 climatology of the weekly maximum (upper left panel). Note that these maps reflect the ice thickness distribution on that week, and not the maximum observed at any given location during the year. That information is shown by the lower panels, showing the 1981–2010 climatology and 2019 distribution of the thickest ice recorded during the season at any location.

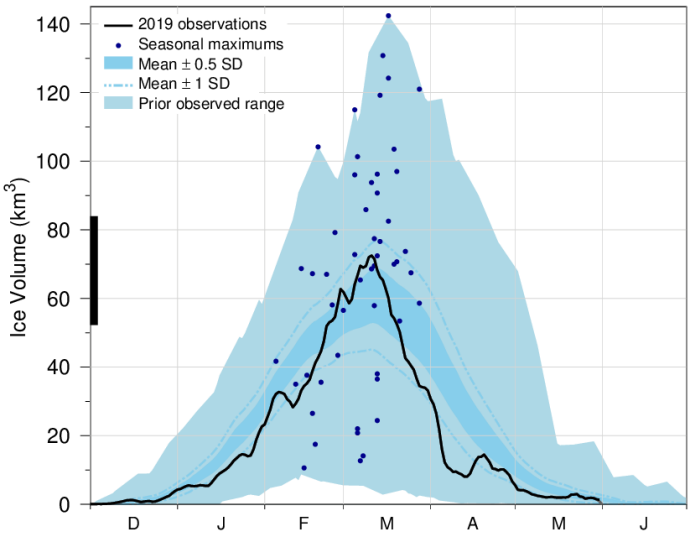

Fig. 30. Time series of the 2018-2019 daily mean ice volume for the Gulf of St. Lawrence and Scotian Shelf (black line), the 1981–2010 climatological mean volume plus and minus 0.5 and 1 SD (dark blue area and dashed line), the minimum and maximum span of 1969-2019 observations (light blue) and the date and volumes of 1969-2019 seasonal maximums (blue dots). The black thick line on the left indicates the mean volume plus and minus 0.5 SD of the annual maximum ice volume, which is higher than the peak of the mean daily ice volume distribution.

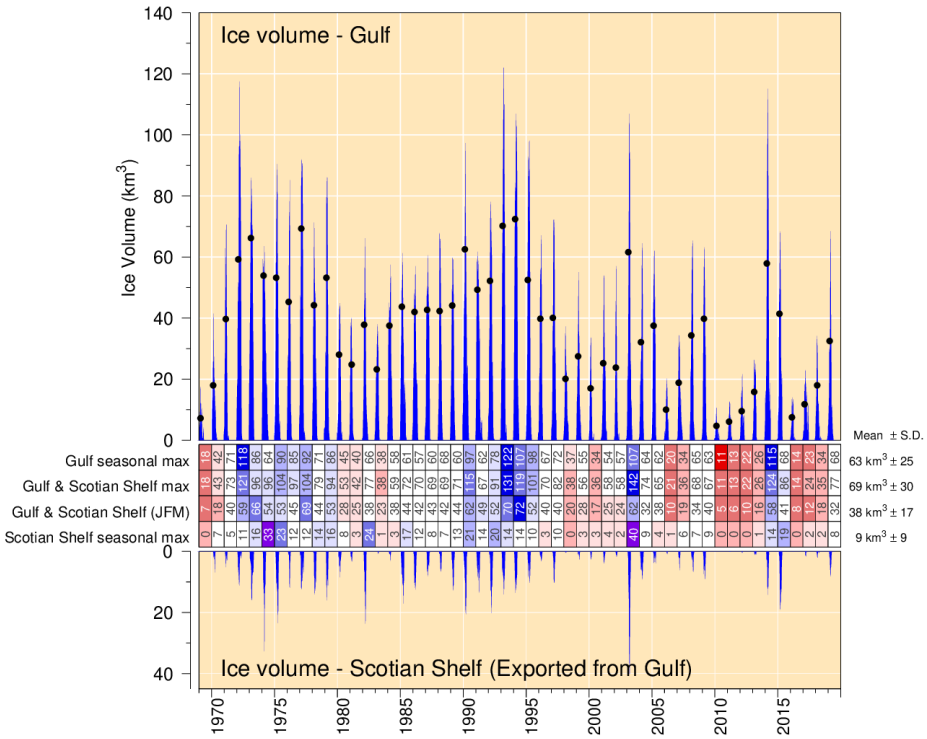

Fig. 31. Estimated weekly maximum ice volume in the Gulf of St. Lawrence (upper panel) and on the Scotian Shelf seaward of Cabot Strait defined by its narrowest crossing (lower panel). Dots show January-March averages of combined Gulf and Scotian Shelf volumes. Scorecards show numbered normalized anomalies for the Gulf, combined Gulf and Scotian Shelf, combined Gulf and Shelf January to March average, and Shelf-only annual maximum volumes from weekly ice data. The mean and standard deviation are indicated on the right side using the 1981–2010 climatology.

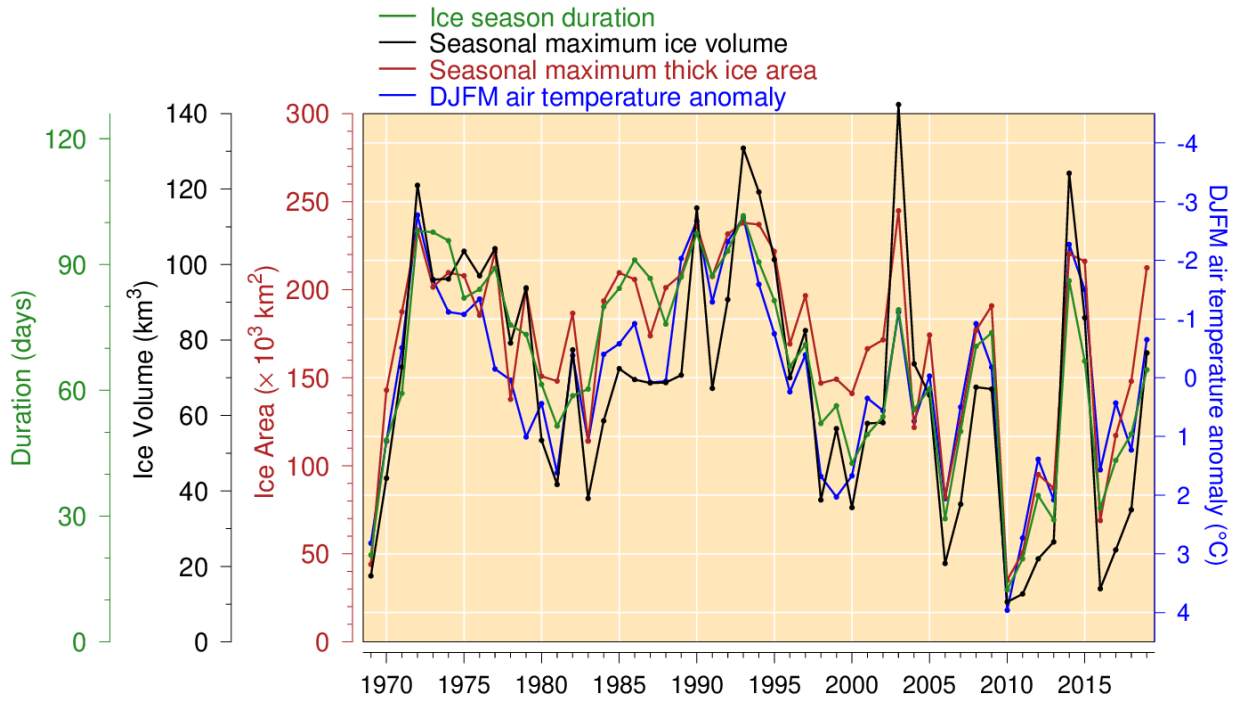

Fig. 32. Seasonal maximum ice volume and area including the portion on the Scotian Shelf (excluding ice less than 15 cm thick), ice season duration and December-to-March air temperature anomaly (Figure adapted from Hammill and Galbraith 2012, but here not excluding small floes and adding February and March data to the air temperature anomalies). All sea-ice products are based on weekly data. Mean duration obtained as spatial average of Fig. 27, excluding the Scotian Shelf, with zeros counted if no ice is present but the climatology has some. Linear relations indicate losses of 18 km^3, 31,000 km^2 and 13 days of sea-ice season for each 1°C increase in winter air temperature (R^2 of 0.72, 0.78 and 0.80 respectively).

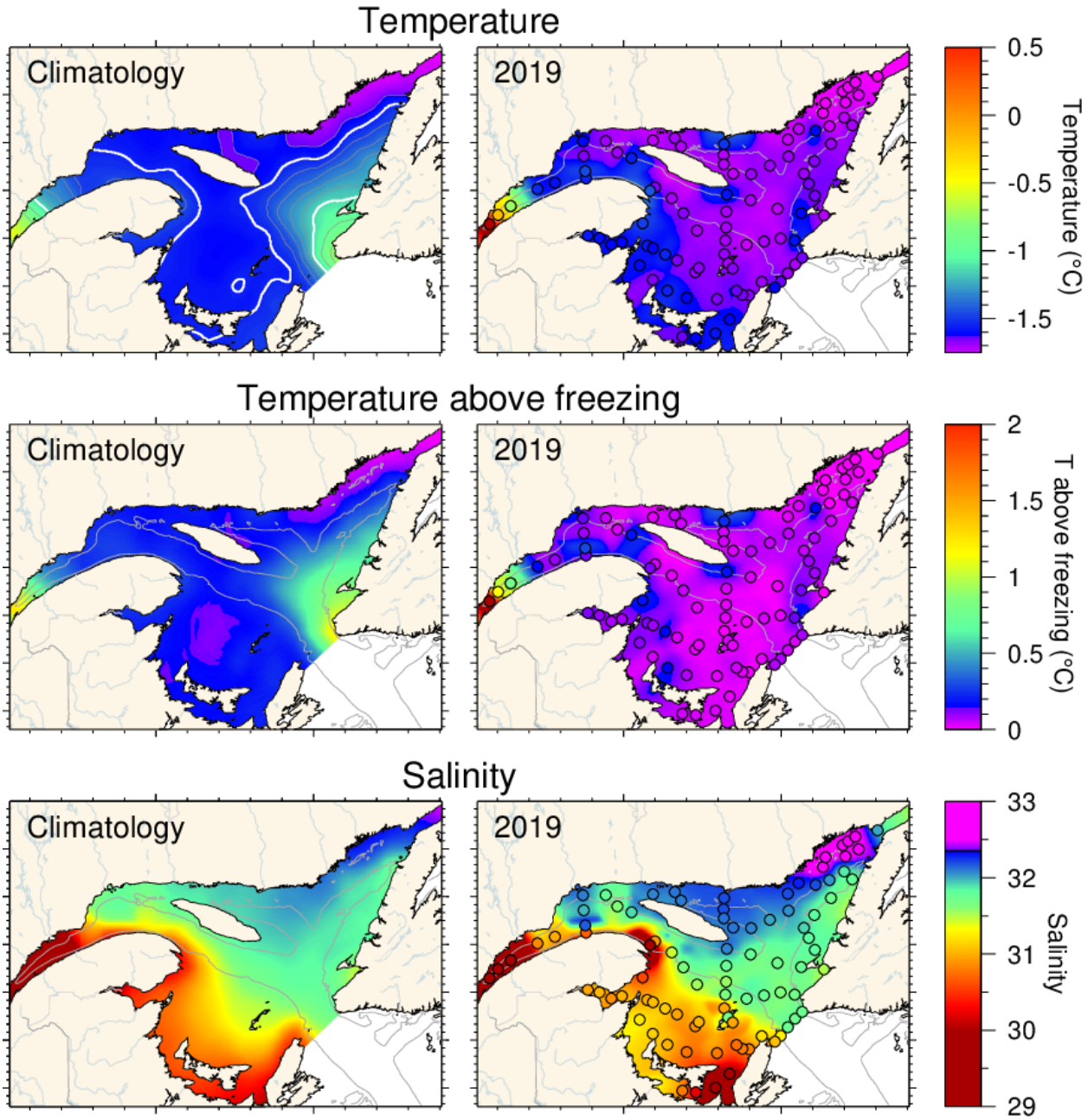

Fig. 33. Winter surface layer characteristics from the March 2019 survey compared with climatological means: surface water temperature (upper panel), temperature difference between surface water temperature and the freezing point (middle panel), and salinity (lower panel). Symbols are coloured according to the value observed at the station, using the same colour palette as the interpolated image. A good match is seen between the interpolation and the station observations where the station colours blend into the background. Black symbols indicate missing or bad data. The climatologies are based on 1996–2019 for salinity but exclude 2010 as an outlier for temperature and temperature above freezing.

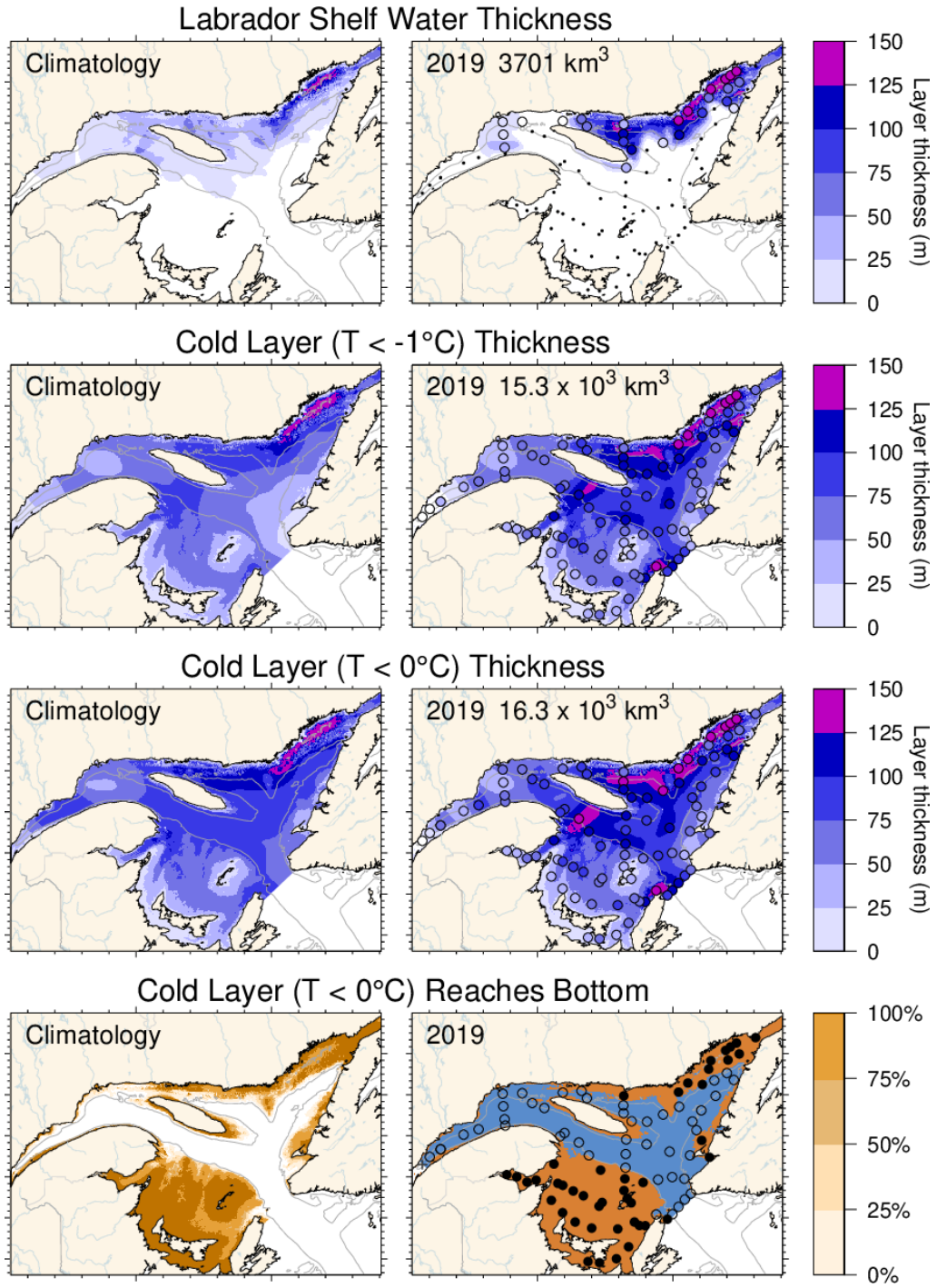

Fig. 34. Winter surface layer characteristics from the March 2019 survey compared with climatological means: estimates of the thickness of the Labrador Shelf water intrusion (upper panels), cold layer (T<-1°C, T<0°C) thickness (middle panels), and maps indicating where the cold layer (T<0°C) reaches the bottom (in brown; lower panels). Station symbols are coloured according to the observed values as in Fig. 33. For the lower panels, the stations where the cold layer reached the bottom are indicated with filled circles while open circles represent stations where the layer did not reach the bottom. Integrated volumes are indicated for the first six panels (including an approximation for the Estuary but excluding the Strait of Belle Isle). The climatologies are based on 1997–2019 for the Labrador Shelf water intrusion, 1996–2019 for the cold layer (T<0°C) but excludes 2010 for T<-1°C.

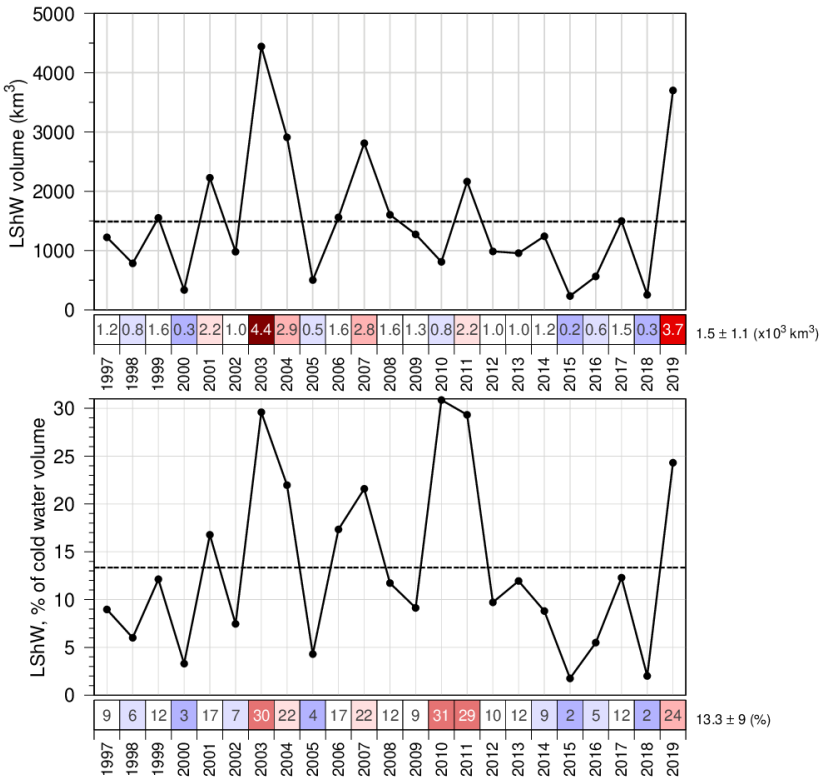

Fig. 35. Estimated volume of cold and saline Labrador Shelf water that flowed into the Gulf over the winter through the Strait of Belle Isle. The bottom panel shows the volume as a percentage of total cold-water volume (<-1ºC). The numbers in the boxes are actual values colour-coded according to their 1997–2019 climatology anomaly. Coverage of Mecatina Trough was insufficient in 1996 to provide an estimated volume.

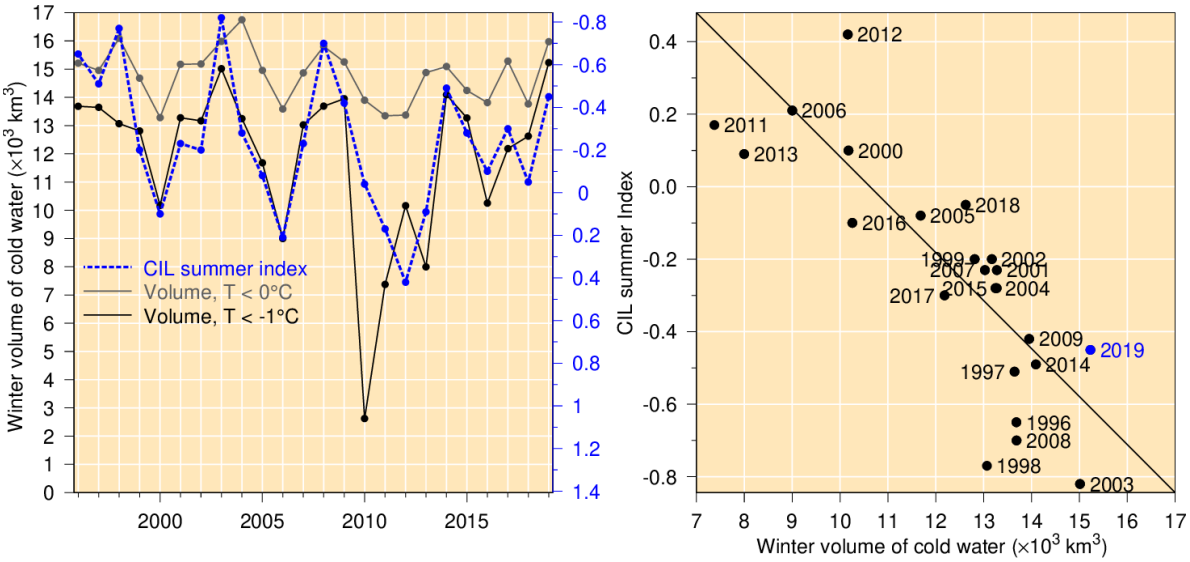

Fig. 36. Left panel: winter surface cold (T<-1°C and T<0°C) layer volume (excluding the Estuary and the Strait of Belle Isle) time series (black and grey lines) and summer CIL index (blue dashed line). Right panel: Relation between summer CIL index and winter cold-water volume with T<-1°C (regression for 1996–2019 data pairs, excluding 1998 [see Galbraith 2006] as well as the 2010 and 2011 mild winters). Note that the CIL scale in the left panel is reversed.

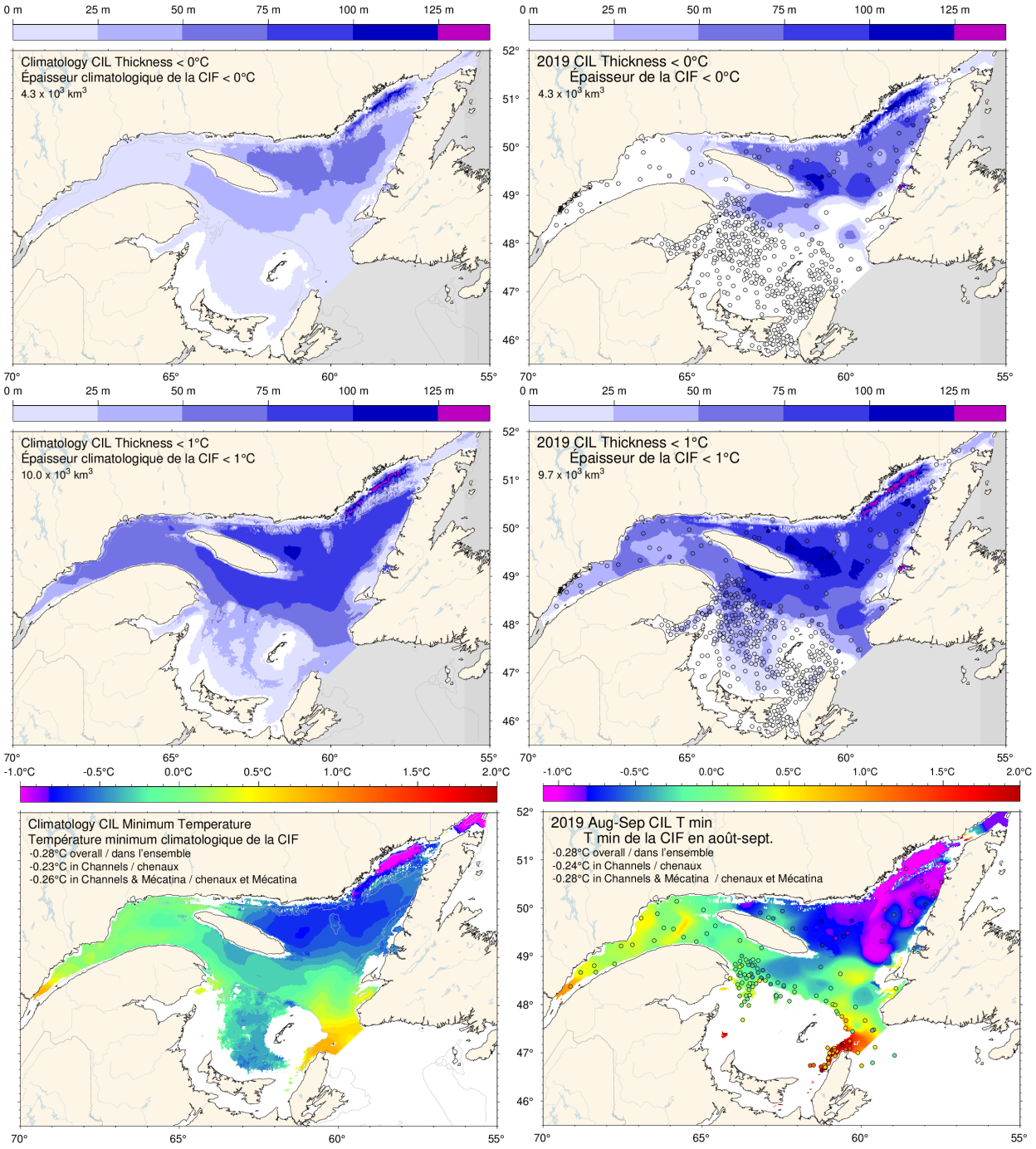

Fig. 37. Cold intermediate layer thickness (T<0ºC, top panels; T<1ºC, middle panels) and minimum temperature (bottom panels) in August and September 2019 (right) and 1981–2010 climatology (left). Station symbols are colour-coded according to their CIL thickness and minimum temperature. Numbers in the upper and middle panels are integrated CIL volumes and in the lower panels are monthly average temperatures.

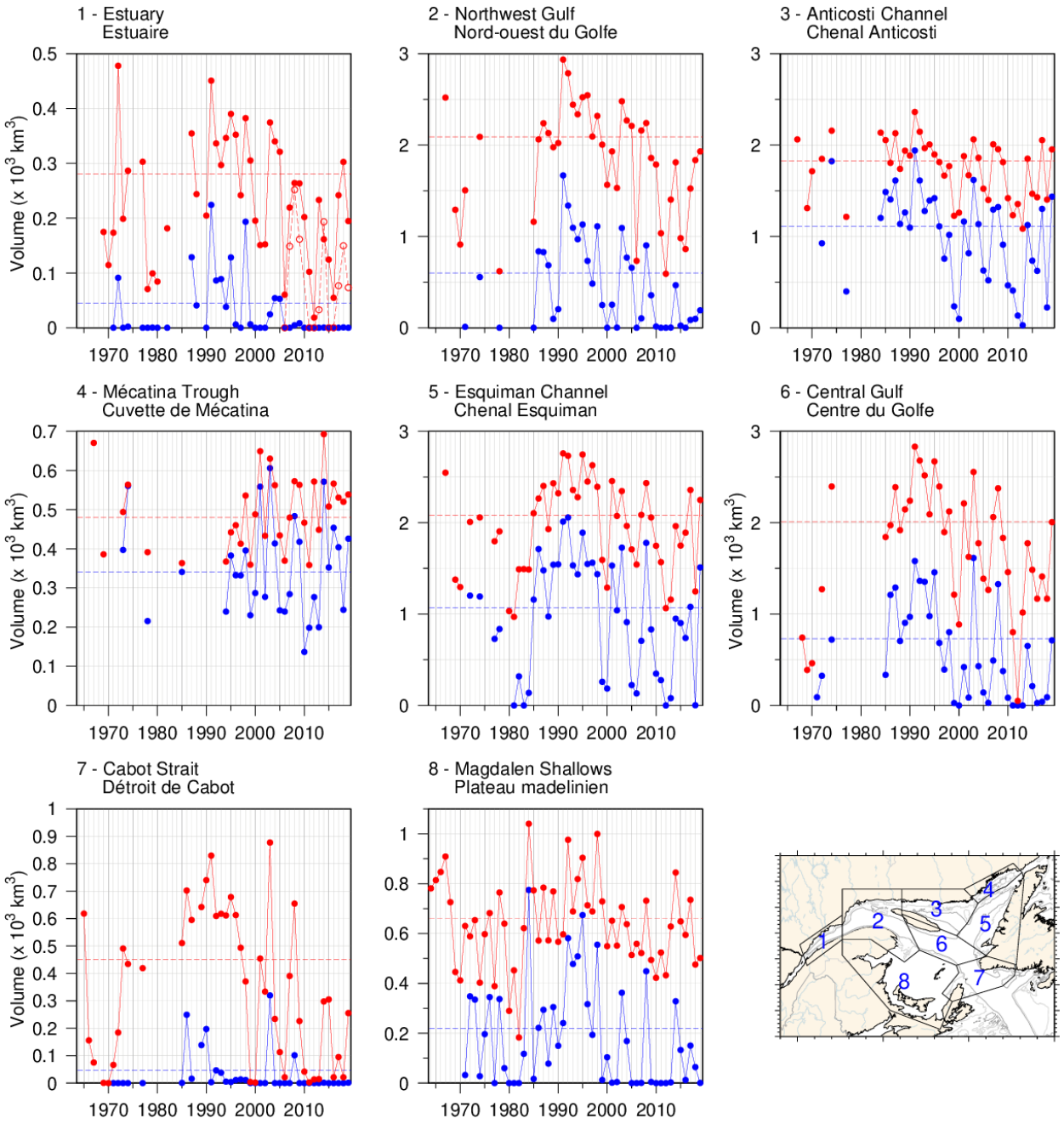

Fig. 38. Volume of the CIL colder than 0ºC (blue) and colder than 1ºC (red) in August and September (primarily region 8 in September). The volume of the CIL colder than 1ºC in November for available years since 2006 is also shown for the St. Lawrence Estuary (dashed line).

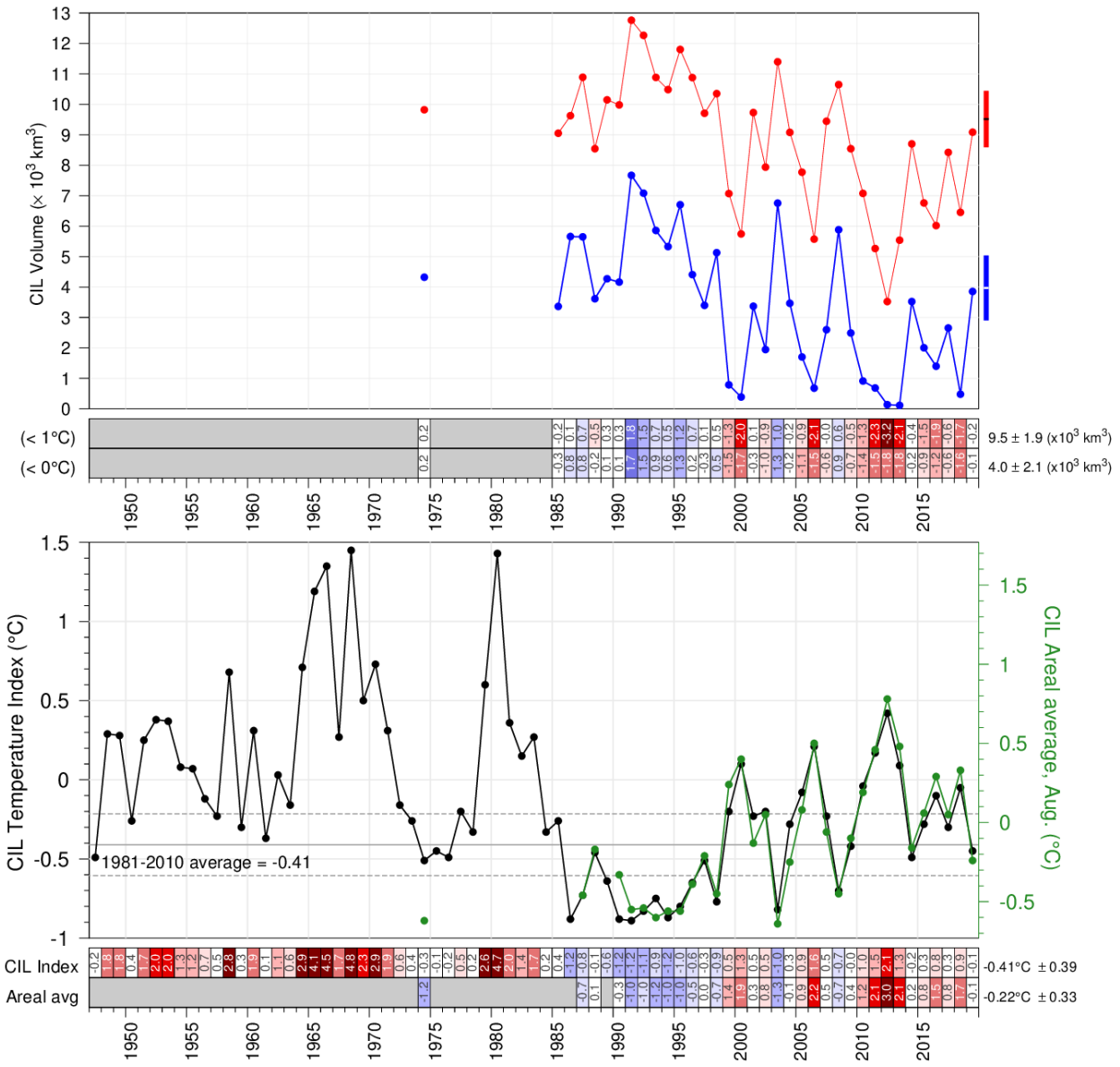

Fig. 39. CIL volume (top panel) delimited by 0ºC (in blue) and 1ºC (in red), and minimum temperature index (bottom panel) in the Gulf of St. Lawrence. The volumes are integrals of each of the annual interpolated thickness grids such as those shown in the top panels of Fig. 37 excluding Mécatina Trough and the Strait of Belle Isle. Rectangles on right side show mean ± 0.5 SD. In the lower panel, the black line is the updated Gilbert and Pettigrew (1997) index interpolated to 15 July (with dashed lines showing mean ± 0.5 SD) and the green line is the spatial average of each of the annual interpolated grid such as those shown in the two bottom panels of Fig. 37, excluding Mécatina Trough, the Strait of Belle Isle and the Magdalen Shallows. The numbers in the boxes are normalized anomalies relative to 1980-2010 climatologies constructed using all available years.

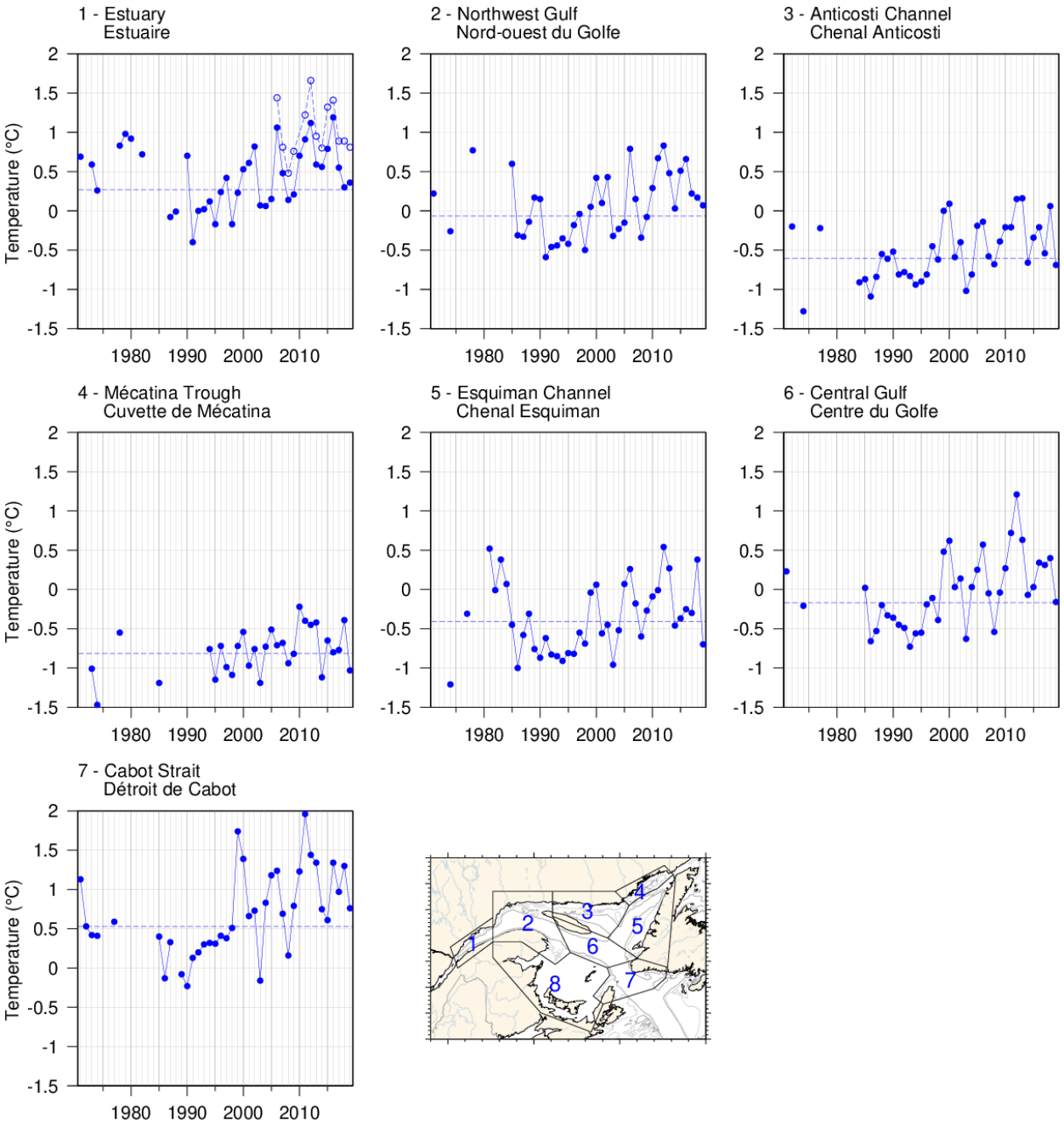

Fig. 40. Temperature minimum of the CIL spatially averaged for the seven areas where the CIL minimum temperature can be clearly identified. The spatial average of the November CIL temperature minimum for available years since 2006 is also shown for the St. Lawrence Estuary (dashed line).

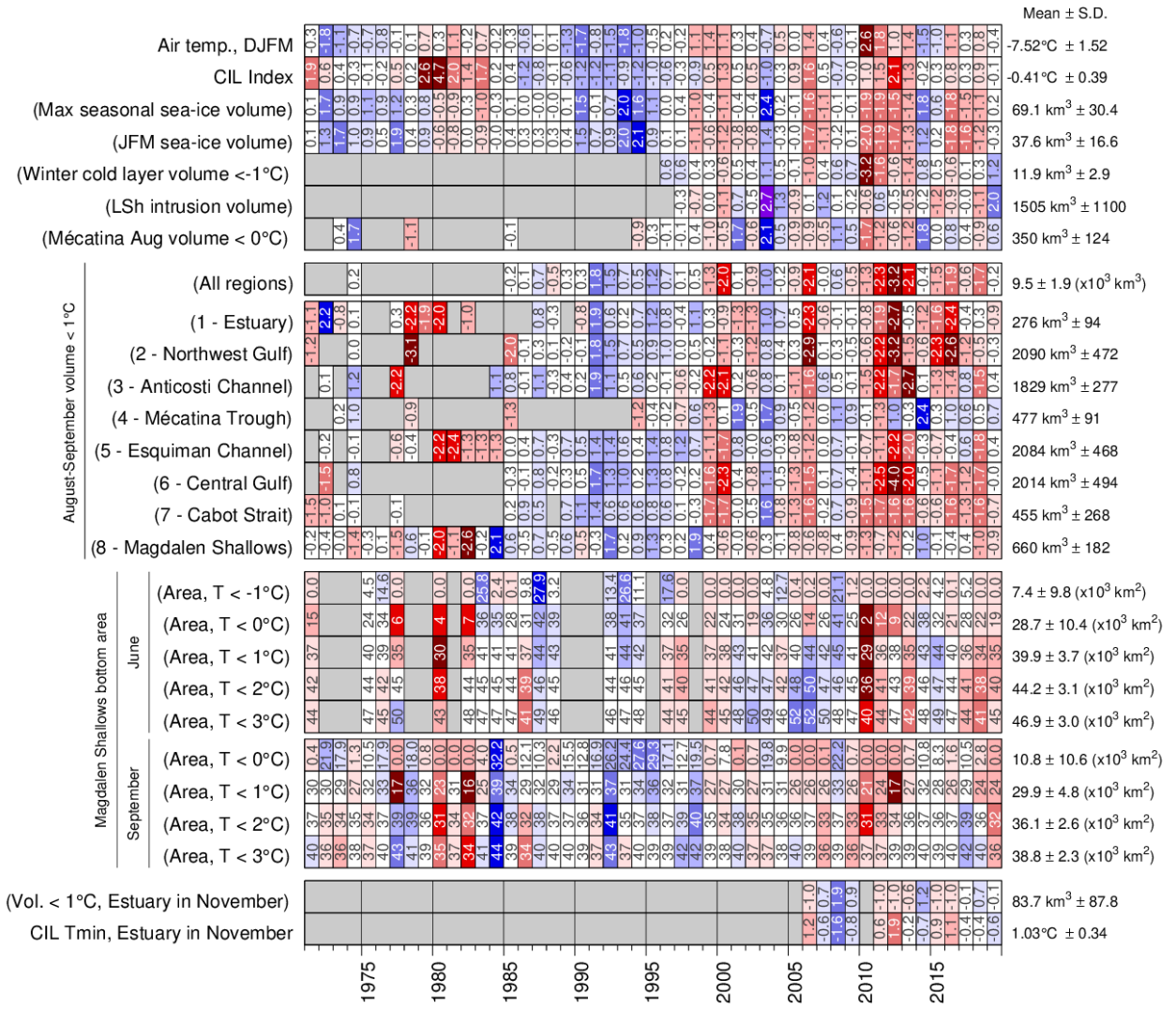

Fig. 41. Winter and summertime CIL related properties. The top block shows the scorecard time series for Dec-Jan-Feb-March air temperature (Fig. 5), the Gilbert and Pettigrew (1997) CIL index, yearly maximum sea-ice volume (Gulf + Scotian Shelf), Dec-Jan-Feb average sea-ice volume, winter (March) cold-layer (<-1°C) volume, volume of Labrador Shelf Water intrusion into the Gulf observed in March, and the August–September volume of cold water (<0°C) observed in the Mécatina Trough. Labels in parentheses have their colour coding reversed (blue for high values). The second block shows scorecard time series for August–September CIL volumes (<1°C) for all eight regions and for the entire Gulf when available. The third block shows the scorecard time series for the bottom areas of the Magdalen Shallows covered by waters colder than 0, 1, 2, and 3°C during the June and September survey. The last block shows the November survey CIL volume (<1°C) and average CIL minimum temperature in the Estuary. Numbers in cells express anomalies in units of standard deviation, except for bottom areas which are expressed in units of area (×10³ km²) (because of the occurrence of zeros).

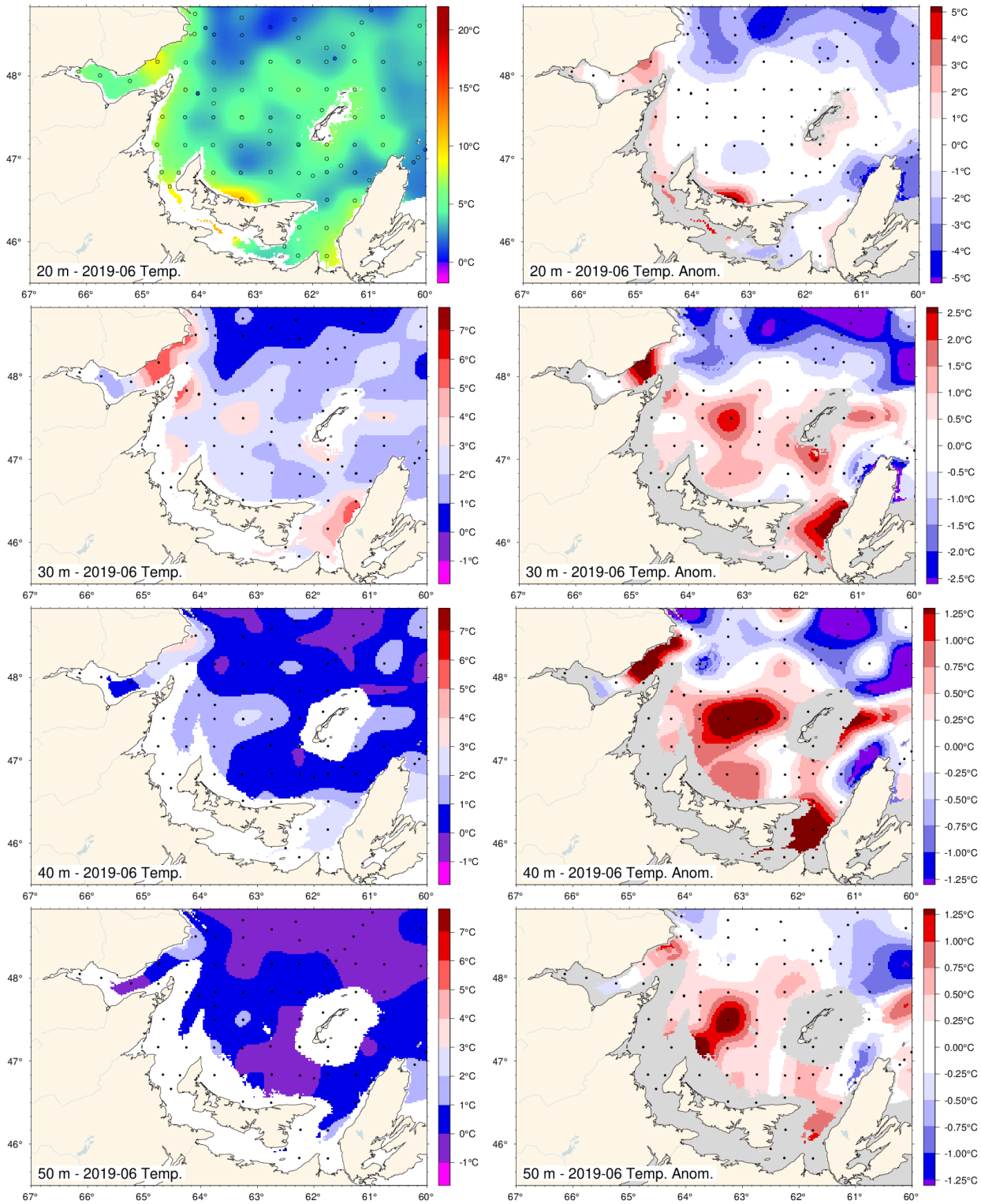

Fig. 42. June depth-layer temperature and anomaly fields on the Magdalen Shallows at 20, 30, 40 and 50 m. Anomalies are based on 1981-2010 climatologies for all available years (appearing on Fig. 43). Dots are station occupations.

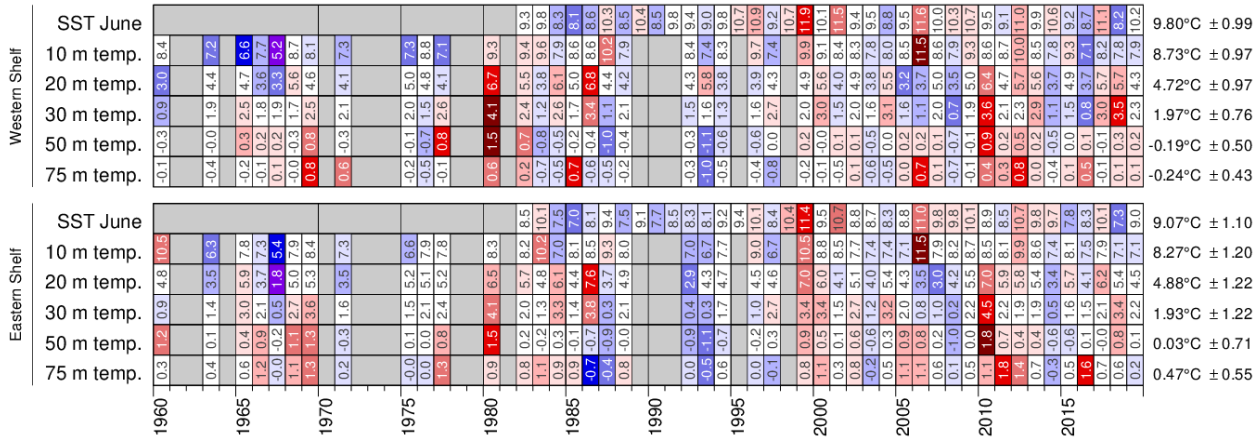

Fig. 43. Depth-layer average temperature anomalies for western and eastern Magdalen Shallows for the June mackerel survey. The SST data are June averages from NOAA remote sensing repeated from Fig. 21. The colour-coding are according to normalized anomalies based on the 1981–2010 climatologies, but the numbers are mean temperatures in ºC.

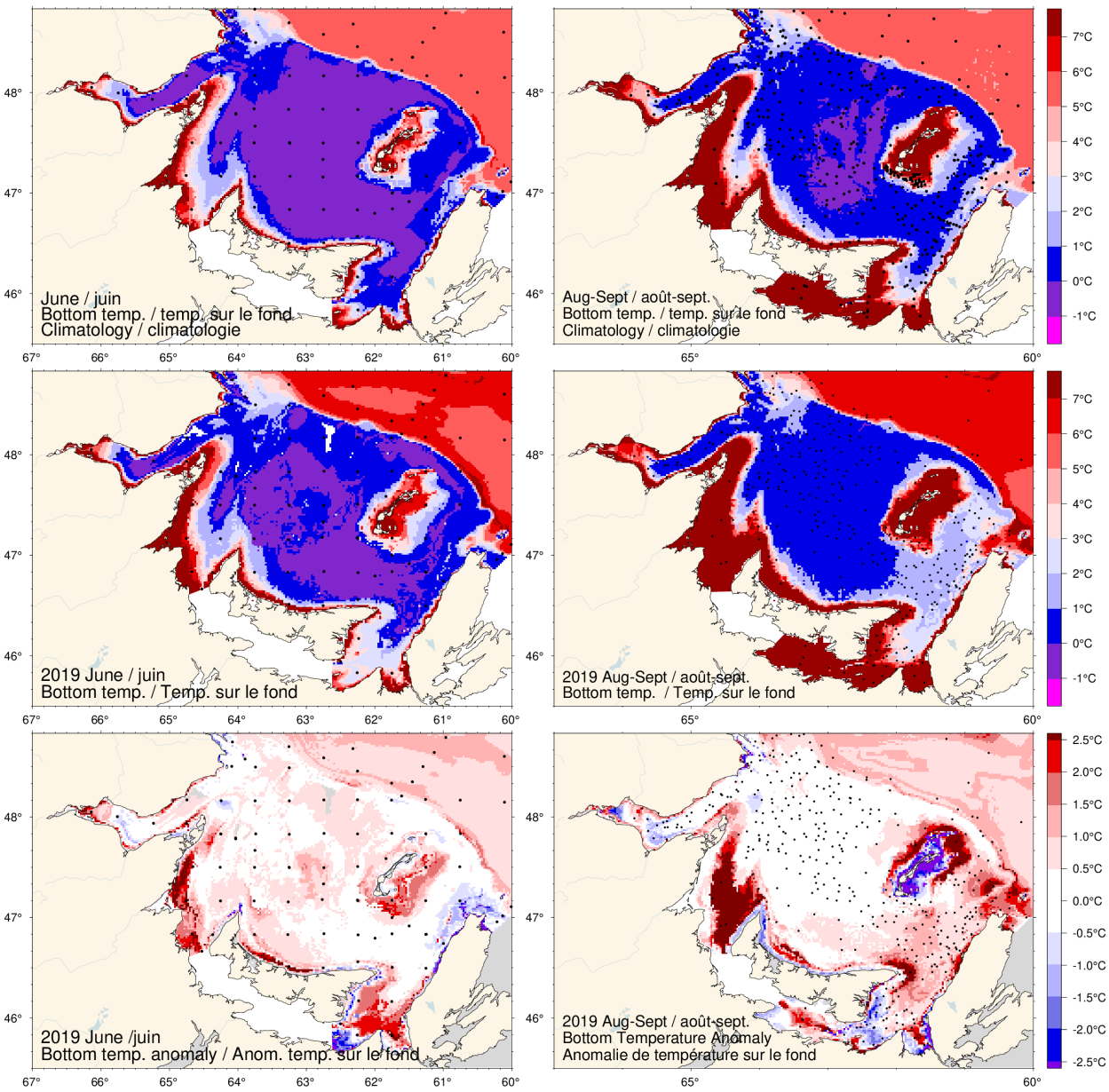

Fig. 44. June (left) and August-September (right) bottom temperature climatology (top), 2019 observations (middle) and anomaly (bottom).

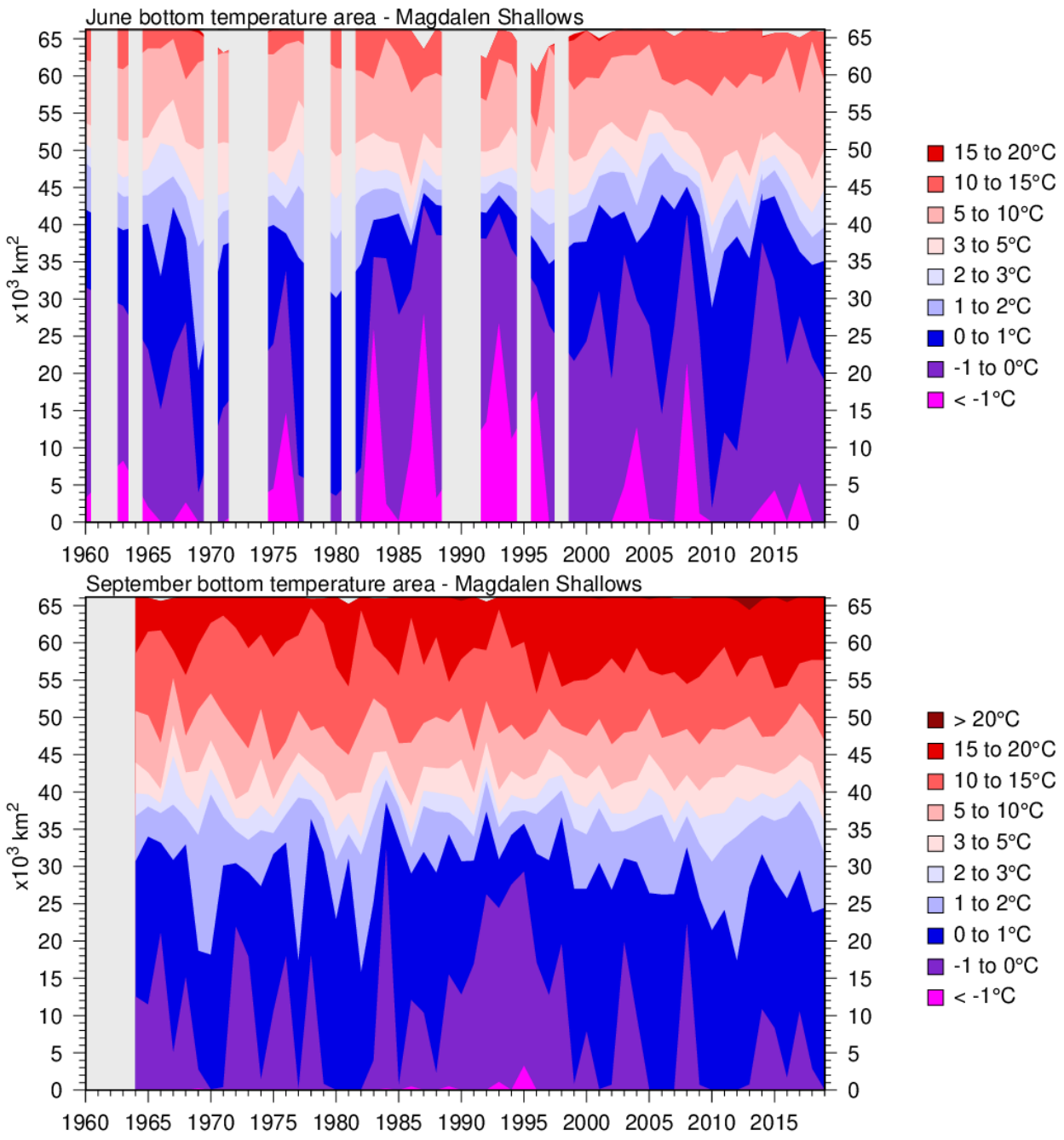

Fig. 45. Time series of the bottom areas covered by different temperature bins in June (top) and August-September (bottom) for the Magdalen Shallows (region 8). Data are mostly from September for the bottom panel.

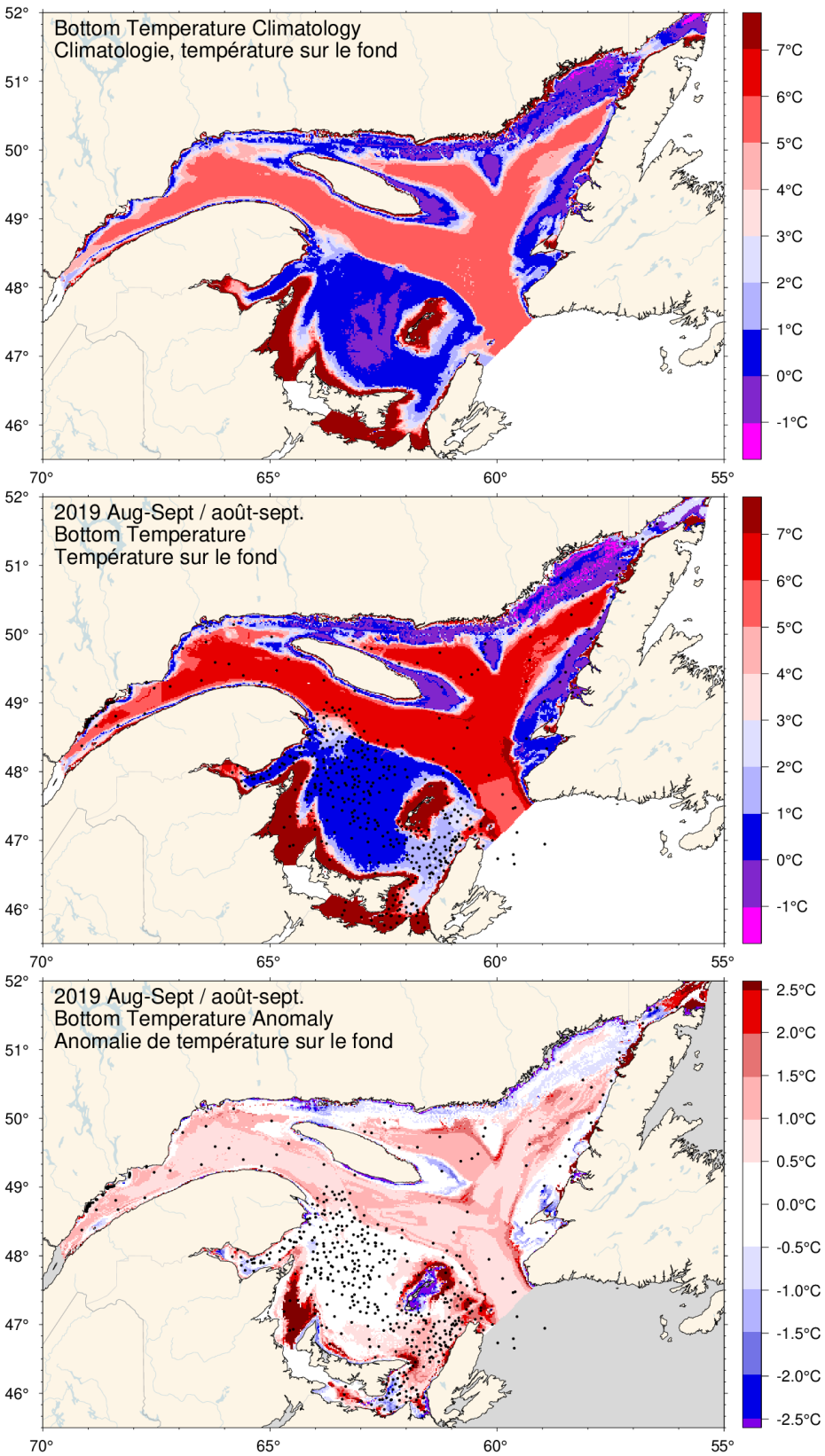

Fig. 46. August-September bottom temperature climatology (top), 2019 observations (middle) and anomaly (bottom).

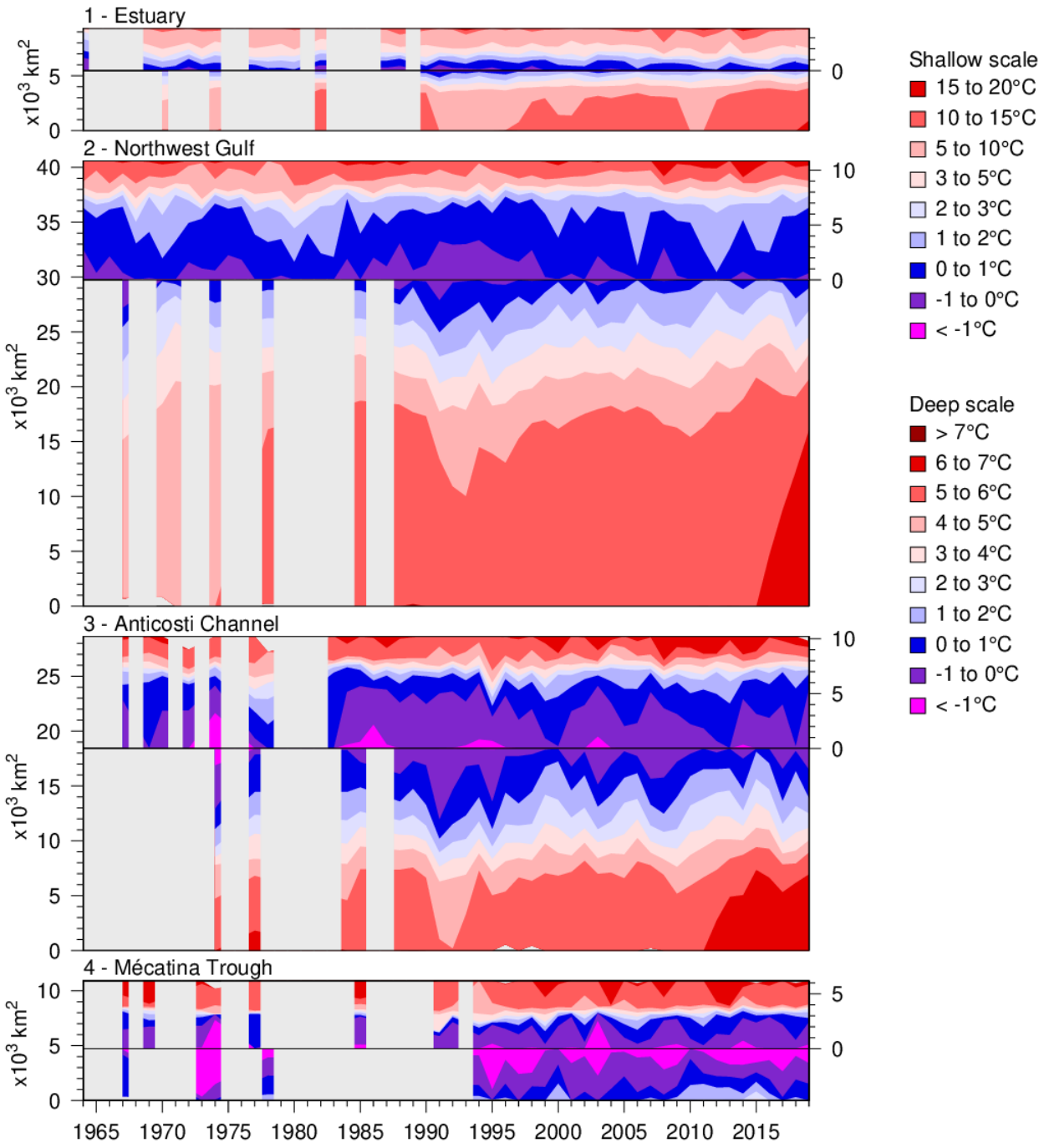

Fig. 47. Time series of the bottom areas covered by different temperature bins in August and September for regions 1 to 4. The panels are separated by a black horizontal line into shallow (<100m) and deep (>100 m) areas to distinguish between warmer waters above and below the CIL. The shallow areas are shown on top using the area scale on the right-hand side and have warmer waters shown starting from the top end. The deep areas are shown below the horizontal line and have warmer waters starting at the bottom end. The CIL areas above and below 100 m meet near the horizontal line.

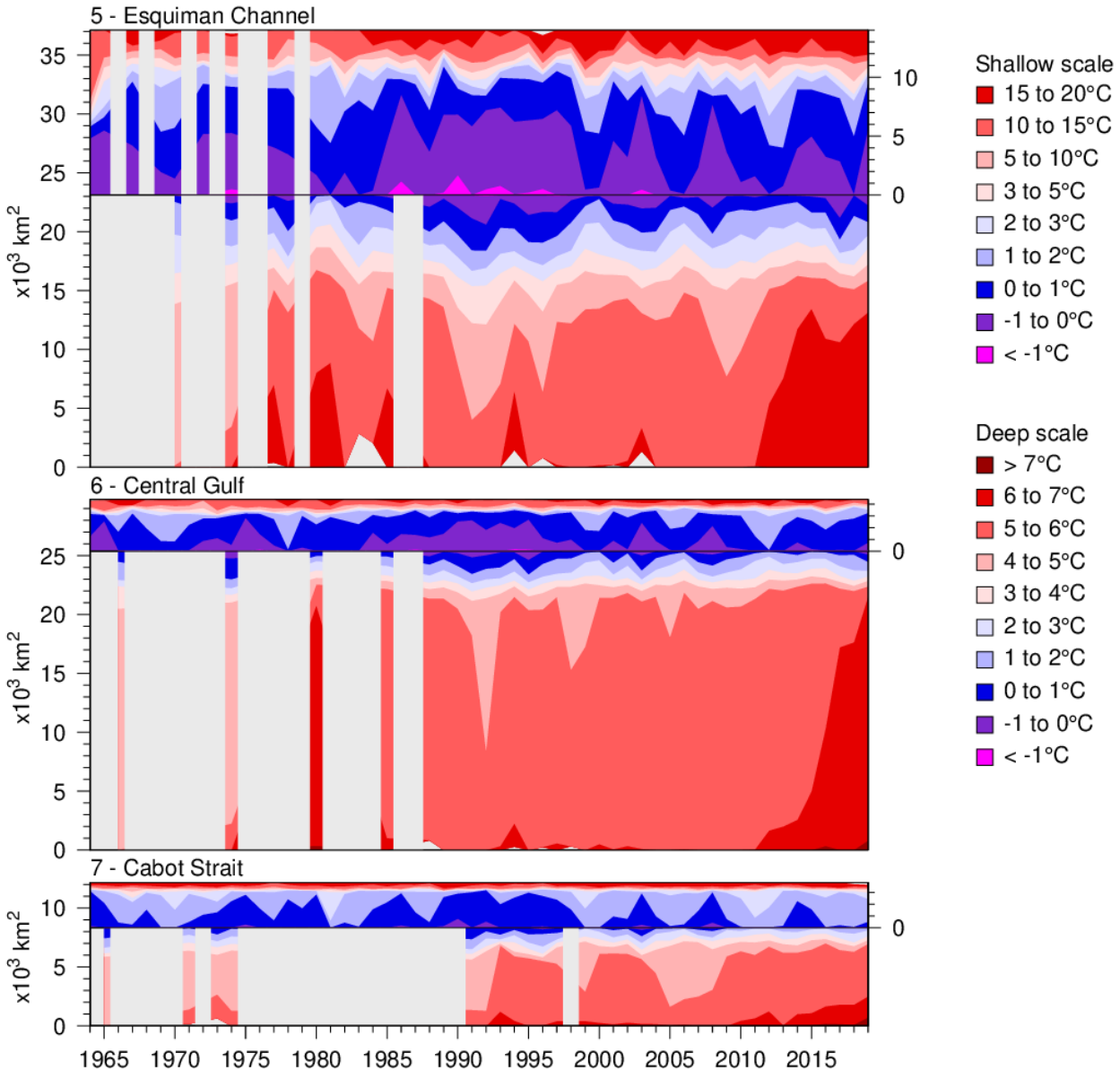

Fig. 48. Time series of the bottom areas covered by different temperature bins in August and September for regions 5 to 7. The panels are separated into shallow (<100 m) and deep (>100 m) areas to distinguish between warmer waters above and below the CIL See Fig. 47 caption.

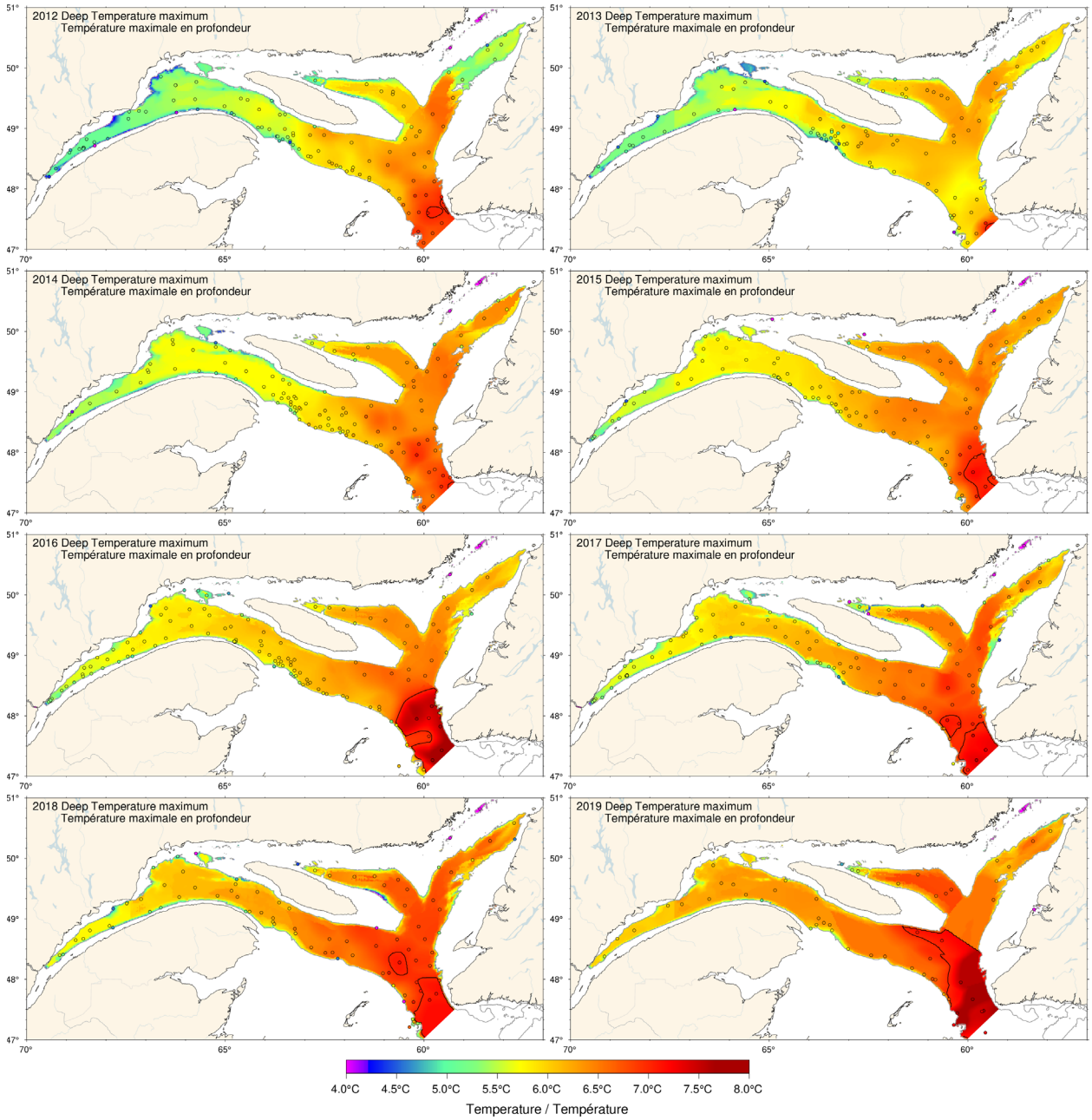

Fig. 49. Map of the deep temperature maximum found typically between 200 and 300 m, 2012–2019. Maps are interpolated from August-September data available for each year. For 2012, 2013 and 2017, casts made in Cabot Strait during the fall survey were used to fill August sampling gaps.

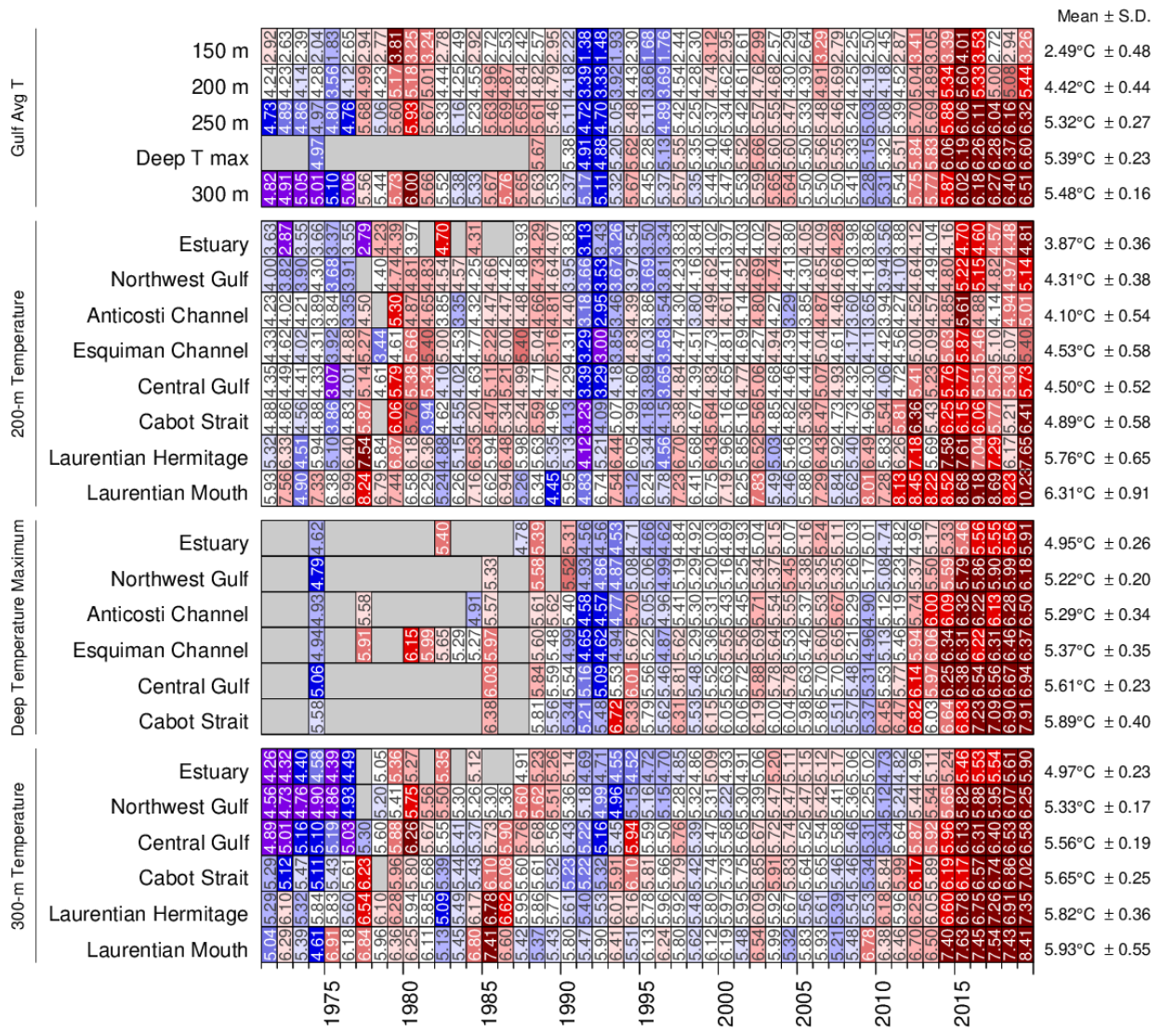

Fig. 50. Deep layer temperature. Gulf averages for temperature are shown for 150, 200, 250, 300 m, as well as for the deep temperature maximum usually found between 200 and 300 m. Regional averages are shown for 200 and 300 m, and deep temperature maximum. The numbers on the right are the 1981–2010 climatological means and standard deviations. The numbers in the boxes are average temperatures. The colour-coding is according to the temperature anomaly relative to the 1981–2010 climatology of each region and depth.

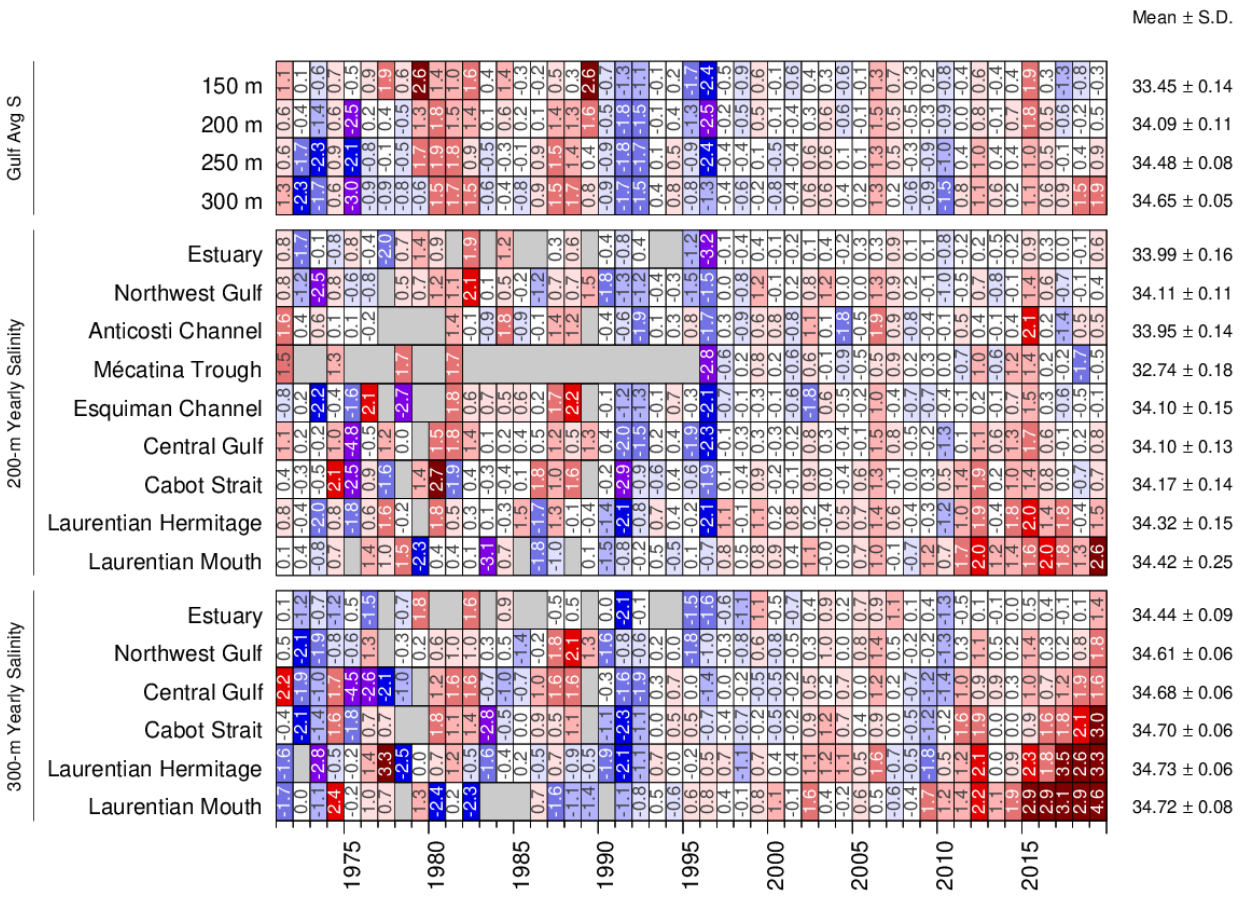

Fig. 51. Deep layer salinity. Gulf averages for salinity are shown for 150, 200, 250, and 300 m. Regional averages are shown for 200 and 300 m. The numbers on the right are the 1981–2010 climatological means and standard deviations. The numbers in the boxes are normalized anomalies.

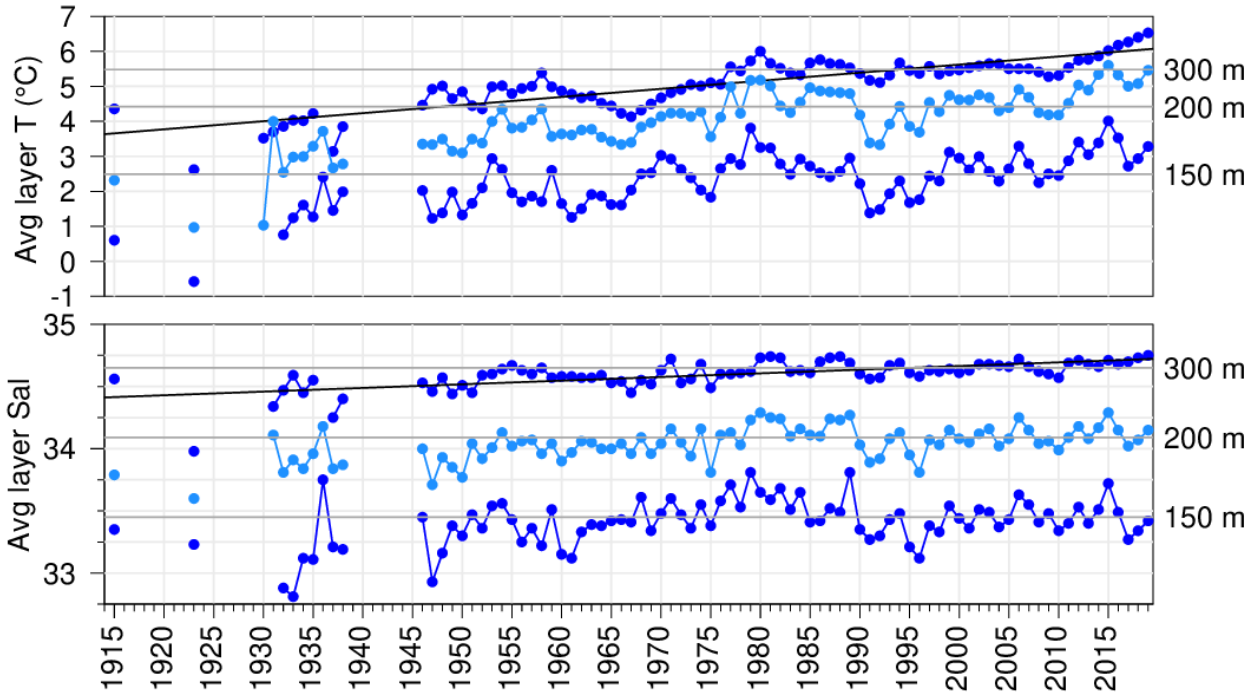

Fig. 52. Layer-averaged temperature and salinity time series for the Gulf of St. Lawrence. The temperature and salinity panels show the 150 m, 200 m, and 300 m annual averages and the horizontal lines are 1981–2010 means. Sloped lines show linear regressions for temperature and salinity at 300 m of respectively 2.3°C and 0.3 per century.

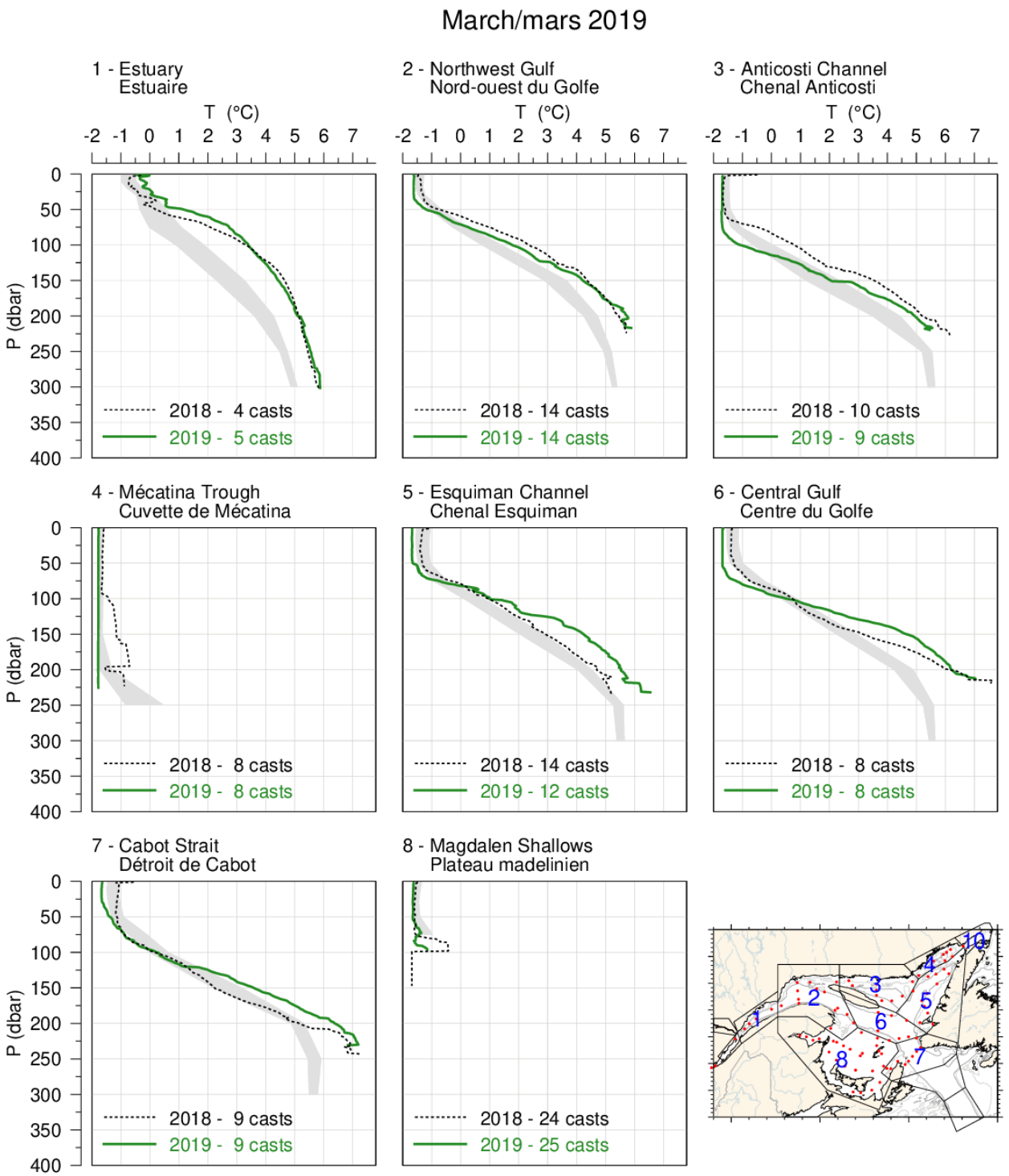

Fig. 53. Mean temperature profiles observed in each region of the Gulf during the March 2019 survey. The shaded area represents the 1981–2010 (but mostly 1996–2010) climatological monthly mean ± 0.5 SD. Mean profiles for 2018 are also shown for comparison.

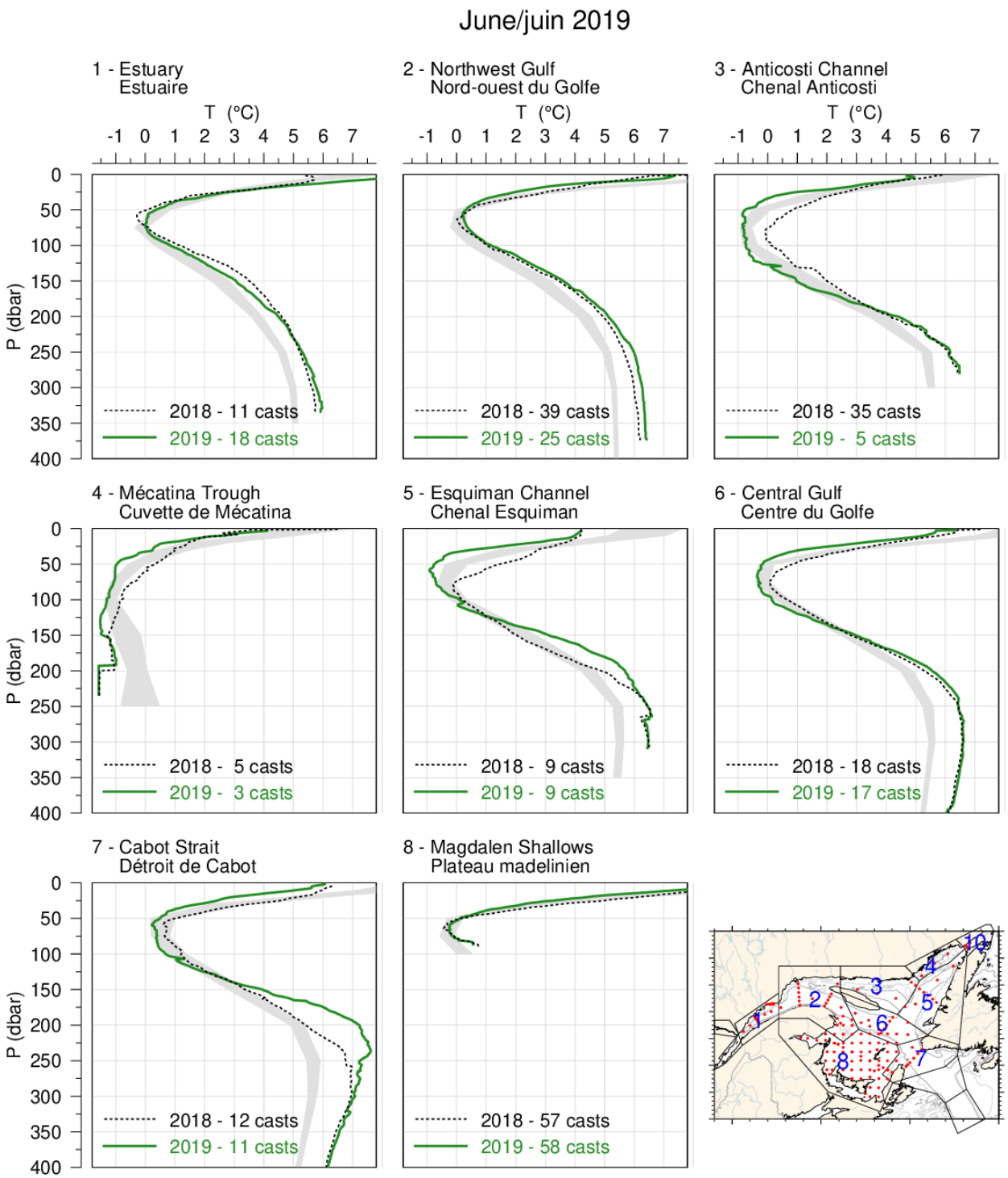

Fig. 54. Mean temperature profiles observed in each region of the Gulf during June 2019. The shaded area represents the 1981–2010 climatological monthly mean ± 0.5 SD. Mean profiles for 2018 are also shown for comparison.

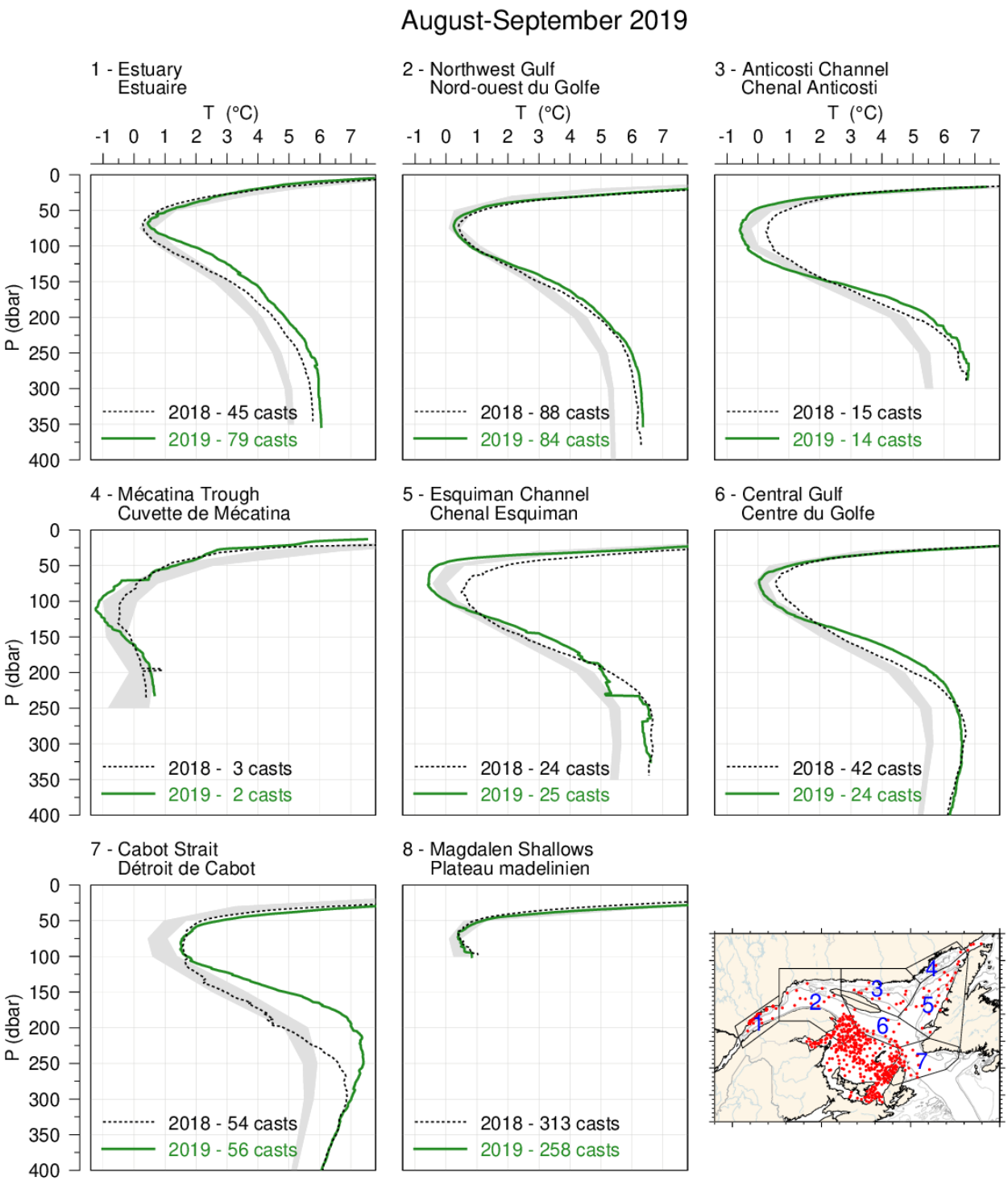

Fig. 55. Mean temperature profiles observed in each region of the Gulf during August and September 2019. The shaded area represents the 1981–2010 climatological monthly mean ± 0.5 SD for August for regions 1 through 7 and for September for region 8. Mean profiles for 2018 are also shown for comparison.

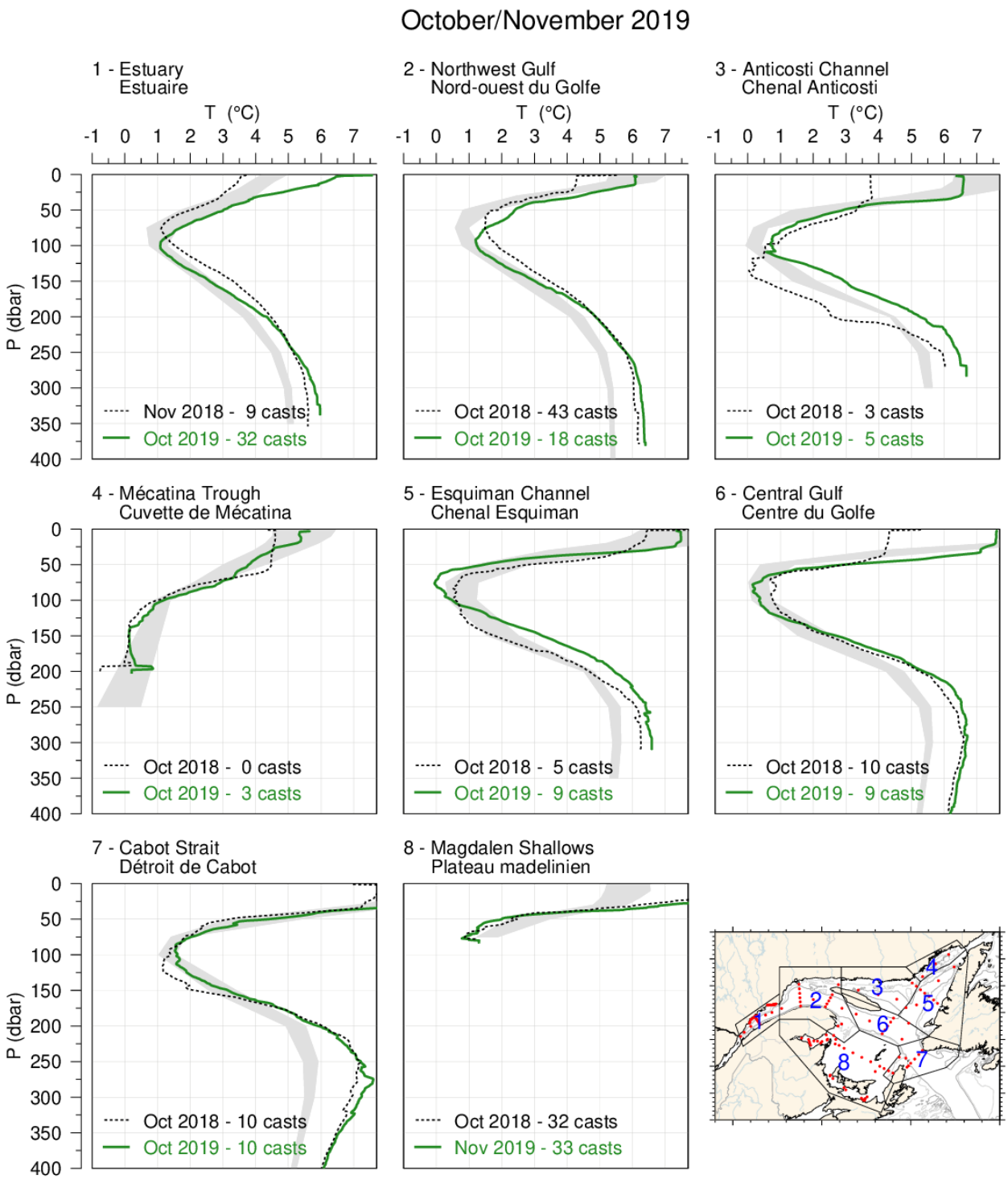

Fig. 56. Mean temperature profiles observed in each region of the Gulf during the October/November 2019 AZMP survey. The shaded area represents the 1981–2010 climatological monthly mean ± 0.5 SD. Mean profiles for 2018 are also shown for comparison.

1 - Estuary / Estuaire

	2018				2019			
	Mar	June	Aug	Nov	Mar	May	Aug	Oct
0 m	-0.56	6.1	8.0	2.3	-0.07	6.0	9.0	6.5
10 m	-0.64	4.7	5.2	2.2	-0.04	4.1	5.8	6.1
20 m	-0.50	3.3	3.3	2.1	0.1	2.7	4.0	5.3
30 m	-0.28	1.8	2.2	2.0	0.4	1.7	2.8	4.2
50 m	-0.20	0.4	0.9	1.9	1.5	0.3	1.1	2.9
75 m	0.4	0.0	0.9	1.2	2.9	0.0	0.6	1.7
100 m	1.5	0.8	1.5	1.2	3.5	0.8	1.8	1.1
150 m	3.8	2.9	3.1	2.4	4.4	3.0	3.8	2.6
200 m	4.85	4.39	4.45	4.12	5.09	4.45	4.88	4.29
250 m	5.17	5.18	5.23	5.14	5.54	5.30	5.68	5.19
300 m	5.51	5.63	5.66	5.60	5.87	5.82	5.96	5.81
350 m		5.75	5.73	5.69		5.96	6.04	5.97

2 - Northwest Gulf / Nord-ouest du Golfe

	2018				2019			
	Mar	June	Aug	Oct	Mar	May	Aug	Oct
0 m	-1.47	6.3	15.9	5.7	-1.60	3.5	16.4	6.7
10 m	-1.36	5.2	13.8	5.6	-1.62	2.4	13.5	6.7
20 m	-1.33	3.8	8.0	5.5	-1.62	1.3	7.3	5.4
30 m	-1.27	2.4	4.3	5.0	-1.62	0.8	3.6	3.9
50 m	-0.71	0.5	1.1	3.2	-1.20	0.3	0.7	2.0
75 m	0.9	0.2	0.4	1.4	0.3	0.5	0.3	1.4
100 m	2.3	1.0	0.8	1.4	1.8	1.3	0.8	1.6
150 m	4.3	3.4	2.9	2.6	4.2	3.7	3.2	3.4
200 m	5.34	4.95	4.88	4.79	5.77	5.17	4.90	4.87
250 m		5.65	5.78	5.82		5.99	5.93	5.88
300 m		6.00	6.05	6.14		6.25	6.24	6.24
350 m		6.11	6.17	6.16		6.36	6.33	6.29
400 m			6.29	6.33				

3 - Anticosti Channel / Chenal Anticosti

	2018				2019			
	Mar	June	Aug	Oct	Mar	June	Aug	Oct
0 m	-1.58	5.6	15.2	5.6	-1.69	4.9	16.3	6.6
10 m	-1.65	4.3	13.5	5.7	-1.70	4.2	15.4	6.6
20 m	-1.66	3.0	5.3	5.5	-1.70	2.3	5.5	6.6
30 m	-1.67	2.1	2.6	5.2	-1.70	0.3	2.2	6.5
50 m	-1.59	0.9	0.9	3.8	-1.70	-0.8	-0.2	2.9
75 m	-0.50	0.1	0.3	2.6	-1.69	-0.8	-0.6	1.2
100 m	0.8	0.1	0.5	1.3	-1.09	-0.7	-0.3	0.7
150 m	3.5	2.0	2.3	3.1	2.0	1.0	2.3	3.0
200 m	5.20	4.17	4.98	5.18	4.82	4.41	5.55	5.27
250 m		6.10	6.41	6.14		6.16	6.53	6.42

4 - Mécatina Trough / Cuvette de Mécatina

	2018			2019			
	Mar	June	Aug	Mar	June	Aug	Oct
0 m	-1.59	4.2	14.7	-1.77	4.0	13.1	5.3
10 m	-1.60	2.5	14.4	-1.77	2.6	9.7	5.4
20 m	-1.61	1.4	10.4	-1.78	0.7	5.2	5.2
30 m	-1.62	0.9	3.2	-1.78	0.2	2.6	4.5
50 m	-1.63	0.3	1.1	-1.78	-1.0	1.3	3.8
75 m	-1.65	-0.4	0.1	-1.78	-1.1	0.4	2.9
100 m	-1.44	-0.8	-0.4	-1.78	-1.3	-1.1	1.2
150 m	-1.16	-1.3	-0.1	-1.78	-1.4	-0.3	0.1
200 m	-0.68	-1.04	0.24	-1.78	-0.99	0.54	0.38

5 - Esquiman Channel / Chenal Esquiman

	2018				2019			
	Mar	June	Aug	Oct	Mar	June	Aug	Oct
0 m	-1.28	4.2	17.5	6.2	-1.67	4.2	17.0	7.5
10 m	-1.34	4.2	16.9	6.2	-1.68	4.0	15.5	7.5
20 m	-1.37	3.6	11.2	6.2	-1.68	2.5	9.5	7.3
30 m	-1.41	2.8	6.6	6.2	-1.68	0.5	4.9	6.3
50 m	-1.32	1.4	1.9	2.1	-1.64	-0.8	-0.3	1.4
75 m	-0.34	-0.0	0.7	0.8	-0.79	-0.7	-0.5	-0.0
100 m	0.7	0.2	0.7	1.1	0.5	0.1	0.0	0.5
150 m	2.9	2.0	2.6	3.1	4.1	3.1	2.9	3.3
200 m	4.47	4.89	5.31	5.61	5.57	5.69	4.91	5.44
250 m		6.47	6.51	6.57		6.45	6.11	6.32
300 m		6.50	6.66			6.47	6.42	6.59

6 - Central Gulf / Centre du Golfe

	2018				2019			
	Mar	June	Aug	Oct	Mar	May	Aug	Oct
0 m	-1.38	6.3	16.8	6.0	-1.70	3.9	17.6	7.7
10 m	-1.38	5.8	16.0	5.9	-1.69	3.9	16.3	7.7
20 m	-1.39	4.1	9.2	5.8	-1.69	3.1	8.6	7.7
30 m	-1.40	2.8	4.2	5.5	-1.69	0.8	3.4	7.2
50 m	-1.31	0.8	1.5	2.6	-1.69	-0.2	0.4	2.6
75 m	-0.74	0.0	0.7	0.6	-1.24	-0.4	-0.0	0.3
100 m	0.7	0.7	1.0	0.9	0.5	-0.2	0.2	0.4
150 m	3.1	2.8	2.5	3.0	4.6	2.6	3.0	2.6
200 m	5.97	5.30	4.98	4.98	6.21	5.82	5.61	5.23
250 m		6.44	6.59	6.18		6.65	6.49	6.45
300 m		6.56	6.71	6.43		6.71	6.60	6.54
350 m		6.37	6.41	6.33		6.53	6.45	6.51
400 m		6.21	6.16	6.19		6.21	6.25	6.22
450 m		5.99	6.01			5.95	6.05	6.02

7 - Cabot Strait / Détroit de Cabot

	2018				2019			
	Mar	June	Aug	Oct	Mar	May	Aug	Oct
0 m	-1.07	6.3	21.9	9.4	-1.65	5.5	20.2	9.6
10 m	-1.08	6.0	21.3	9.4	-1.66	4.6	18.7	9.6
20 m	-1.11	5.1	12.0	9.0	-1.67	2.7	12.8	9.4
30 m	-1.15	3.5	5.2	8.0	-1.63	1.8	6.6	8.8
50 m	-1.14	1.0	1.7	5.4	-1.38	0.6	1.5	4.4
75 m	-0.92	0.7	1.5	2.6	-0.88	0.4	0.8	2.0
100 m	0.1	1.2	1.6	1.8	0.2	0.7	1.3	1.6
150 m	2.2	3.4	2.6	3.1	3.6	3.9	4.8	3.2
200 m	5.02	5.41	5.00	5.03	6.02	7.22	7.16	5.93
250 m	6.86	6.77	6.76	6.72		7.24	7.54	7.22
300 m		6.95	6.95	6.86		7.08	7.01	7.22
350 m		6.43	6.52	6.56		6.55	6.49	6.54
400 m		6.11	6.08	6.11		6.15	6.05	6.08
450 m		5.95	5.94	5.91		5.98	5.95	6.00
500 m		5.91	5.88			5.91	5.95	

8 - Magdalen Shallows / Plateau madelinien

	2018				2019			
	Mar	June	Sep	Oct	Mar	June	Sep	Nov
0 m	-1.52	9.1	17.0	8.8	-1.62	9.5	13.3	8.4
10 m	-1.55	8.4	16.8	8.7	-1.63	8.0	13.1	8.4
20 m	-1.56	6.2	12.9	8.3	-1.64	4.6	12.0	7.9
30 m	-1.59	3.8	6.0	7.5	-1.65	2.7	8.3	6.4
50 m	-1.58	0.3	1.6	2.9	-1.65	0.4	1.7	2.0
75 m	-1.54	-0.1	0.7	1.3	-1.42	-0.1	0.9	0.9
100 m	-0.43	0.8		1.1	-1.15		0.6	

Fig. 57. Depth-layer monthly average temperature summary for months during which the eight Gulf-wide oceanographic surveys took place in 2018 and 2019. The colour-coding is according to the temperature anomaly relative to the monthly 1981–2010 climatology of each region.

1 - Estuary / Estuaire

	2018				2019			
	Mar	June	Aug	Nov	Mar	May	Aug	Oct
Strat.	2.53	4.3	3.9	2.7	3.64	6.6	5.3	2.5
0 m	28.1	26.3	27.7	27.6	27.8	23.9	26.0	28.3
10 m	29.0	27.5	29.1	28.1	29.3	25.6	28.7	28.8
20 m	29.5	28.5	30.1	28.8	30.6	28.3	29.8	29.6
30 m	30.2	29.7	30.8	29.4	31.4	30.4	30.6	30.2
50 m	31.3	31.2	31.7	30.9	32.5	31.7	31.7	31.0
75 m	32.3	32.0	32.2	31.9	33.2	32.2	32.4	31.7
100 m	32.8	32.5	32.7	32.4	33.5	32.6	32.9	32.3
150 m	33.7	33.3	33.4	33.1	33.9	33.4	33.7	33.2
200 m	34.12	33.94	33.96	33.83	34.18	33.94	34.12	33.89
250 m	34.25	34.27	34.28	34.24	34.38	34.30	34.46	34.27
300 m	34.41	34.46	34.47	34.44	34.55	34.53	34.58	34.52
350 m		34.53	34.50	34.48		34.59	34.62	34.59

2 - Northwest Gulf / Nord-ouest du Golfe

	2018				2019			
	Mar	June	Aug	Oct	Mar	May	Aug	Oct
Strat.	0.84	2.9	4.5	1.7	0.49	1.8	5.5	1.9
0 m	31.0	28.6	28.4	29.4	31.3	29.9	27.5	30.1
10 m	31.4	29.6	28.8	29.5	31.4	30.6	28.3	30.1
20 m	31.6	30.4	29.9	29.9	31.5	31.2	29.8	30.6
30 m	31.7	30.9	30.6	30.4	31.7	31.3	30.8	31.2
50 m	32.1	31.6	31.5	31.2	31.9	31.9	31.7	31.9
75 m	32.6	32.2	32.0	32.0	32.4	32.4	32.2	32.3
100 m	33.1	32.6	32.4	32.4	32.9	32.8	32.6	32.6
150 m	33.9	33.5	33.4	33.1	33.8	33.6	33.4	33.5
200 m	34.27	34.10	34.06	34.03	34.38	34.18	34.05	34.08
250 m		34.42	34.47	34.47		34.54	34.52	34.52
300 m		34.62	34.66	34.69		34.71	34.70	34.72
350 m		34.72	34.74	34.74		34.82	34.78	34.76
400 m			34.81	34.88				

3 - Anticosti Channel / Chenal Anticosti

	2018				2019			
	Mar	June	Aug	Oct	Mar	June	Aug	Oct
Strat.	0.09	2.4	2.8	0.6	0.00	2.1	4.0	1.0
0 m	31.7	29.1	30.6	30.8	32.1	29.9	29.8	30.8
10 m	31.7	30.4	30.7	31.0	32.1	30.6	29.8	30.8
20 m	31.7	31.0	31.3	31.0	32.1	31.4	30.9	30.9
30 m	31.8	31.4	31.5	31.1	32.1	31.6	31.4	31.0
50 m	31.8	31.7	31.7	31.4	32.1	31.9	31.9	31.6
75 m	32.2	31.9	32.0	31.6	32.1	32.1	32.2	31.9
100 m	32.6	32.3	32.3	31.9	32.3	32.3	32.4	32.2
150 m	33.6	33.1	33.2	33.4	33.0	32.9	33.2	33.4
200 m	34.13	33.75	34.02	34.10	33.97	33.81	34.19	34.12
250 m		34.45	34.57	34.48		34.45	34.61	34.59

4 - Mécatina Trough / Cuvette de Mécatina

	2018			2019			
	Mar	June	Aug	Mar	June	Aug	Oct
Strat.	0.15	1.3	2.9	0.03	2.3	2.8	0.5
0 m	31.6	30.3	30.4	32.5	29.2	30.2	31.1
10 m	31.7	30.9	30.5	32.5	30.9	30.7	31.1
20 m	31.7	31.3	30.8	32.6	31.2	31.3	31.1
30 m	31.7	31.4	31.4	32.6	31.4	31.7	31.4
50 m	31.8	31.6	31.7	32.6	31.7	31.9	31.6
75 m	31.9	31.8	31.9	32.6	32.0	32.0	31.8
100 m	32.0	32.0	32.0	32.6	32.2	32.3	32.0
150 m	32.2	32.2	32.4	32.6	32.5	32.5	32.5
200 m	32.43	32.35	32.52	32.67	32.58	32.75	32.62

5 - Esquiman Channel / Chenal Esquiman

	2018				2019			
	Mar	June	Aug	Oct	Mar	June	Aug	Oct
Strat.	0.13	0.4	3.4	0.8	0.08	0.9	3.8	1.3
0 m	31.5	31.4	30.3	31.1	31.8	31.1	30.1	31.0
10 m	31.5	31.4	30.4	31.1	31.9	31.1	30.3	31.0
20 m	31.5	31.4	31.0	31.1	31.9	31.3	30.8	31.0
30 m	31.6	31.5	31.3	31.1	31.9	31.6	31.2	31.2
50 m	31.7	31.6	31.6	31.6	31.9	31.9	31.8	31.9
75 m	31.9	31.8	31.9	32.0	32.2	32.1	32.1	32.3
100 m	32.5	32.2	32.3	32.4	32.6	32.5	32.5	32.6
150 m	33.4	33.1	33.2	33.4	33.7	33.3	33.2	33.4
200 m	33.84	33.96	34.11	34.23	34.18	34.17	33.89	34.10
250 m		34.55	34.56	34.62		34.57	34.41	34.48
300 m		34.56	34.75			34.56	34.55	34.61

6 - Central Gulf / Centre du Golfe

	2018				2019			
	Mar	June	Aug	Oct	Mar	May	Aug	Oct
Strat.	0.06	1.1	3.6	0.9	0.04	0.7	4.4	1.4
0 m	31.6	30.7	30.0	30.7	31.7	31.3	29.4	30.6
10 m	31.6	30.8	30.1	30.7	31.7	31.3	29.6	30.7
20 m	31.6	31.1	30.7	30.7	31.8	31.3	30.7	30.7
30 m	31.6	31.3	31.3	30.8	31.8	31.6	31.3	30.8
50 m	31.7	31.6	31.6	31.4	31.8	31.8	31.9	31.7
75 m	31.9	31.8	31.9	32.0	31.9	32.1	32.2	32.2
100 m	32.6	32.4	32.3	32.5	32.4	32.4	32.4	32.4
150 m	33.5	33.3	33.2	33.4	33.8	33.2	33.3	33.2
200 m	34.30	34.11	34.02	34.03	34.38	34.14	34.14	34.05
250 m		34.55	34.60	34.52		34.57	34.56	34.55
300 m		34.75	34.82	34.75		34.80	34.77	34.76
350 m		34.87	34.92	34.92		34.92	34.90	34.92
400 m		34.91	34.96	34.94		34.94	34.95	34.96
450 m		34.97	34.97			34.98	34.99	34.98

7 - Cabot Strait / Détroit de Cabot

	2018				2019			
	Mar	June	Aug	Oct	Mar	May	Aug	Oct
Strat.	0.29	1.1	6.2	1.5	0.21	1.1	5.6	1.9
0 m	31.4	30.6	28.2	30.0	31.3	30.8	28.2	30.2
10 m	31.4	30.7	28.3	30.0	31.4	30.8	28.6	30.2
20 m	31.4	30.9	29.4	30.2	31.4	31.0	29.4	30.4
30 m	31.5	31.1	30.6	30.4	31.4	31.3	30.5	30.8
50 m	31.7	31.4	31.6	31.2	31.6	31.6	31.5	31.7
75 m	31.8	31.9	32.1	31.9	31.9	32.1	32.2	32.3
100 m	32.2	32.4	32.5	32.4	32.3	32.4	32.6	32.6
150 m	33.1	33.5	33.2	33.3	33.3	33.4	33.7	33.2
200 m	34.08	34.14	34.01	33.97	34.16	34.42	34.51	34.12
250 m	34.59	34.60	34.60	34.56		34.69	34.82	34.60
300 m		34.84	34.85	34.79		34.84	34.90	34.83
350 m		34.93	34.95	34.89		34.94	34.96	34.95
400 m		34.97	34.97	34.97		34.97	34.98	34.98
450 m		34.98	34.98	34.98		34.98	34.99	34.98
500 m		34.98	34.98			34.98	34.98	

8 - Magdalen Shallows / Plateau madelinien

	2018				2019			
	Mar	June	Sep	Oct	Mar	June	Sep	Nov
Strat.	0.37	2.8	4.4	1.8	0.07	3.1	3.6	2.6
0 m	30.8	28.7	28.6	29.6	30.9	28.5	28.6	28.9
10 m	30.8	29.0	28.7	29.6	30.9	29.0	28.7	29.1
20 m	30.8	29.8	29.3	29.7	30.9	29.8	29.0	29.5
30 m	31.0	30.5	30.3	30.0	30.9	30.5	29.8	30.1
50 m	31.2	31.1	31.3	31.1	31.0	31.2	31.3	31.3
75 m	31.4	31.7	31.7	31.7	31.2	31.9	31.9	31.9
100 m	32.0	32.2		31.9	31.8		31.8	

Fig. 58. Depth-layer monthly average stratification and salinity summary for months during which the eight Gulf-wide oceanographic surveys took place in 2018 and 2019. Stratification is defined as the density difference between 50 m and the surface and its colour-coding is reversed (blue for positive anomaly).

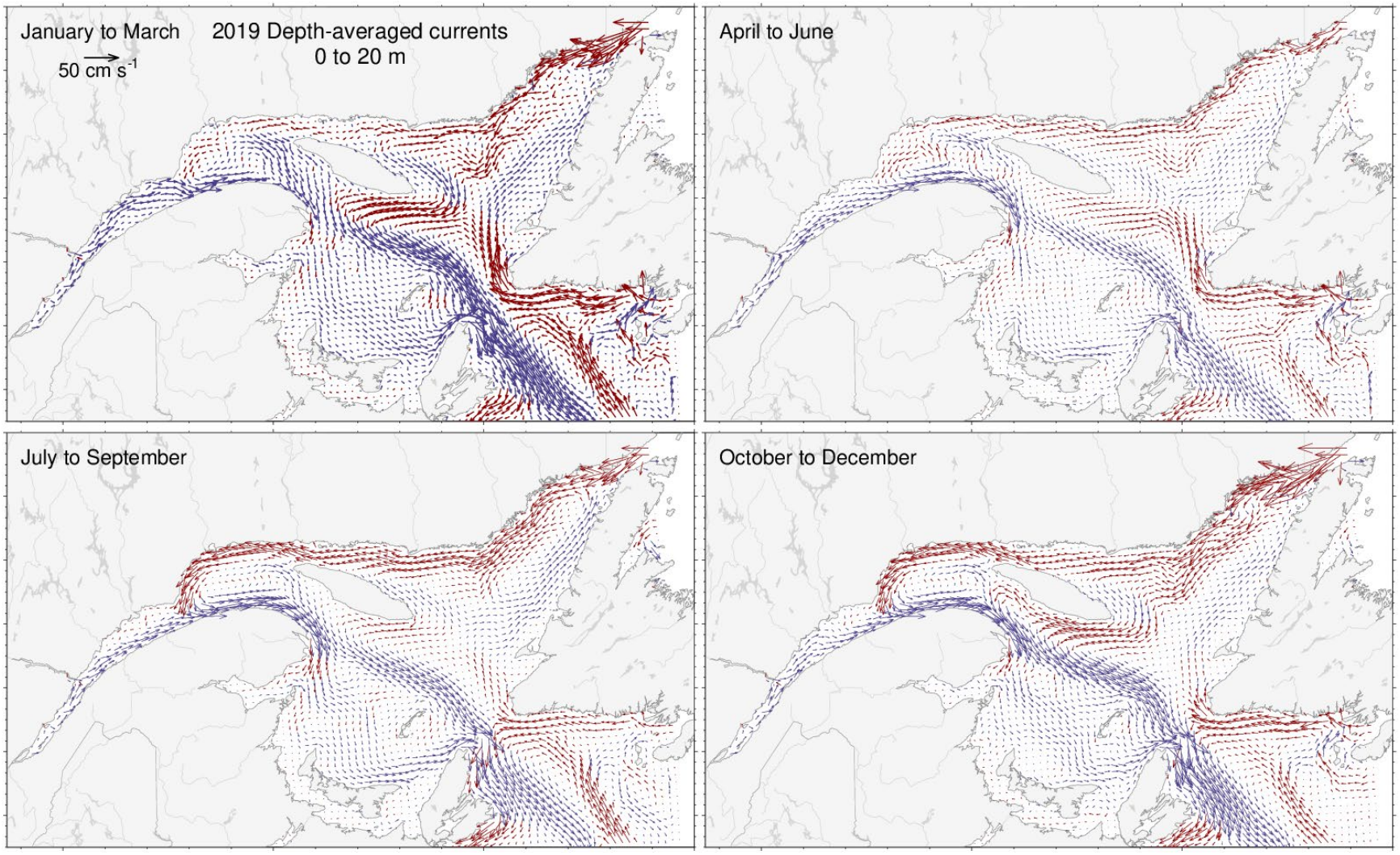

Fig. 59. Depth-averaged currents from 0 to 20 m for each three-month period of 2019. Vectors drawn in blue are towards the East and those drawn in red are towards the West.

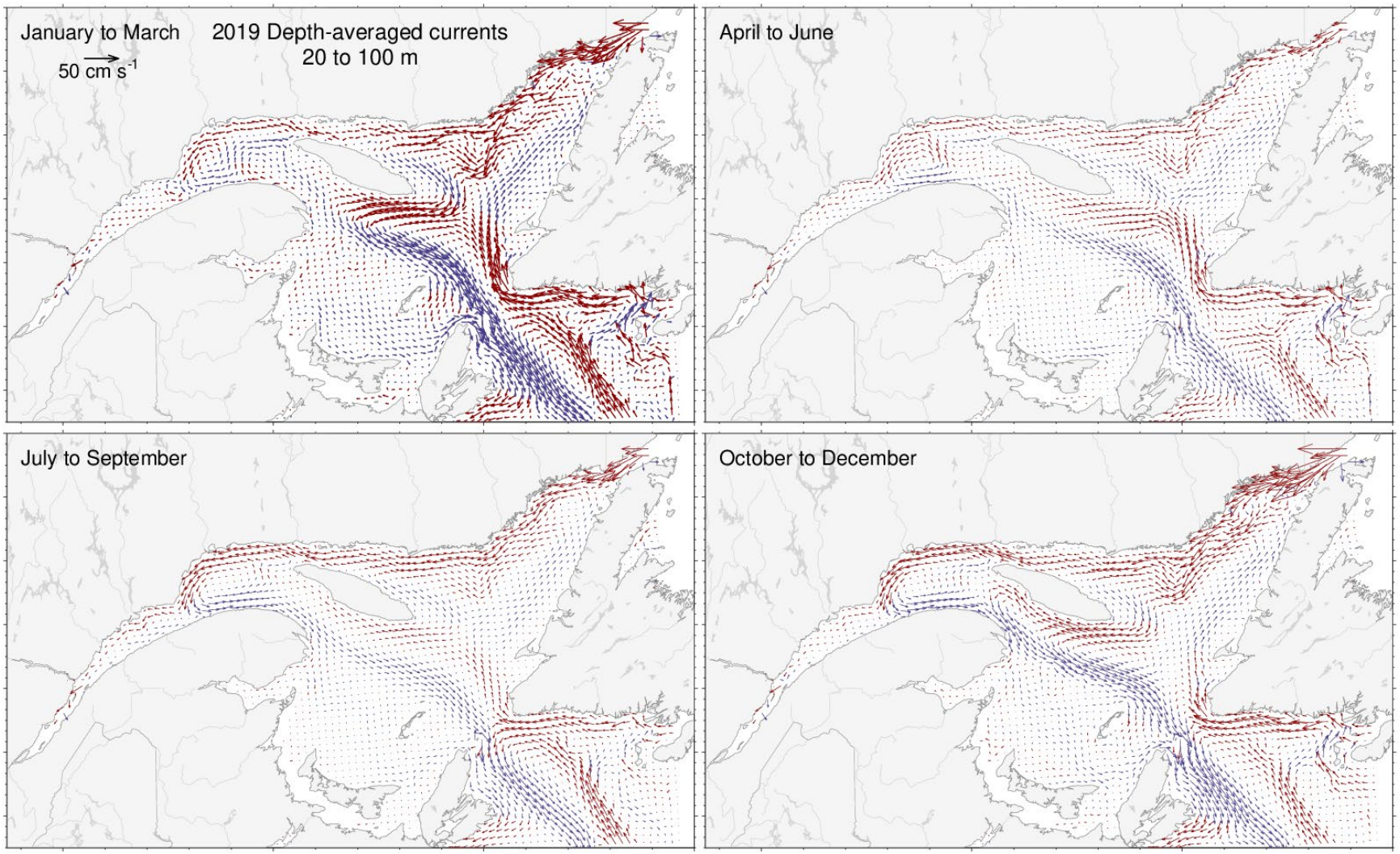

Fig. 60. Depth-averaged currents from 20 to 100 m for each three-month period of 2019. Vectors drawn in blue are towards the East and those drawn in red are towards the West.

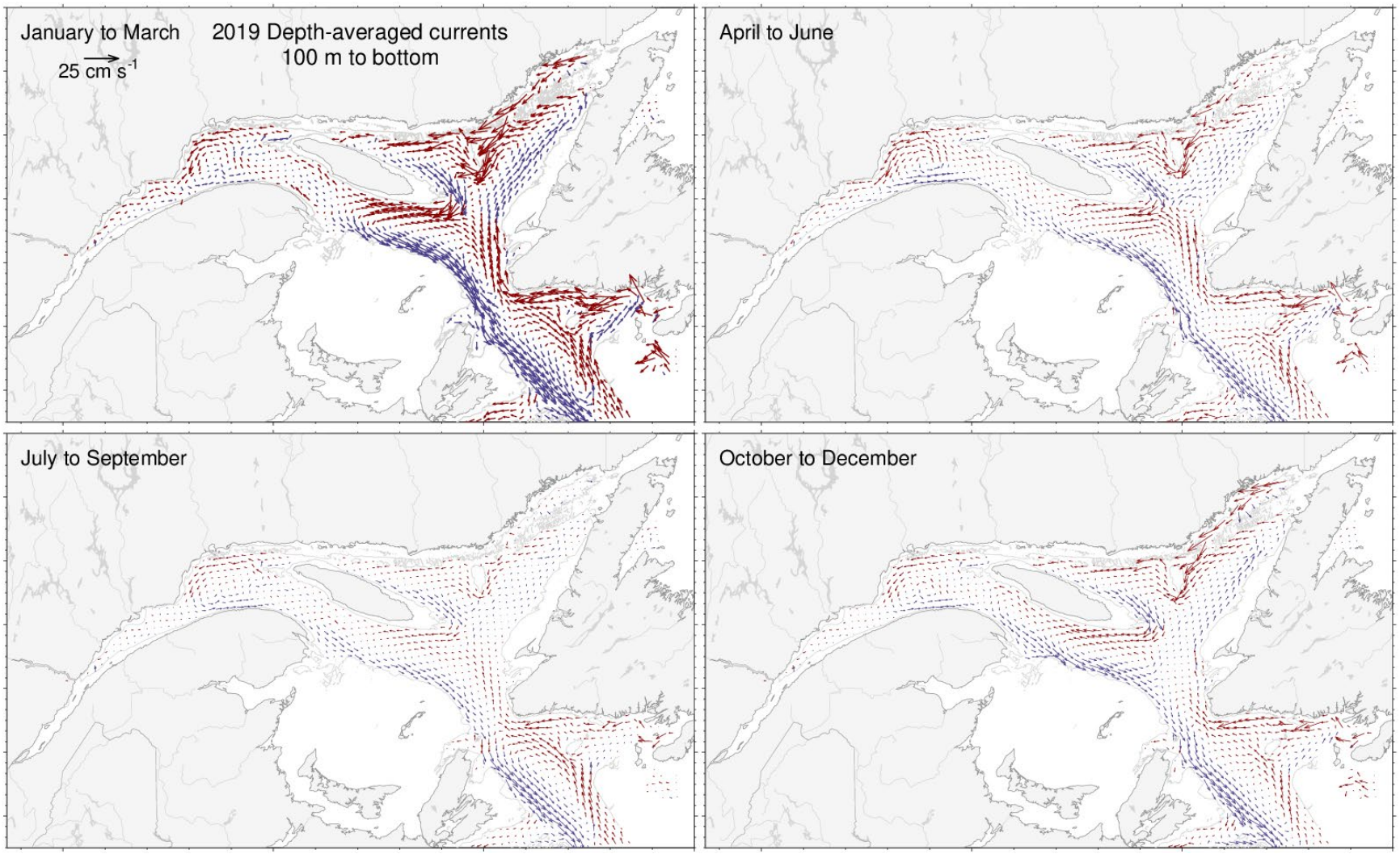

Fig. 61. Depth-averaged currents from 100 m to the bottom for each three-month period of 2019. Vectors drawn in blue are towards the East and those drawn in red are towards the West.

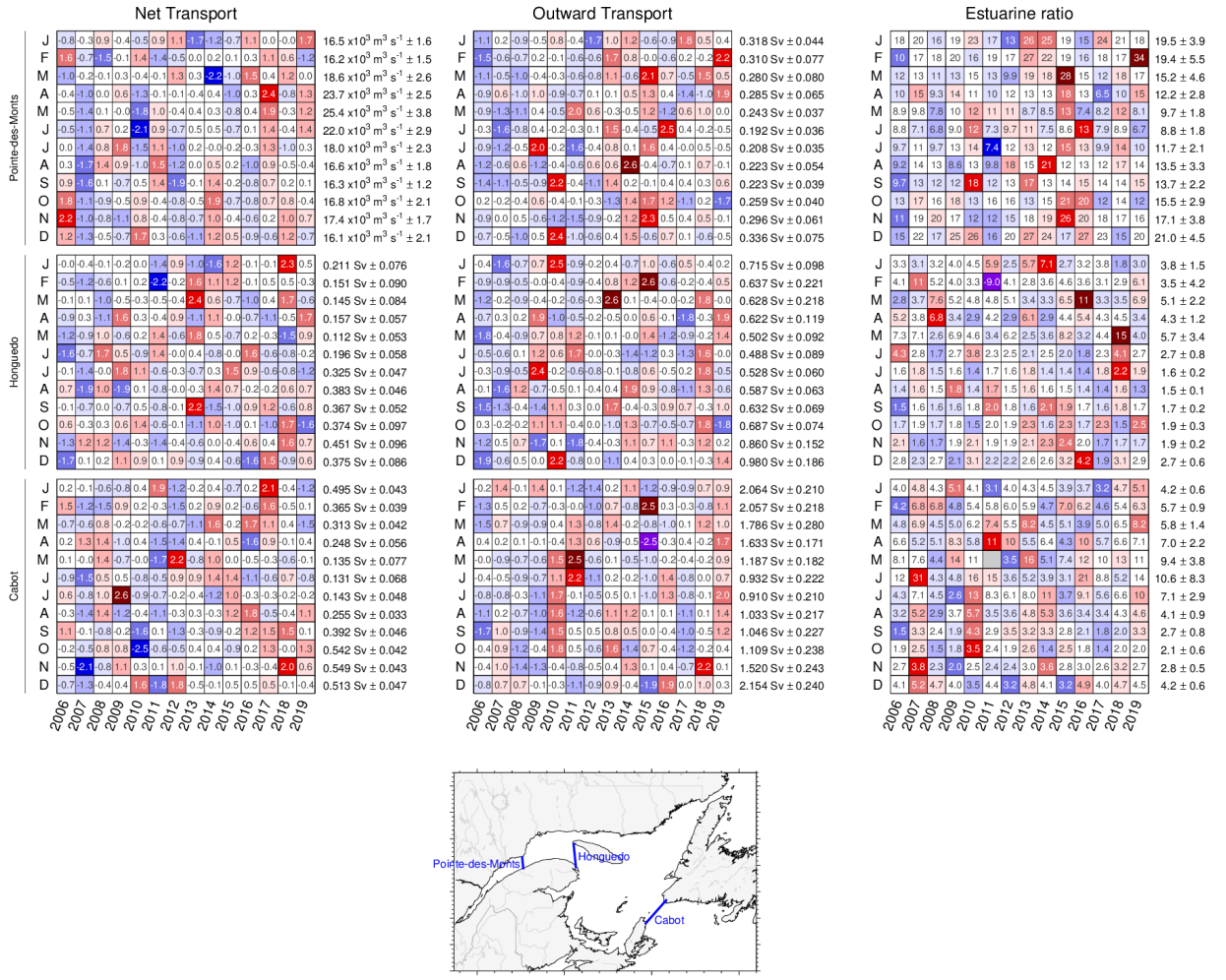

Fig. 62. Monthly averaged modelled transports and estuarine ratio across sections of the Gulf of St. Lawrence since 2006. The numbers on the right are the 2006–2019 means and standard deviations. The numbers in the boxes are normalized anomalies for transport panels, but ratio values are indicated in the right panel. Colours indicate the magnitude of the anomaly. Sv (Sverdrup) are units of transport equal to 10^6 m^3s^{-1}.

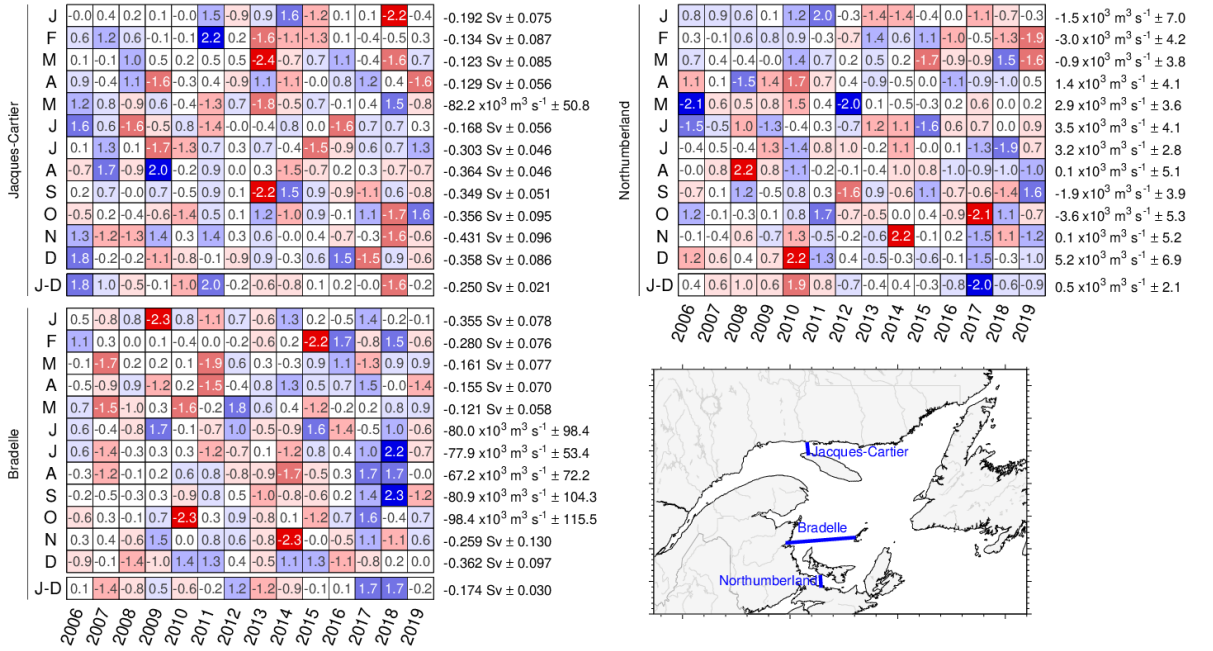

Fig. 63. Monthly and annual averaged modelled transports across sections of the Gulf of St. Lawrence since 2006. The numbers on the right are the 2006–2019 means and standard deviations, with positive values toward east and north. The numbers in the boxes are normalized anomalies. Colours indicate the magnitude of the anomaly (e.g., negative anomalies are still shown in red when the mean transport is negative across the section).

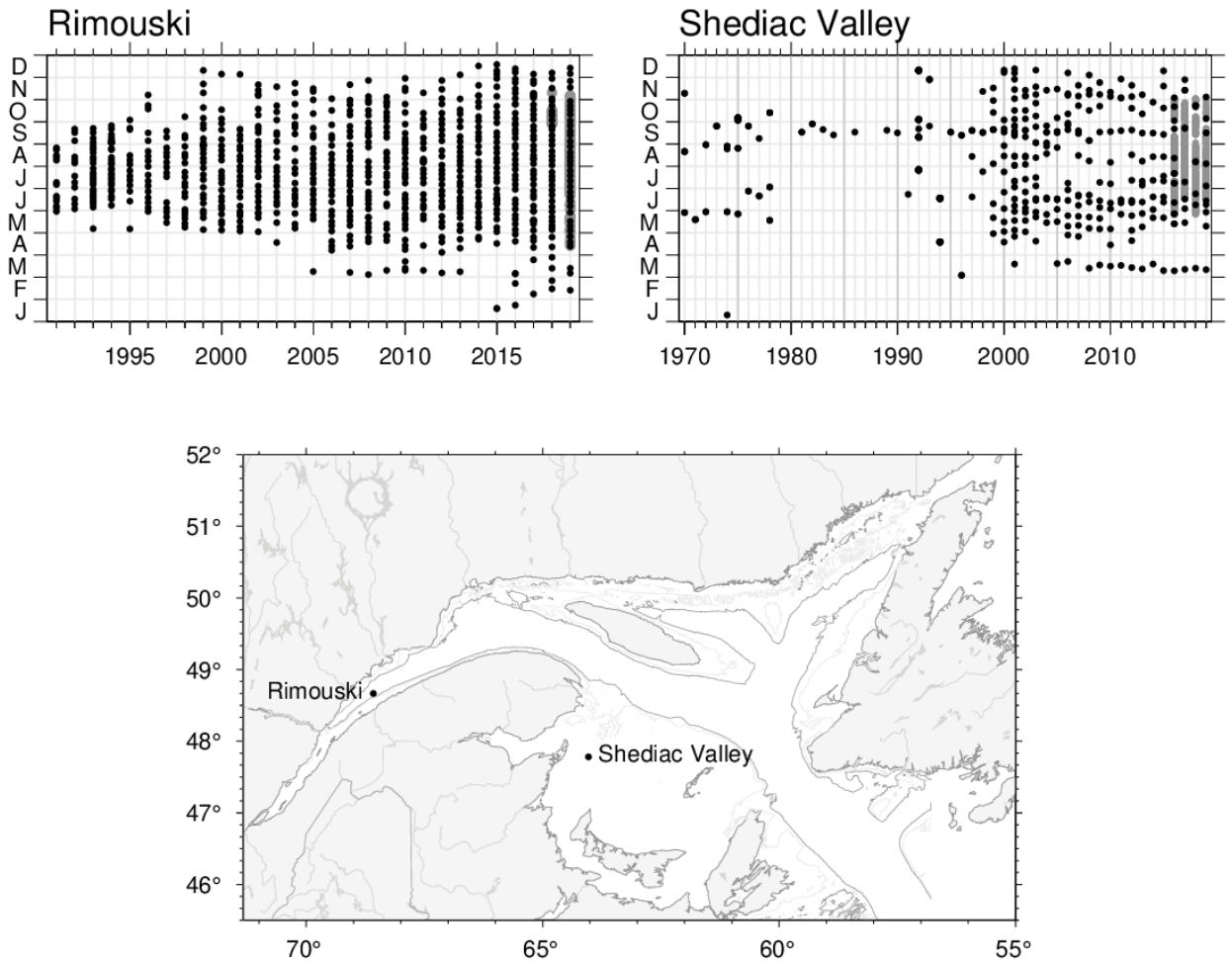

Fig. 64. Sampling frequency and positions of the AZMP stations Rimouski and Shediac Valley. Gray overlay in 2019 at Shediac Valley shows span of 193 temperature and salinity profiles made by the PMZA-VAS automatic oceanographic buoy between 2019-06-16 and 2019-11-02. The grey overlay at Rimouski station shows 388 full depth temperature and salinity profiles made by the PMZA-Riki automatic oceanographic buoy between 2019-04-13 and 2019-11-06.

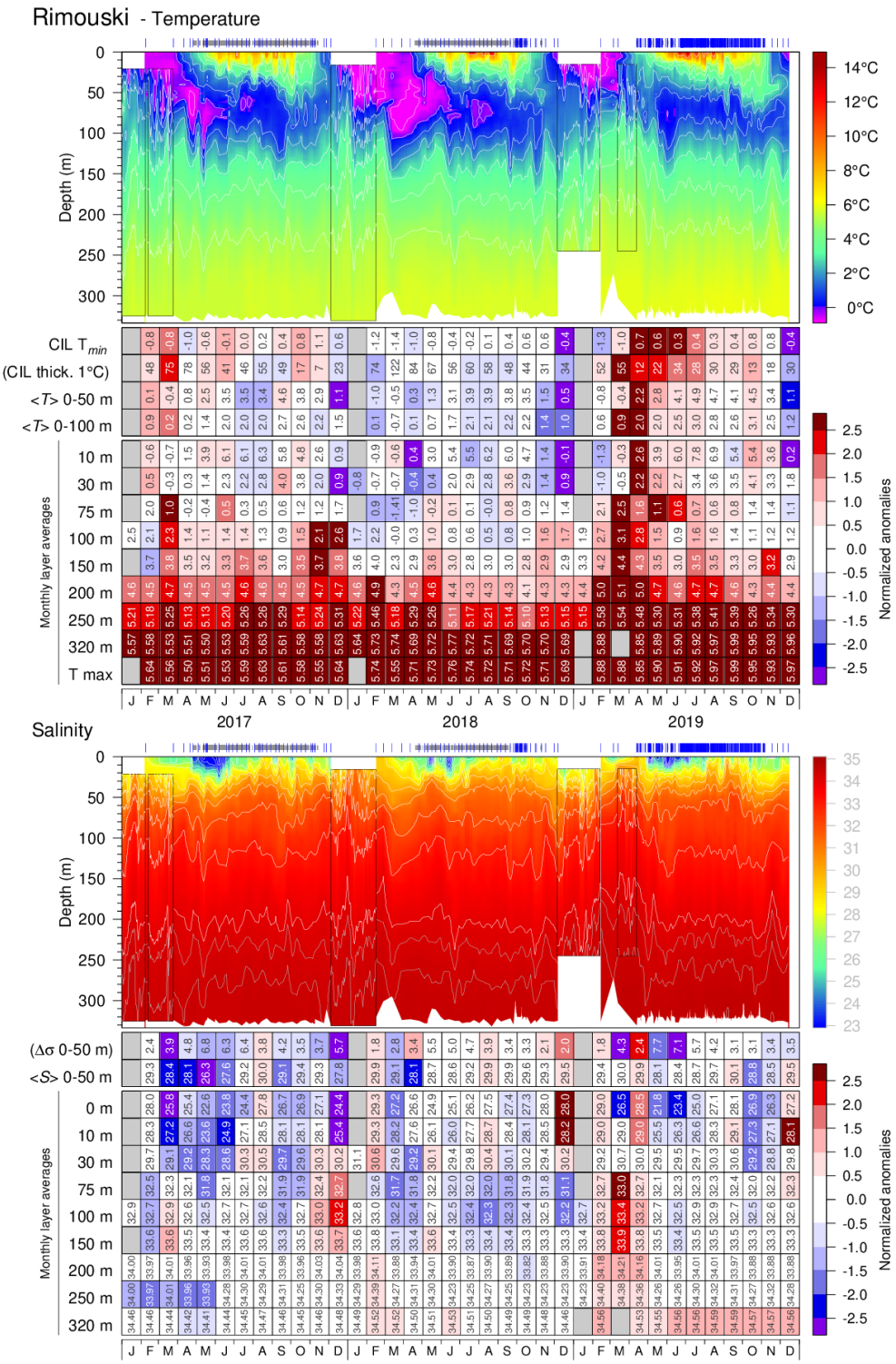

Fig. 65. Isotherm (top) and isohaline (bottom) time series at the Rimouski station; tick marks above indicate full-depth casts (mostly from a Viking buoy) and shaded area indicates earlier shallow casts made by a Viking automatic buoy. The scorecard tables are monthly layer averages colour-coded according to the anomaly relative to the 1991–2010 monthly climatology for the station (yearly climatology for 200 m and deeper). Thickness of the CIL and stratification have reversed colour codes where blue indicates thicker CIL (associated with colder water) and more stratification (associated with low surface salinity). The box insets and some of the monthly averages are from mooring data.

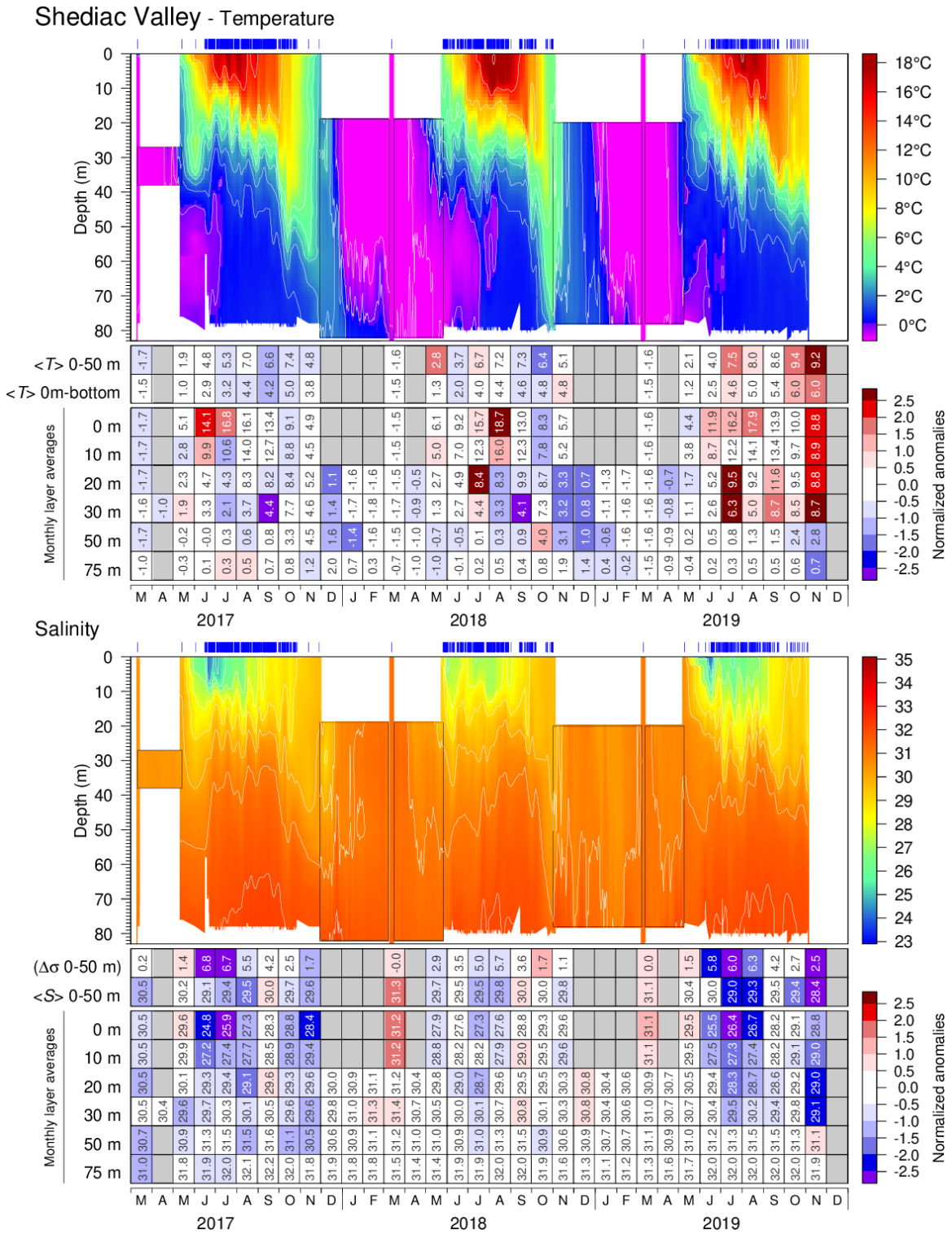

Fig. 66. Isotherm (top) and isohaline (bottom) time series at the Shediac Valley station; tick marks above indicate casts (mostly from automatic buoy starting in 2016). Scorecard tables are monthly layer averages colour-coded according to the anomaly relative to the 1981–2010 monthly climatology for the station (input to climatology is sparse prior to 1999). Higher than normal stratification is coded in blue (associated with low surface salinity). The box insets and 20, 30, 50 and 75 m monthly layer averages are mostly from mooring data. Internal tide oscillations are smoothed out.

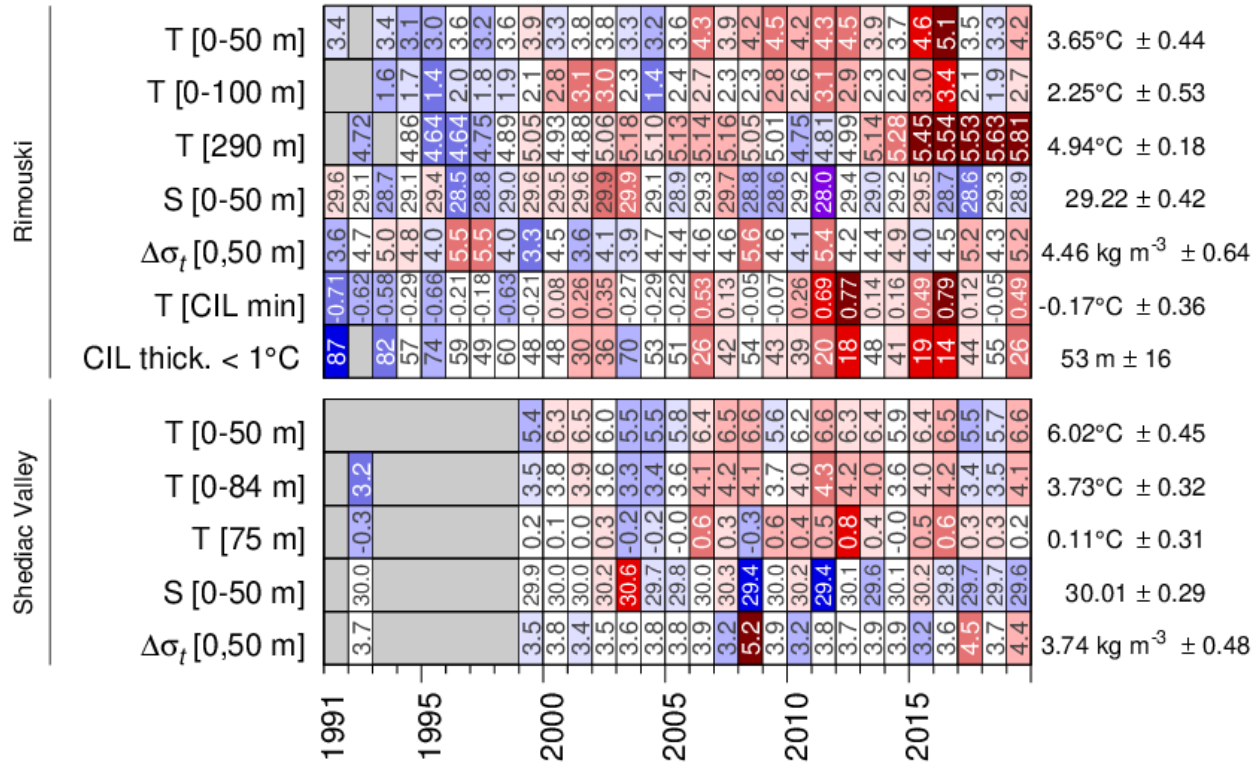

Fig. 67. May to October temperature and salinity layer averages, stratification (expressed as the density difference between 0 and 50 m), and CIL temperature minimum and thickness (T<1°C) for high frequency monitoring stations. Numbers in panels are monthly average values colour-coded according to the anomaly relative to the 1991–2010 climatology. Three months of anomaly data, between May and October, are required to show an average anomaly for any given year, except for deep water temperature at Rimouski station. Temperatures at 290 m and 75 m at Rimouski station and Shediac Valley station are considered to represent near-bottom temperatures.

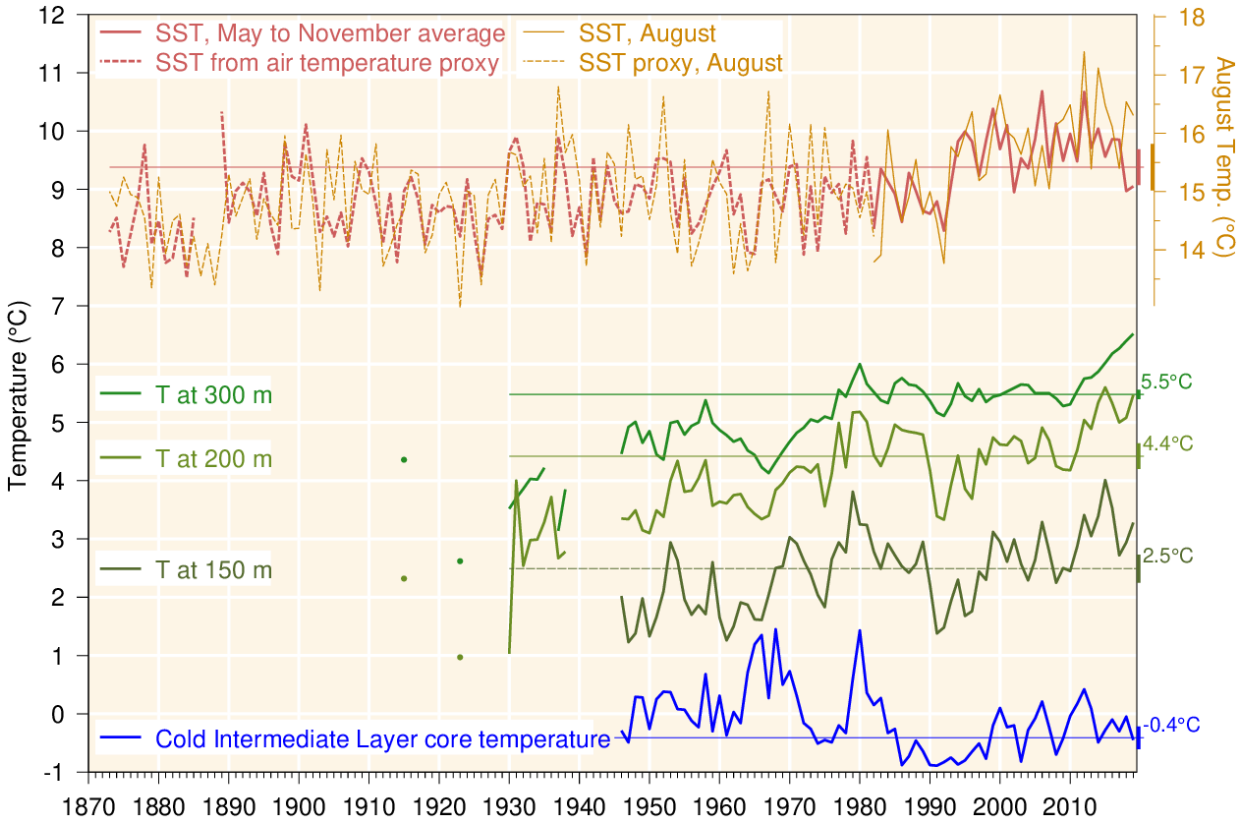

Fig. 68. Water temperatures in the Gulf of St. Lawrence. May–November SST averaged over the Gulf excluding the Estuary (1982–2019, red line), completed by a proxy based on April–November air temperature (1873–1981, red dashed line; average of all AHCCD stations in Fig. 4 but excluding Estuary stations at Baie Comeau and Mont-Joli). August SST is shown using temperature scale offset by 6°C; its proxy is based on the average air temperature in July and August. Layer-averaged temperature for the Gulf of St. Lawrence at 150, 200 and 300 m (green lines). Cold intermediate layer minimum temperature index in the Gulf of St. Lawrence (blue line). SST air temperature proxy is similar to that of Galbraith et al. (2012). Climatological averages based on the 1981–2010 period are indicated by thin lines labeled on the right side, and half the standard deviation is shown by vertical bars on the right side. Figure adapted from Benoît et al. (2012).

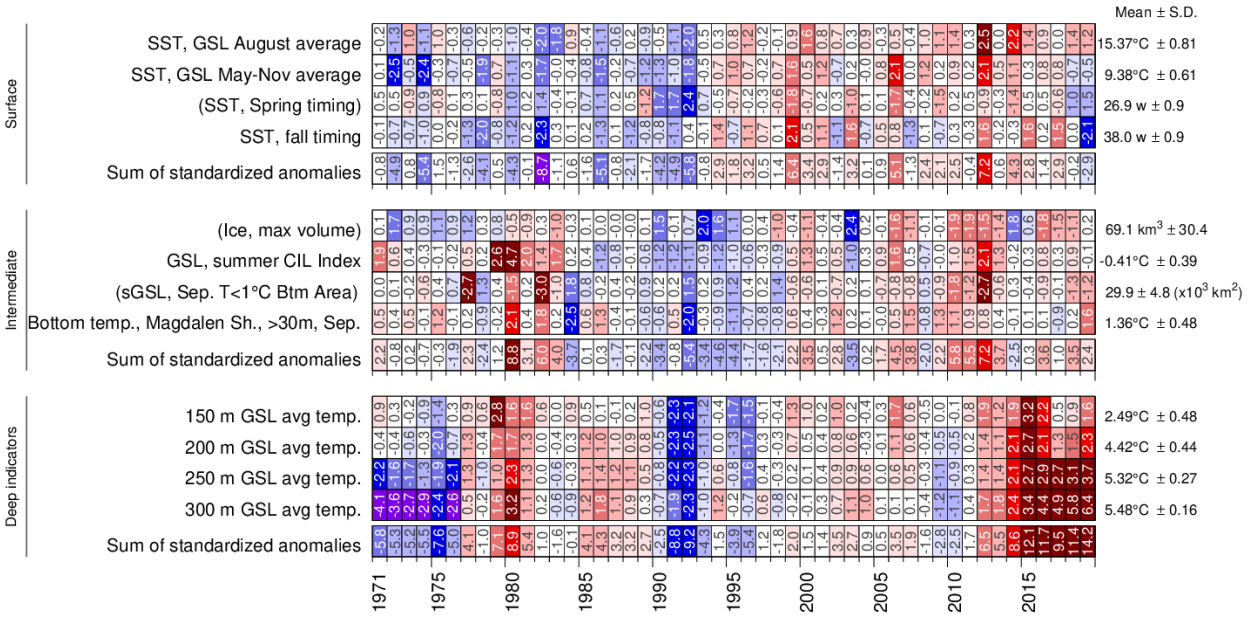

Fig. 69. Surface, intermediate (and sea-ice) and deep indicators used in the composite climate index (Fig. 70). The SST spring and fall timing are for 12°C.

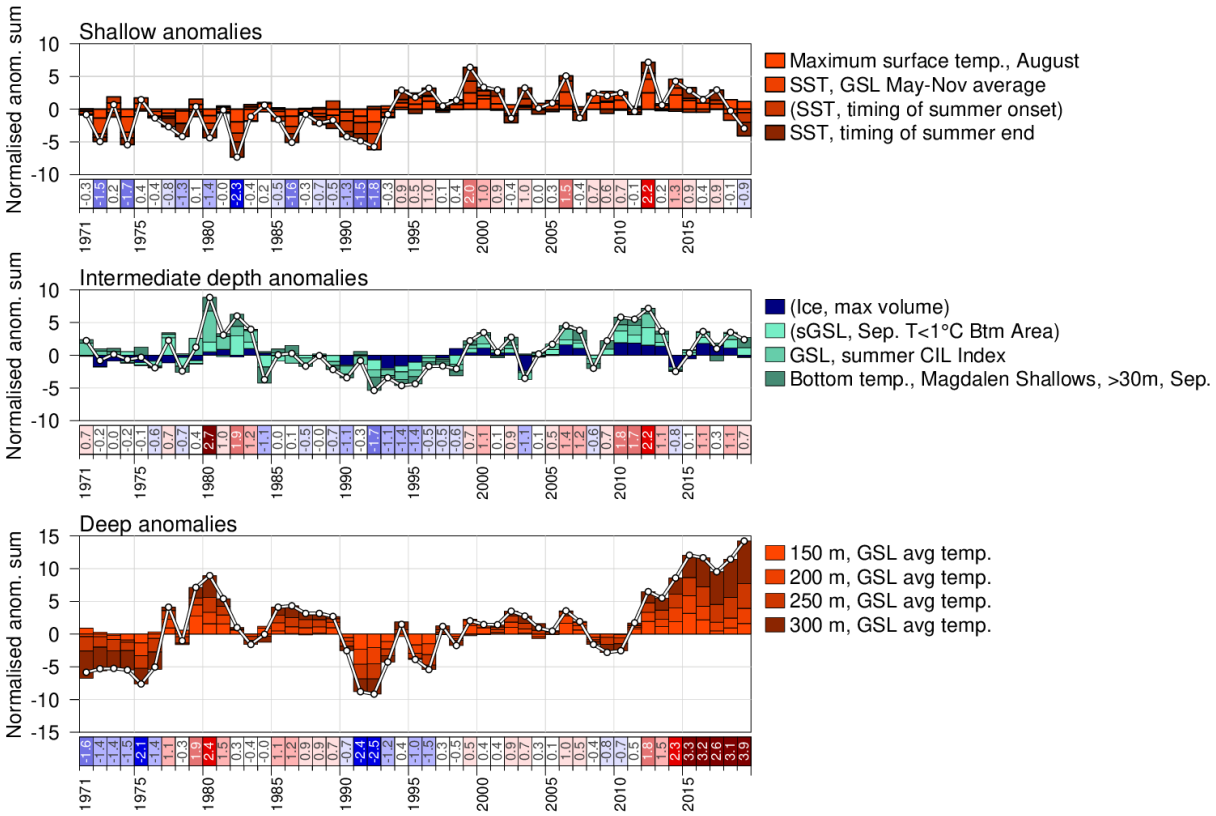

Fig. 70. Composite climate indices (white lines and dots) derived by summing various normalized anomalies from different parts of the environment (colored boxes stacked above the abscissa are positive anomalies, and below are negative). Top panel sums anomalies representing shallow temperature anomalies, middle panel sums intermediate depth temperature anomalies and sea-ice (all related to winter formation), and bottom panel sums deep temperature anomalies.

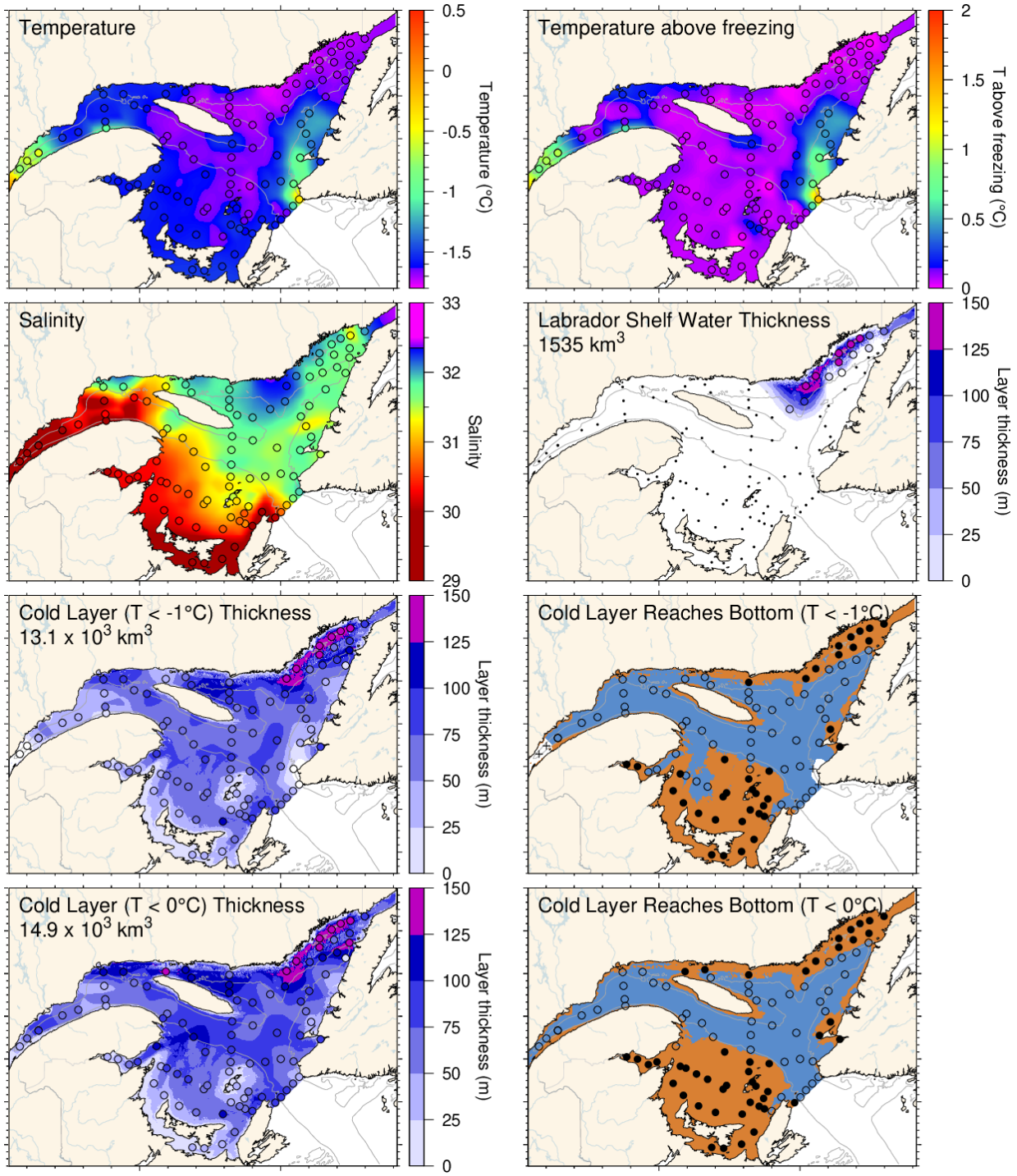

Fig. 71. March 2020 surface cold layer characteristics: surface water temperature (upper left), temperature difference with the freezing point (upper right), salinity (second row left), estimate of the thickness of the Labrador Shelf water intrusion (second row right), and cold layer (T<-1°C and <0°C) thicknesses and where they reach bottom. The symbols are coloured according to the value observed at the station, using the same colour palette as the interpolated image. A good match is seen between the interpolation and the station observations where the station colours blend into the background.